Multi-Objective Optimization of Solar Thermal Combisystems

Anthony Rey

A Thesis
in the Department
of
Building, Civil, and Environmental Engineering

Presented in Partial Fulfillment of the Requirements
for the Degree of
Doctor of Philosophy (Building Engineering) at
Concordia University
Montreal, Quebec, Canada

August 2017

Concordia University

School of Graduate Studies

This is to certify that the thesis prepared

By: Anthony Rey

Entitled: Multi-Objective Optimization of Solar Thermal Combisystems

and submitted in partial fulfillment of the requirements for the degree of

DOCTOR OF PHILOSOPHY (Building Engineering)

complies with the regulations of this University and meets the accepted standards with respect to originality and quality.

Signed by the final examining committee:

_____ Chair
Dr. Thomas G. Fevens

_____ External Examiner
Dr. Mikhail V. Sorin

_____ External to Program
Dr. M. Y. Chen

_____ Examiner
Dr. H. Ge

_____ Examiner
Dr. A. Athienitis

_____ Supervisor
Dr. R. Zmeureanu

Approved by _____
Dr. F. Haghighat , Graduate Program Director

August 30, 2017 _____
Dr. Amir Asif, Dean, Faculty of Engineering and Computer Science

Abstract

Multi-Objective Optimization of Solar Thermal Combisystems

Anthony Rey, Ph.D.

Concordia University, 2017

Solar thermal combisystems can significantly reduce primary energy consumption for residential buildings and therefore cut down greenhouse gas emissions; however, the overall performance of such systems depends on their design (i.e., configuration and sizing of their components) and operating conditions. Designing solar thermal combisystems can be improved by using optimization methods. Therefore, this doctoral thesis introduces a multi-objective optimization framework for optimizing the configuration and equipment sizing of solar thermal combisystems. A micro-time variant multi-objective particle swarm optimization (micro-TVMOPSO) algorithm is developed for handling engineering optimization problems, such as the multi-objective optimization of solar combisystems, where evaluating objective functions is time-consuming. The proposed framework uses a generic solar combisystem model coupled with the micro-TVMOPSO algorithm to find a set of optimized combisystem designs. Applied to two case studies, the multi-objective optimization framework was able to find designs reducing the life cycle cost, life cycle energy use, and life cycle exergy destroyed of solar thermal combisystems. The proposed multi-objective optimization framework can therefore be used to get the most out of solar thermal combisystems given specific economic and environmental conditions.

Acknowledgments

I would like to sincerely acknowledge the person without whom this thesis would not exist, Dr. Radu Grigore Zmeureanu. During the time I spent working under his supervision, he has been attentive professionally as well as personally. I, undoubtedly, benefited from his great knowledge and excellent advice that guided my research whilst letting me conduct it with the autonomy that I needed. I would like to thank all the members of the committee, especially Dr. Andreas Athienitis whom I had the chance to have as a teacher on solar building design. I would like to extend my gratitude to all the staff at Concordia University who has been helpful and accommodating, particularly Ms. Dalia Radwan. A thought goes to all my colleagues on the 16th floor who are always ready to help.

To Dr. Aiman Hanna, I hope someday to be as good at teaching as you are. Special thanks go to Drs. Sébastien Dutour, Richard Fournier, and Arnaud Lepadelec, from Paul Sabatier University, whose passion has inspired me. I would not have considered a research career if it were not for you. I cannot thank Kaitlin Manning enough for her incommensurable help regarding my English skills. I am sure that I would not have been able to carry out this doctoral program at Concordia University and write this thesis in William Shakespeare's language without her.

I will never forget all the wonderful people I have met here. Living on the other side of the Atlantic ocean had its ups and downs, but their friendliness made me feel at home. I almost enjoyed extreme winters thanks to Bora and our ice-skating trips as well as our gathering at his place with David and Chris. I had fun playing games with you, Drogheda, even if it meant losing most of the time. Thank you for showing me that veganism is not only about eating grass. Thanks to all the brunches I had with my friends and ex-roommates Valérie, Marie-André, Kayla, and Louis. I found a home away from home. It goes without saying that my Canadian experience would have not been the same without you. Special thanks go to Kayla for her assistance in proofreading this work.

To Golia, Pooya, Kasra, Masha, and Kaveh. You have no idea how grateful I am. All of you know that a doctoral program comes with its downs and you helped me surpass them. You are

more than drinking buddies who I had so much fun with, you are real friends. A special thanks goes to you, Salman, I could not have imagined that free sandwiches will lead to such an amazing friendship. You are the best, I owe you one.

I would like to thank my family and friends outside of Canada for supporting me. I strongly believe that I would not have achieved this without you. To Jérémy, Thomas, and Pierre, with whom I have so much fun every time. I cannot skip Tom and Oliver, since we would all go insane if we could not laugh. For every whatsapp text, I thank you, David. I wish that you arrived earlier, because I had missed you, Andrés and Aliénor. You all are amazing people. To my sister, although you were so mean to me when we were kids, you have always watched over me. I do not say it enough, but I do believe – despite our squabbling – that you are the best big sister ever. To my grand-mother and uncle, as well as my cousins and their parents, who gave me the best memories of my childhood. I would also like to thank my parents as I could not have wished for better ones. Last but not least, I would like to give a special thanks to the person who has shared this experience with me, Ingrid. Your love has been one of the best fuel to accomplish this adventure. I cannot fully express how grateful I am for all you have done.

Looking at how long is my acknowledgments makes me realize how lucky I am. Although I did my best to properly acknowledge everybody without offending anybody, it would have been way to long if I had mentioned everything I wanted to. Therefore, I would love to make sure that people know that I am thankful and keep them all in my heart.

To my grandfather, I wish I had more time with you.

Table of Contents

List of Figures

List of Tables

Nomenclature

Abbreviations

AbYSS	Archive-based hYbrid Scatter Search
BPS	Building Performance Simulation
CFSR	Climate Forecast System Reanalysis
COP	Coefficient Of Performance
CVRMSE	Coefficient of Variation of the Root Mean Square Error
DHW	Domestic Hot Water
DTLZ	Deb-Thiele-Laumanns-Zitzler
EA	Evolutionary Algorithm
EE	Embodied Energy
EEH	Energy Efficient House
EFR-RR	Ensemble Fitness Ranking with Ranking Restriction
EHX	External Heat Exchanger
ETC	Evacuated Tube Collector
FPC	Flat-Plate Collector
FSC	Fractional Solar Consumption
FW	Future Worth
GA	Genetic Algorithm
GenOpt	Generic Optimization program
GHG	GreenHouse Gas
GrEA	Grid-based Evolutionary Algorithm
HJ	Hooke and Jeeves

HUSP	Hours Under Set Point
HV	HyperVolume
HX	Heat Exchanger
IAM	Incidence Angle Modifier
IEA	International Energy Agency
IGD	Inverted Generational Distance
IHX	Internal Heat Exchanger
IQR	InterQuartile Range
KnEA	Knee point-driven Evolutionary Algorithm
KUR	KURsawe
LCC	Life Cycle Cost
LCE	Life Cycle Energy use
LCX	Life Cycle eXergy destroyed
MAD	Median Absolute Deviation
MATLAB	MATrix LABoratory
MINLP	Mixed Integer NonLinear Programming
MOEA/D-DE	Multiobjective Evolutionary Algorithm/Decomposition-Differential Evolution
MOEA	Multi-Objective Evolutionary Algorithm
MOO	Multi-Objective Optimization
MOPSO	Multi-Objective Particle Swarm Optimization
NMBE	Normalized Mean Bias Error
NSGA	Nondominated Sorting Genetic Algorithm
NZEB	Net Zero Energy Building
NZEH	Net-Zero Energy House
OECD	Organisation for Economic Co-operation and Development
OE	Operating Energy

PAES	Pareto Archived Evolution Strategy
PCCS	Parallel Cell Coordinate System
PCD	Parallel Cell Distance
PEN	PENalty function
PMAE	Percentage Mean Absolute Error
PME	Percentage Mean Error
PMV	Predicted Mean Vote
PPD	Percentage of People Dissatisfied
PSO	Particle Swarm Optimization
PV/T	Photovoltaic/Thermal
PW	Present Worth
RF	Radiant Floor
RMSE	Root-Mean-Square Error
SHC	Solar Heating and Cooling
SH	Space Heating
SPEA	Strength Pareto Evolutionary Algorithm
SWH	Solar Water Heating
TESS	Thermal Energy Systems Specialists
TRNSYS	TRaNsient System Simulation Tool
TVMOPSO	Time Variant Multi-Objective Particle Swarm Optimization
VNT	VieNneT
WSM	Weighted Sum Method
ZDT	Zitzler-Deb-Thiele

Greek Symbols

χ	constriction coefficient
Δ	difference

ϵ_m	constraint applied to the m-th objective function
η	thermal efficiency
X	exergy
λ	thermal conductivity
ϕ	sum of the cognitive and social coefficients
φ	positive random number between zero and one
τ	exergy/energy ratio

Roman Symbols

A	area
a_0	optical efficiency
a_1	first order heat loss coefficient
a_2	second order heat loss coefficient
K	archive size
b	constant involved in the definition of the MAD
B	Boolean variable or bias error
C	initial cost
c_1	cognitive coefficient
c_2	social coefficient
p	degree of freedom
n	dimension of decision set (number of decision variables) or sample size
M	dimension of objective set (number of objective functions)
d	discount rate
D	physical distance or thickness
h	specific enthalpy
s	specific entropy
G	solar irradiance

G^{best}	global best position
Q	heat transfer
I	inflation rate
$L_{k,m}$	integer label number for the m-th objective of the k-th non-dominated solution
E_{KE}	kinetic energy
l^j	lower limit of the j-th decision variable
m	mass
P	power
P_i^{best}	best position of the i-th particle
E_{PE}	potential energy
c_{p}	specific heat capacity at constant pressure
t	time, generation index, or t-value
T	temperature
U	overall heat transfer coefficient or overall uncertainty
u^j	upper limit of the j-th decision variable
v_i^j	velocity of the i-th particle for the j-th decision variable
V	volume or hypercube
w	inertia weight
w_m	weight assigned to the m-th objective function
W	Work transfer
x_i^j	the position of the i-th particle for the j-th decision variable

Mathematical Symbols

$\lceil x \rceil$	ceiling function: $\min\{k \in \mathbb{Z} \mid k \geq x\}$
$\mathcal{D}$	decision search space
$\prec$	Pareto dominance relation
$d(p, q)$	Euclidean distance: $d(p,q) = \sqrt{(q_1 - p_1)^2 + \ldots + (q_M - p_M)^2}$

$F(\cdot)$	vector function (composed of objective functions)
$f(\cdot)$	objective function
$\in$	is an element of
$lt(x_1, x_2)$	TRNSYS function which returns one if x_1 is less than x_2 and zero otherwise
$\max(\cdot)$	maximum function
$\overline{\square}$	overline symbol: arithmetic mean
$\mathrm{M}(\cdot)$	median operator
$\min(\cdot)$	minimum function
$\lvert\cdot\rvert$	absolute value or cardinality
P^*	Pareto front
$\hat{\square}$	hat over symbol: predicted (or estimated) value
$\dot{\square}$	dot over symbol: time rate of change
$\mathbb{R}$	set of real numbers
$\mathrm{rand}(\min, \max)$	return a uniformly distributed pseudo-random number between min and max
s_x	standard deviation of a variable x
$\subset$	is a subset of
x	decision vector (composed of decision variables) or observations
x^*	Pareto solution (or Pareto decision vector)
y	function
$\mathbb{Z}$	set of integers
$z(\cdot)$	global objective function

Subscripts and superscripts

amb	ambient
aux	auxiliary
avg	average
coll	solar thermal collector

comb	combisystem
cplg	internal convective gains due to air flow from adjacent zones
cross	cross-sectional area
d	destroyed
elec	electricity
env	environment
fin	final value
g,c	convective gains
ini	initial value
in	inlet
inv	initial investment
L	leaked
max	maximum value
min	minimum value
N	Nadir point
n	nominal
op	operating
out	outlet
phys	physical boundary
r	real
0	reference environment
rep	replacement
s	stored
tech	technical boundary
th	thermal
tot	total

up	upper boundary
U	Utopia point

Chapter 1

Introduction

This chapter provides an overview of the context in which this research has been conducted, and then presents the motivations that drove it. Afterwards, the outlines of this doctoral thesis are reported.

1.1 Background

Since the 1970s energy crisis, people have become more and more concerned about energy and its utilization. As human beings, we use energy every day for heating water, illuminating streets, transporting people, and so on. As a consequence, energy resource management is one of the biggest challenges for humanity. Energy demand is constantly growing as the world population increases. Since energy supply does not increase at the same rate as the energy demand, a supply-demand problem arises. In addition, our current energy infrastructures depend heavily on fossil fuels, which are consumed faster than they are produced. Fossil fuels are not sustainable energy sources, so they tend to disappear. Finally, burning fossil fuels produces greenhouse gases (GHGs), which are responsible for climate change. Consequently, we must look for alternative energy sources.

1.2 Motivations

As reported in (OECD/IEA, 2013), the buildings sector accounts for one-third of total final energy consumption, and that energy demand in buildings set to rise 50% by 2050. The buildings sector has therefore a significant impact on the environment. Global warming has led to a worldwide consciousness regarding the importance of renewable energy. For instance, the International Energy

Agency (IEA) is an autonomous organization which was establish in November 1974, within the framework of the Organisation for Economic Co-operation and Development (OECD), in response to the 1973 oil crisis. Renewable energy is defined by (IRENA, 2016) as "all forms of energy produced from renewable sources in a sustainable manner". Despite their beneficial effects, all of them cannot be integrated easily into buildings. Solar energy appears to be one of the most suitable sources for buildings. Nonetheless, solar energy technologies have faced difficulties in imposing themselves as the first choice in the buildings sector. A solar energy review (Timilsina et al., 2012) concluded that the main barrier to the deployment of solar thermal energy technologies is their cost, which remains less affordable than that of any conventional technologies for power generation. This explains why the solar energy growth observed over the past decade is primarily driven by policy support. The same observation was made in (Landry & Gagnon, 2015).

As pointed out in (Nyboer & Lutes, 2011), the most common use of solar energy in Canada is the direct heating of air and water. Figures reported in (Mauthner & Weiss, 2013) indicate that such a tendency is global. In 2012, the estimated total capacity of solar thermal collectors in operation worldwide was 268.1 GW_{th}, whereas that of solar photovoltaic panels was equal to 102.2 GW. Moreover, between 2000 and 2011, the average growth rate worldwide of the market development of glazed water collectors was around 20%. Consequently, technologies related to solar thermal collectors have a significant potential to save energy, and therefore reduce the buildings sector primary energy consumption. Solar energy, through solar thermal collectors, is a promising alternative to the use of fossil fuels in buildings.

An increasing interest in solar water heating (SWH) systems to reduce fossil fuel consumption and greenhouse gas emissions of residential building has already emerged (Hang et al., 2012). However, as mentioned in (Bornatico et al., 2012), priority should be given to solar thermal combisystems whose purpose is twofold, that is, providing heat for both domestic hot water (DHW) and space heating (SH) needs. Solar combisystems are relatively complex (Hadorn et al., 2002) and their performance depends on many factors, such as, orientation and tilt angle of solar thermal collectors, DHW usage profiles, weather conditions, and so on. Therefore, optimization techniques can be an efficient way to get the most out of solar thermal combisystems.

Optimization refers to finding the optimum feasible solution to a given problem without violating a set of constraints (Coello Coello, 2006). Optimization problems can be defined as single-objective,

if there is only one objective to be optimized, or as multi-objective, if more than one objective are involved. Real-world optimization problems having only one objective function are rather the exception than the rule for example, time against money or industrial development against wildlife preservation are multi-objective optimization problems. Most problems usually imply conflicting objectives (Fesanghary et al., 2012). Multi-objective optimization (MOO) problems require a different approach than the one used for single-objective, since the concept of optimality changes. A solution can be better according to one objective, but worse according to the others. MOO problems do not have a unique solution, but rather a set of trade-off optimal solutions, known as Pareto solutions. The concept of Pareto optimality lies in the fact that a Pareto solution cannot be improved according to an objective without being degraded according to another. For instance, reducing the insulation of a house to save money increases energy consumption. As mentioned in (Nguyen et al., 2014), the use of optimization methods in the buildings sector has significantly increased since 2005. Nevertheless, no multi-objective optimization method has been proposed or applied to completely design solar thermal combisystems.

Designing a solar thermal combisystem implies selecting a configuration, and then sizing all its components. Due to time and financial limitations, building performance simulation (BPS) programs can be preferred to physical experiments. Predicting the performance of a building plays a key role in reducing the buildings sector energy consumption, since 80-90% of a building's life-cycle operational energy demand is due to its operation (Ramesh et al., 2010). As a result, using multi-objective optimization methods to design solar thermal combisystems could be a way of reducing the buildings sector primary energy consumption and greenhouse gas emissions.

1.3 Thesis overview

This section gives an overview of the outlines of this doctoral thesis, which covers two main topics: (i) solar thermal combisystems and (ii) multi-objective optimization methods. Chapter 2 reviews previous research studies conducted in these two areas and introduces the research objectives based on a critical analysis of the literature review.

A preliminary study on multi-objective optimization methods for optimizing solar combisystems is conducted in Chapter 3. For comparison purposes, both a classical and a non-classical

optimization method is used to optimize a residential solar thermal combisystem, approached as a multi-objective optimization problem.

Chapter 4 presents a research methodology for optimizing solar thermal combisystems, which is composed of two main sections: (i) the development of a multi-objective optimization framework for optimizing solar combisystems, and (ii) the multi-objective optimization of the design of solar combisystems.

A generic model for solar thermal combisystems is presented in Chapter 5 in order to take into account the effect of the solar combisystem configurations and their sizing on the overall performance of solar thermal combisystems.

Chapter 6 introduces the multi-objective optimization framework developed in this doctoral thesis to optimize solar thermal combisystems. This framework goes from the selection of decision variables and their constraints up to objective and penalty functions.

A micro multi-objective optimization algorithm and a way of coupling it with the generic solar combisystem model are included in Chapter 7.

Two case studies are reported in Chapters 8 and 9. The first case study concentrates on a simulation-based residential solar thermal combisystem in Montreal, Quebec, Canada. The second focuses on an actual solar thermal combisystem installed in Massachusetts, USA.

Finally, Chapter 10 concludes this thesis by summarizing all conclusions that have been drawn and by presenting all contributions and potential future work.

Chapter 2

Literature review

This chapter reports previous research studies that have been conducted in areas of interest related to this doctoral thesis. This literature review is mainly related to two topics: (i) solar thermal combisystems, and (ii) multi-objective optimization methods. Research studies on solar thermal combisystems and their optimization are first presented. Special attention is then paid to multi-objective optimization methods in general. Finally, a summary identifies areas where further research could be valuable.

2.1 Solar thermal combisystems

The most common use of solar energy is the direct heating of air and water. For this reason, a special interest has been given to solar water heating systems. Such systems use solar energy for domestic hot water purposes. Solar thermal combisystems are designed to supply thermal energy for both domestic hot water and space heating needs. An additional heat distribution system increases complexity compared to solar water heating systems (Hadorn et al., 2002). New solar combisystems have extended the initial definition to space cooling needs; however, such systems – known as solar combi plus systems – are beyond the scope of this research, and therefore they will not be studied herein. In order to improve solar combisystems as a whole, all components and their interactions need to be enhanced.

2.1.1 Design of solar combisystems

Designing a solar thermal combisystem implies selecting a configuration and sizing all its components, which both have an impact on the overall performance of solar combisystems. Established in

1977, the Solar Heating and Cooling (SHC) Programme was one of the first IEA projects. Aiming to advance and promote the use of solar energy in buildings, the SHC Programme has allowed the creation of many projects, also known as Tasks. Task 26 was an exhaustive project conducted by a group of 35 experts and 16 solar industries from nine European countries and the United States of America, from 1998 to 2002, so as to analyze and optimize solar combisystems (Suter et al., 2000). This collaborative work led to 21 different solar generic combisystem configurations (Weiss, 2003).

From 2001 to 2003, the European Alterner Programme Project studied more than 200 solar combisystems installed in seven European countries. Since then, many independent studies have been related to solar combisystems, but no similar projects have focused on solar combisystem designs.

A review of research studies related to solar thermal combisystems, from 2004 to present, is therefore conducted herein to identify research areas that have not been explored yet. A distinction is made between simulation-based and experimental-based research studies. Solar combisystem configurations from manufacturers are also presented to have practical insights.

Simulation-based studies

Due to time and financial limitations, building performance simulation programs are preferred to physical experiments. Since simulations enable more flexibility than experiments, many simulation-based research studies were conducted.

One thermal storage tank

The environmental benefits of using a DHW or a solar combisystem instead of a conventional system was assessed in (Kalogirou, 2004a). For the specific configuration and sizing selected, 40% savings in greenhouse gas emissions was achieved for the solar thermal combisystem leading to an environmental payback varying from 0.9 to 9.5 years depending on the fuel and particular pollutant considered.

The effect of solar collector area and storage tank volume on a specific solar combisystem configuration was studied in (Lund, 2005) using TRNSYS (Klein et al., 2017), a BPS software. Increasing the thermal storage tank size to overcome overheating in summer was not found to be economically justified.

Two combined solar and pellet combisystem configurations based on Task 26 were compared in (Fiedler et al., 2006) using TRNSYS. Emphasis was put on the auxiliary heating system, either an integrated pellet burner or an external pellet boiler. For the former, storage tank losses should be addressed carefully while flue gas losses were the main heat losses for the latter.

The influence of different thermal storage tanks on the performance of solar combisystems was investigated in (Andersen & Furbo, 2007) using TRNSYS. Higher solar fractions, increased by 5-10%, were achieved with a stratifying device in the solar collector loop.

A simplified procedure for sizing solar thermal combisystem was presented in (Raffenel et al., 2009) and compared with TRNSYS. Although it cannot provide an optimal sizing, it can be used as a first step for energy feasibility. To characterize and compare the performance of solar combisystems, the fractional solar consumption (FSC) was developed in (Letz et al., 2009). This research study showed that the design of solar thermal combisystems has an impact on their thermal performance.

An economic analysis for a given solar combisystem was performed in (Ataei et al., 2009). The solar collector surface area was varied to find an optimal value, which led to a payback period of 5.4 years and 86 years, depending on the natural gas price considered (i.e., subsidized or not).

The influence of thermal storage volume dimensions on the solar combisystem performance was investigated in (Lundh et al., 2010) using TRNSYS. Well-insulated storage tanks were found to be insensitive to their geometry. External auxiliary volumes yielded lower energy savings than an external auxiliary heater using the thermal storage tank as a thermal buffer.

The impact of bikini and tank-in-tank stores on the thermal performance of solar combisystem was assessed in (Yazdanshenas & Furbo, 2010). Low flow bikini tanks were found to be promising for low energy buildings, while tank-in-tank stores were more suitable for houses with medium or high energy demands.

The economic and environmental impact of the auxiliary heat source (as, electricity, biomass, and coal) for a solar combisystem was investigated in (Yan & Li, 2012). Biomass was found to be the more favorable according to both criteria for northern China.

The effect of different charge and discharge strategies for the storage tank on the thermal performance of solar combisystems was studied in (Glembin & Rockendorf, 2012) using TRNSYS. The simulations revealed that installing three-way valves in both solar collector and heating loops to improve thermal stratification was not worthwhile.

A solar combisystem, using a 100 kW pellet boiler as an auxiliary heater, installed in a 4-story apartment building in Latvia was analyzed in (Žandeckis et al., 2013). Emphasis was put on the boiler's efficiency, which was increased by adjusting its operational parameters based on the results of laboratory tests.

A hybrid model predictive controller for the auxiliary heating of a solar thermal combisystem, developed in TRNSYS, was presented in (Pichler et al., 2014). Equipped with one thermal storage tank using a stratifying device and two external heat exchangers (EHXs), on the solar flat collector and DHW loops, a reduction of auxiliary energy demand up to 40% was achieved.

Nine different sized solar combisystems were simulated in (Martinopoulos & Tsalikis, 2014), which revealed that solar combisystems present a viable solution towards net zero energy building (NZEB) in Greece. The solar combisystem configuration was composed of one thermal storage tank with two internal heat exchangers (IHXs), on the solar flat-plate collector and SH loops. The minimum solar contribution among all the four climatic zones studied was 45% of the total heating loads, which led to a payback period of 4.5 years and a reduction of CO_2 around 50 tons.

The performance of a pellet and solar combisystem at four different temperature ranges for space heating was studied in (Žandeckis et al., 2016) using TRNSYS. Results showed that reducing the SH temperature increases solar gains and diminishes CO emissions.

The potential of a direct solar integration into the space heating circuit for solar thermal combisystems, instead of a storage tank to store thermal energy, was investigated in (Glembin et al., 2016) using TRNSYS. In such a configuration, flat-plate collectors can be connected only to the tank or to both tank and indoor heating distribution system. Three different configurations were studied based on a prototype installed in Germany. For a solar fraction of approximately 50%, direct integration was able to reduce the thermal storage volume by three compared to a conventional solar combisystem.

Two thermal storage tanks

A residential solar thermal combisystem, based on the configuration no. 14 of Task 26, was studied in (Leckner & Zmeureanu, 2011) using TRNSYS. The shortest financial payback was higher than the life expectancy of the house; however, an energy payback time varying between 7.5 and 9.5 years, depending on the number of flat-plate collectors, was achieved.

A preliminary study for solar combisystem potential in the four main climates regions of Canada was investigated in (Asaee et al., 2014). For each climate, varying the normalized tank volume (volume/baseline volume) showed a maximum annual solar fraction value. Solar fraction was found to decrease if the storage tank volume exceeds available solar energy. Savings within 70-80% highlighted the benefits of solar combisystems.

A techno-economic feasibility of retrofitting solar combisystems to houses in Canada was performed in (Asaee et al., 2016). Results showed that approximately 40% of houses in the Canadian housing stock are eligible for solar combisystem retrofit, which would reduce the annual energy consumption and GHG emissions by about 19%, if all houses were retrofitted.

Seasonal thermal storage

A solar thermal combisystem equipped with a seasonal storage tank was studied in (Hugo et al., 2010). Results showed that the initial embodied energy was recovered within six years, no matter the type of solar collectors being used; however, the financial payback period was between 26 and 55 years, depending on the type of solar collectors, lack of substantial financial incentives, and low electricity price.

A commercial developing prospect of solar heating combisystems with seasonal heat storage for district heating in China was conducted in (Ruicheng & Jingjingm, 2015). Such systems were found to be more suitable in the north-west of China where larger uncultivated lands and solar resources are available.

A life cycle analysis of a low-energy single-family house in Ireland, equipped with a solar combisystem, was presented in (Colclough & McGrath, 2015). The solar combisystem has one 300 L DHW tank and one seasonal thermal storage tank. Among the different configurations tested, the use of both solar thermal collectors and photovoltaic panels was the most attractive option with an energy savings of 28,763 MJ and a payback period of approximately 8.4 years.

Recent research activities

Different configurations have been tested over the past twenty years to improve the overall performance of solar thermal combisystems. Recent research activities have focused on: (i) solar thermal combisystems with a more efficient storage (Mette et al., 2013); (ii) solar thermal combisystems

equipped with a heat pump (Deng et al., 2013; Poppi, Bales, Haller, & Heinz, 2016; Poppi, Bales, Heinz, et al., 2016; Schimpf & Span, 2015; ur Rehman et al., 2016), (iii) solar combi-plus systems for cooling needs (Bahria et al., 2016); and (iv) solar thermal combisystems using photovoltaic/thermal (PV/T) hybrid solar collectors to produce electricity (Hazami et al., 2017).

The performance of a solar thermal combisystem using thermochemical energy storage (where heat is stored in a reversible chemical reaction instead of a temperature difference) was studied in (Mette et al., 2013) using TRNSYS for a building located in Germany. Emphasis was put on a regeneration process for the thermochemical energy storage to increase the solar thermal combisystem's efficiency (an increase of 6.1% of the fractional energy saving was achieved).

A solar combisystem equipped with a carbon dioxide heat pump was developed in (Deng et al., 2013) using TRNSYS. An average coefficient of performance (COP) value of 2.38 and a solar faction of 69% for the entire heating season was achieved for Shanghai after a parametric optimization.

An economic feasibility of a solar thermal combisystem coupled with a heat-pump organic Rankine cycle system was conducted in (Schimpf & Span, 2015). Their results indicated that the organic Rankine cycle operation reduces the net electricity demand from the grid while mitigating the potentially harmful stagnation of the solar collector loops in a cost-effective way.

An air source and solar thermal heat pump combisystem was developed in (Poppi, Bales, Haller, & Heinz, 2016; Poppi, Bales, Heinz, et al., 2016) using TRNSYS for Carcassonne and Zurich. Heat pumps losses were shown to be an important factor to take into account. Results also show that variations in electricity price affects the additional investment limit far more than the other economic parameters.

A parametric study of a solar combi-plus system was conducted for different houses and climates of Algeria using TRNSYS in (Bahria et al., 2016). A solar fraction greater than 45% was achieved with optimal parameters.

An energetic, exergetic, and economic analysis of a solar thermal combisystem equipped with PV/T hybrid solar collectors was conducted in (Hazami et al., 2017) using TRNSYS. Under the Tunisian climate, a payback period of 10.2 years was found with an annual energy saved of 7,618.3 kWh/year.

Experimental-based studies

Building performance simulations rely on mathematical models, which must be verified and validated to be used. The validation process assures models' accuracy by way of a comparison with experimental data. Models are thus similar to but simpler than systems they represent (Maria, 1997).

One thermal storage tank

An energy analysis of an experimental solar thermal combisystem was performed in (Kaçan & Ulgen, 2012). Experiments were conducted to verify and increase the solar combisystem's performance, which led to an annual FSC value of approximately 83%. An energetic and exergetic analysis of a solar combisystem was performed in (Kaçan & Ulgen, 2014), based on an experimental setup built in Turkey. Tank volume was found to be one of the most important parameters to save energy effectively and avoid excessive energy production. Depending on the climatic conditions, system components, system efficiencies and energy demand, 10% to 100% of the energy demand was covered by the solar combisystem. The effect of the exergetic efficiency of some solar combisystem components on the overall system exergetic efficiency was assessed in (Kaçan, 2015) by using a combination of response surface method and central composite design. A net exergetic efficiency of 11.95% was achieved for the entire solar combisystem by finding the optimum values for each component.

Seasonal thermal storage

An analysis of the solar thermal market in Latvia was conducted in (Žandeckis et al., 2011), followed by a data analysis of a solar combisystem implemented in a multi-family building. Reducing the use of natural gas by installing solar combisystems should ensure a more stable price for DHW and SH needs. An optimization was mentioned in order to enhance the performance of the solar combisystem since data showed that it was not working in the most efficient way.

Experimental data from a solar thermal combisystem, installed in Ireland, were used to calibrate a TRNSYS model in (Clarke et al., 2014). Afterwards, a parametric analysis was performed which showed that increasing the collector area from 10.6 m^2 to 20.0 m^2 could increase the total solar

fraction from 47% to 67%, decreasing fossil-fuel-derived energy demand by up to 30%.

Manufacturers' solar combisystem configurations

The characteristics of several solar thermal combisystem configurations were presented at a conference held by Affordable Comfort, Inc. (Home Performance Coalition, 2012). Out of five configurations, two were similar to those used in (Ng Cheng Hin & Zmeureanu, 2014) and (Martinopoulos & Tsalikis, 2014). The use of two thermal storage tanks or external heat exchangers are not common practice. Two configurations used an internal boiler.

A collaboration with Viessmann (S. Royce, personal communication, March 2014) and Stiebel Eltron (E. Wilson, personal communication, April 2014), which are two of the leading international manufacturers of solar water heating technology, showed that one or two thermal storage tanks are viable. Each of the configurations proposed by the manufacturers use the hot water within the thermal storage tank for DHW purposes. Space heating is mainly ensured by an immersed heat exchanger; however, Viessmann proposes two configurations where no heat exchanger or an external one can be used on the SH loop side. The solar configuration proposed by Stiebel Eltron has no equivalent among the 21 generic solar thermal combisystems considered by Task 26, except the generic solar combisystem no. 14 that shares however similar characteristics. The main difference between the two configurations is the solar collector loop, which is equipped with an internal (Stielbel Eltron) or an external heat exchanger (no. 14). The Viessmann group proposes four different solar combisystem configurations. The Viessmann configuration no. 1 is similar to the generic solar combisystem no. 4 of Task 26; however, the former uses one dual-coil storage tank, whereas the latter employs three immersed heat exchangers. The generic solar combisystem no. 9 is the most analogous to the Viessmann solar combisystem no. 2. Nonetheless, the DHW storage tank in the generic solar combisystem no. 9 is built in the space heating storage tank (i.e., a tank-in-tank). The Viessmann solar combisystem no. 3 and no. 4 have no equivalent among the solar combisystems reported in Task 26.

2.1.2 Optimization of solar combisystems

An optimization of a simulation-based solar combisystem was performed in (Bornatico et al., 2012) using MATLAB (MATLAB, 2017). Three objective functions (solar fraction, energy use, and cost

of the installation) were agglomerated into one global objective function, then a single-objective optimization algorithm was used to optimize the sizing of the given combisystem configuration.

The fluid mass flow rate in the solar collector and storage loops of a solar thermal combisystem was optimized in (Kusyy & Vajen, 2012) using TRNSYS and GenOpt (Wetter, 2011), an optimization software. An improvement of only 0.3 percent points for the thermal fractional savings was achieved by reducing the fluid mass flow rate from 30 L/(h·m$^2_{\text{coll}}$) to 10 L/(h·m$^2_{\text{coll}}$).

A hybrid particle swarm optimization/Hooke and Jeeves (PSO/HJ) algorithm was used in (Ng Cheng Hin & Zmeureanu, 2014) to minimize the life cycle cost, life cycle energy use, and life cycle exergy destroyed of a solar thermal combisystem in an energy efficient house in Montreal, Canada. The result show that the life cycle cost, life cycle energy use, and life cycle exergy destroyed were reduced by 19%, 34%, and 33%, respectively.

2.2 Multi-objective optimization

Any optimization problem formulation has at least three components: (i) one or several objective functions, (ii) a set of decision variables, and (iii) a set of constraints for the objective functions and decision variables. Multi-objective optimization (MOO) problems intend to determine the optimum feasible sets of values of decision variables, which minimize or maximize at best objective functions while respecting all constraints. MOO problems can be formally formulated as follows:

$$\min_{x\in\mathcal{D}} \left(\text{or } \max_{x\in\mathcal{D}}\right) F(x) \tag{2.1}$$

where x is the decision vector (composed of decision variables); $F(x)$ and $\mathcal{D}$ are the function vector and decision search space defined as:

$$F(x) = [f_1(x), f_2(x), \ldots, f_M(x)] \tag{2.2}$$

$$X = \{x \subset \mathbb{R}^n \mid l^j \leq x^j \leq u^j, j \in \{1, \ldots, n\}\} \tag{2.3}$$

with $-\infty \leq l^j < u^j \leq \infty$ for all $j \in \{1, ..., n\}$; M is the number of objective functions; n is the number of decision variables; l^j and u^j are the lower and upper limits of the j-th decision variable, respectively.

Determining an optimal solar combisystem design implies finding a set of values of the decision variables $x^* \in \mathcal{D}$ that optimizes the function vector $F(x)$, while satisfying all the constraints. As explained by the duality optimization principle (Ravindran et al., 2006), any maximization optimization problems can be turned into minimization ones by multiplying their objective functions by (-1). Without loss of generality, it is assumed that all future objective functions must be minimized. Such optimization problems do not have a unique optimal solution, but rather a set of trade-off optimal solutions, known as Pareto solutions.

Most of the multi-objective optimization problems involve conflicting objective functions (R. Yang & Wang, 2012), where it is impossible to make the most of each objective function with the same decision vector x. Therefore, multi-objective optimizations aim at finding solutions where any improvement of an objective function can be made without degrading the others. This concept is known as Pareto optimality. For any multi-objective optimization problem defined by Equation 2.1, a decision vector x_1 in the decision search space $\mathcal{D}$ is said to be Pareto optimal if, and only if, for all $x_2 \in \mathcal{D}$,

1. $f_m(x_1) \leq f_m(x_2)$ for all $m \in \{1, \ldots, M\}$; and
2. $f_m(x_1) < f_m(x_2)$ for at least one $m \in \{1, \ldots, M\}$.

If x_1 is Pareto optimal, then x_1 can be written x_1^* and is said to dominate any x_2, which is expressed as $x_1^* \prec x_2$. A set of Pareto optimal solutions, or simply Pareto solutions, is referred to as Pareto front. The Pareto front associated with a multi-objective optimization problem is the set P^* such that $P^* \in \mathcal{D}$ and for all $x_1^* \in P^*$, there is no $x_2^* \in P^*$ such that $x_2^* \prec x_1^*$.

2.2.1 Main issues of multi-objective optimizations

Any multi-objective optimization aims at finding the optimum feasible non-dominated solutions according to all the objective functions involved (i.e., the Pareto front). Since objective functions are evaluated by external BPS programs for solar thermal combisystems, additional issues arise in the optimization search. These issues are then added to common existing multi-objective optimization challenges.

Intercommunication

Communication between BPS programs and multi-objective optimizers is not without difficulties. Communication involves an information source, which sends a message to a receiver. The objective of such a process is to exchange information, and therefore receivers must understand messages. Coupling a building performance simulation software with an optimizer requires that they are both information source and receiver. As mentioned in (Wetter, 2004), objective functions evaluated by most of the BPS programs – that have been developed so far – have discontinuities (e.g., discontinuities due to iterative solvers which cannot find an accurate approximate solution). Since optimization optimizers depend on the properties of objective functions, optimization methods need to take this problem of discontinuities into account.

Multi-dimensional optimizations

Decision variables can be seen as the degree of freedom of the problem to be optimized. The more decision variables are used, the more difficult multi-objective optimization problems become (Mahdavi et al., 2015). The curse of dimensionality, also known as Bellman's curse of dimensionality, refers to difficulties that occur when the size of an optimization problem increases. For instance, if the design of a solar combisystem is defined by nine decision variables, each able to take on 10 different values, one billion possibilities must be considered to know all the Pareto solutions. Even though constraints make some possibilities unfeasible, a considerable amount of time is required to test all decision vectors.

Selection of optimizers

Selecting a suitable optimizer is a key step in multi-objective optimization problems. The *No Free Lunch* theorem for search and optimization, introduced in (Wolpert & Macready, 1997), states that "all optimization algorithms are equivalent when their performance is averaged across all possible problems". In other words, there exists no optimization algorithm able to outperform all others in all multi-objective optimization problems. Accordingly, optimization algorithms are problem-dependent. For this reason, the challenge is to select the most suitable optimization algorithm for a given multi-objective optimization problem.

2.2.2 Multi-objective optimization methods

As mentioned in Section 2.2.1, the performance of an optimizer strongly depends on the optimization problem it is applied to. As a result, this section introduces different optimization methods in order to define the most suitable for the multi-objective optimization of solar combisystems. As mentioned in (Nguyen et al., 2014), optimization algorithms can be classified as: deterministic or stochastic, derivative-based or derivative-free, bio-inspired or non-bio-inspired, and so on. Since building performance simulation programs can entail discontinuities in objective functions, derivative-based algorithms are not suitable for optimizing solar thermal combisystems and are not considered herein. Among derivative-free algorithms, two methods have been mainly used for solving multi-objective optimization problems (Machairas et al., 2014): (i) classical, and (ii) non-classical methods. The term non-classical is used as opposed to classical, which is taken from (Deb, 2001).

Classical methods

An overview of the main classical methods used for multi-objective optimization problems are presented herein. The idea behind all of the following methods is to turn multi-objective optimization problems into single objective ones.

Weighted Sum Method

The weighted sum method (WSM) is one of the most widely used method for multi-objective optimizations (Kim & de Weck, 2006; Marler & Arora, 2010). The WSM consists of aggregating all objective functions of a MOO problem into only one global objective function, in which each objective function is assigned a weight as follows (Deb, 2001):

$$z(x) = \sum_{m=1}^{M} w_m \cdot f_m(x) \tag{2.4}$$

where $z(x)$ is the global objective function; w_m is the weight assigned to the m-th objective function $f_m(x)$.

The WSM gives importance to one or more criteria by increasing their respective weights compared to the others. Nevertheless, this method has five main disadvantages: (i) one optimization

run leads to only one Pareto solution; (ii) time-consuming for approximating a Pareto front; (iii) the combination of weights are difficult to select; (iv) different weight vectors do not necessarily lead to different Pareto points; (v) some Pareto solutions in non-convex search domains cannot be found.

ϵ-constraint method

The ϵ-constraint method focuses on one of the selected objectives, while the rest of them are set as constraints. Proposed in (Haimes et al., 1971), the optimization problem is formulated as:

$$\begin{aligned} &\min_{x \in \mathcal{D}} \ f_l(x) \\ &\text{subject to} \\ &f_m(x) \leq \epsilon_m, \forall m \neq l \end{aligned} \tag{2.5}$$

Unlike the WSM, the ϵ-constraint method can find Pareto solutions in non-convex regions; however, the Pareto solutions strongly depend on the selection of the ϵ-vector which requires information about the selected objectives. Thus, the ϵ-constraint method belongs to *a priori* methods, that is to say methods implying previous knowledge about the selected objective functions. One optimization run still leads to only one Pareto solution. Therefore, like the WSM, the ϵ-constraint method is time-consuming for approximating a Pareto front.

Non-classical methods

Non-classical methods, as opposed to classical ones, use multi-objective optimization algorithms which can directly deal with MOO problems. Two main families of non-classical methods are introduced herein because of their current popularity and effectiveness (Britto & Pozzo, 2014; Pasandideh et al., 2013; Y. Zhang et al., 2011): (i) evolutionary algorithm, and (ii) swarm intelligence.

Evolutionary algorithms

Evolutionary algorithm (EA) is a generic term used to designate any population-based metaheuristic optimization algorithms, of which the search process consists in imitating natural selection. Evolutionary algorithms are hence inspired by evolution. At each generation, the best individuals

(i.e., candidate solutions) are selected, based on their fitness, and go through operators such as reproduction, recombination, and mutation to engender the next generation. Over the generations, the population evolves and becomes more suitable for the given optimization problem.

As mentioned in (Evins, 2013; Nguyen et al., 2014; Roy et al., 2008), the most popular evolutionary algorithms are genetic algorithms (GAs), whose concept was first introduced by John Holland at the University of Michigan in the 1970s (Luke, 2015). The working principle of genetic algorithms is shown in Figure 2.1.

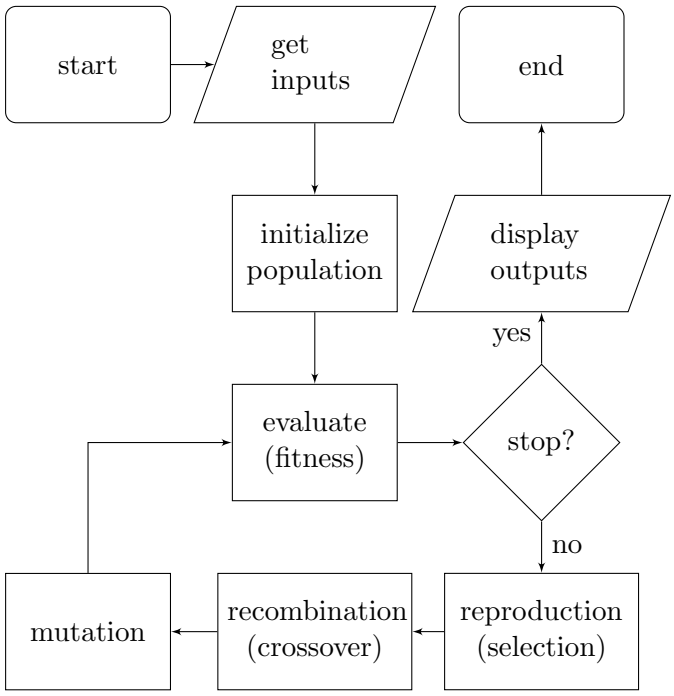

Figure 2.1: Flowchart of the GA process

GAs start with an initial population of individuals, which can be initialized through three different mechanisms: (i) random, (ii) seeded, or (iii) mixed selections. The first uses a pseudo random number generator to create the initial population, whereas the second assigns a user-defined candidate solution to each individual. The last is a mix of the first two mechanisms. Once the initial population is created, the individuals are evaluated to know their fitness. One or more termination criteria are implemented to ensure conditions under which the algorithm stops execution. For example, a user-defined percentage of the individuals converging to the same solution or a maximum number of generations can be set as termination criteria. If these conditions are

not met, the best individuals (i.e., solutions having the fittest fitness) are selected for reproduction. These individuals undergo recombination and mutation operators to generate offspring. These new individuals, often called children, replace those from the initial population having the fittest fitness. This procedure continues until one of the termination criteria is met.

Genetic algorithms are single objective optimizers, and therefore they cannot directly handle MOO problems. To overcome the disadvantages of the classical methods, multi-objective evolutionary algorithms (MOEAs) have been developed. Based on (Goldberg, 1989), a multi-objective version of genetic algorithms, named nondominated sorting genetic algorithm (NSGA), was introduced in (Srinivas & Deb, 1994). Since then, this multi-objective genetic algorithm has been improved in (Deb et al., 2002), which is referred to as NSGA-II, and applied to buildings-related problems (Chantrelle et al., 2011; Magnier & Haghighat, 2010; Wang et al., 2005). It has thus become one of the most commonly used approaches for MOO problems (Ghiasi et al., 2011; Roy et al., 2008). A more recent version, named NSGA-III, was proposed in (Deb & Jain, 2014) in order to handle many-objective optimization problems. Many-objective optimization problems (i.e., four up to 15 objectives) is one of the most recent research activities, which has led to GrEA (S. Yang et al., 2013), KnEA (X. Zhang et al., 2015), or EFR-RR (Yuan et al., 2016). Each of them has proved their effectiveness and competitiveness compared with other MOO algorithms on benchmark problems with six or more objectives. Since four objective functions are considered in this thesis for optimizing solar thermal combisystems, such MOO algorithms are not taken into account.

Swarm intelligence

As mentioned in (Luke, 2015), swarm intelligence algorithms are somewhat similar to EAs; however, they differ in their philosophy, since they are modeled after swarming behaviors in animals. Swarm intelligence algorithms do not use any selection mechanism. All particles at the end of the search process are the same as the ones in the initial population, they only moved through the search space. Although more and more swarm intelligence algorithms come into beings, such as artificial bee colony, bat algorithm, or even wolf search, particle swarm optimization (PSO), remains the most widely used swam intelligence algorithm (Fister et al., 2013; Peyvanddi et al., 2011; Shakerian et al., 2011).

Particle swarm optimization

Particle swarm optimization is a population-based stochastic optimization algorithm presented in (Kennedy & Eberhart, 1995). PSO solves single-objective problems by mimicking the collective behavior of certain animal species searching for food, such as flocks of birds or schools of fish. Each candidate solution is called a particle, which is characterized by its position and velocity. The former corresponds to a vector of decision variables, while the later represents the speed and direction at witch a particle is moving from one location to another. At each iteration, also called generation, each particle's velocity is updated based on its own memory and that of the entire swarm. The particle's position is then tweaked to find a better location that is, a decision vector leading to a decrease of the selected objective function's value. Each particle memorizes its position having the lowest objective function value, which is stored in P^{best}. The lowest objective function value of the whole swarm is stored in G^{best}. Therefore, each particle *flies* through the search space by using its best experience and that of the entire swarm, as depicted in Figure 2.2. The update pattern of each particle is given by (Shi & Eberhart, 1998):

$$v_i^j(t+1) = w(t) \cdot v_i^j(t) + \varphi_1(t) \cdot c_1(t) \cdot \left[P_i^{\text{best}}(t) - x_i^j(t)\right] + \varphi_2(t) \cdot c_2(t) \cdot \left[G^{\text{best}}(t) - x_i^j(t)\right] \quad (2.6)$$

$$x_i^j(t+1) = x_i^j(t) + v_i^j(t+1) \quad (2.7)$$

where v_i^j is the velocity of the i-th particle for the j-th decision variable; w is the inertia weight; φ_1 and φ_2 are positive random numbers between zero and one; c_1 and c_2 are the cognitive and social coefficients, respectively; P_i^{best} is the best position of the i-th particle; G^{best} is the global best position (i.e., the best position found by the entire swarm); x_i^j is the position of the i-th particle for the j-ith dimension; t is the generation index.

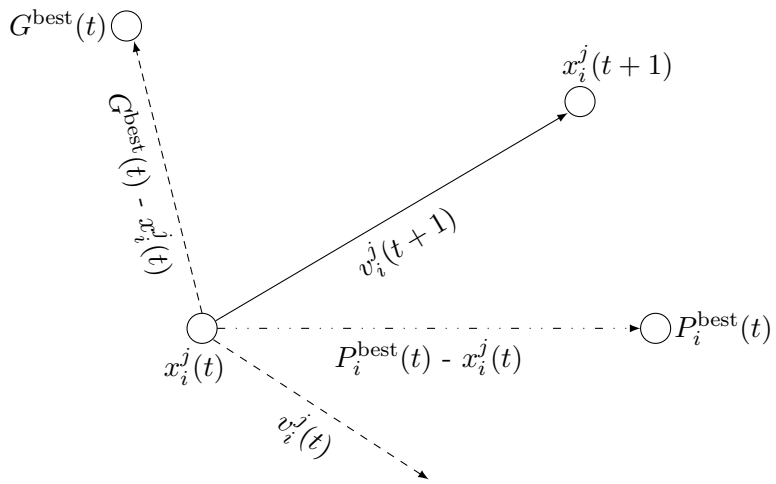

Figure 2.2: Representation of the PSO pattern

As reported in (Deb, 2001), multi-objective optimization algorithms usually derive from a single-objective version. PSO has proved to be effective at solving single objective optimization problems in several studies (Bornatico et al., 2012; Coelho et al., 2005; Hasni et al., 2011; Wetter & Wright, 2004). Unlike GA, PSO does not have many user-defined parameters to be tuned and its concept is easy to implement. As a result, special attention is paid to multi-objective particle swarm optimization (MOPSO), which is the multi-objective version of PSO.

Multi-objective particle swarm optimization

A proposal extending the PSO algorithm to solve multi-objective optimization problems was presented in 2002 (Coello Coello & Lechuga, 2002). The authors called this proposal MOPSO, which stands for multi-objective particle swarm optimization. At that time, using the PSO concept for MOO problems was innovative, as only two other proposals were related to this possibility (Moore & Chapman, 1999; Ray et al., 2001). Since MOO problems do not have a unique optimal solution, but rather a set of Pareto solutions, three main issues arose in extending PSO (Reyes-Sierra & Coello Coello, 2006):

1. How to select particles (to be used as leaders) in order to guide the optimization search?
2. How to retain a well spread set of non-dominated solutions?
3. How to maintain diversity in the swarm to avoid converging to local minimums?

Although MOPSO was first introduced in (Coello Coello & Lechuga, 2002), an improved version published by the same authors in (Coello Coello et al., 2004) is often considered in the specialized literature as the original MOPSO. Therefore, the next paragraphs focus on how this improved version answered the three aforementioned questions.

Leader selection

The strength of MOPSO lies in its external archive, named repository. Non-dominated solutions found during the optimization search are stored in the repository. To ensure diversity, an adaptive grid taken from (Knowles & Corne, 2000) divides the repository into hypercubes, based on the value of each objective function found so far. The repository can be viewed as a matrix, where each hypercube is associated with a row and column number. Each Pareto solution is stored using these hypercubes. The hypercubes having more than one particle are assigned a fitness equal to the ratio of a fixed number, e.g., equal to 10 in (Coello Coello et al., 2004), to the number of particles that it contains. The fitness assigned to a hypercube is thus inversely proportional to the number of particles that are within the hypercube. For example, if a hypercube contains 20 particles, its fitness is equal to 0.5 (i.e., 10 divided by 20). The global best solution G^{best}, which serves as a leader, is then chosen by using the roulette-wheel selection based on the calculated fitness values of all hypercubes. Therefore, the non-dominated solutions located in the less crowded regions of the repository have a higher probability to be selected to guide the swarm.

Retaining non-dominated solutions

The size of the repository, which is a user-defined parameter, is limited. As a result, some solutions must be removed when the repository reaches its maximum capacity. Since the repository contains only non-dominated solutions, the roulette-wheel selection based on the calculated fitness values of the hypercubes is used to maintain the size of the repository. Non-dominated solutions located in the less crowded hypercubes are more like to remain in the repository to obtain a well spread set of solutions. So, the non-dominated solutions located in the more crowded regions of the repository are more likely to be removed.

Maintaining diversity

MOPSO uses a mutation operator to increase its exploration, and therefore maintains diversity. The mutation operator acts on both the particles and the range of each decision variable. At the beginning, it acts on all the particles and covers the full range of each design variable. As the number of generations increases, fewer and fewer particles are mutated and the range of each decision variable being mutated is narrowed using a non-linear function. The mutation operator aims at exploring remote regions of the search space and ensure that the full range of each decision variable is explored, so as to prevent premature convergence. The working principle of the MOPSO algorithm presented in (Coello Coello et al., 2004) can be illustrated as shown in Figure 2.3.

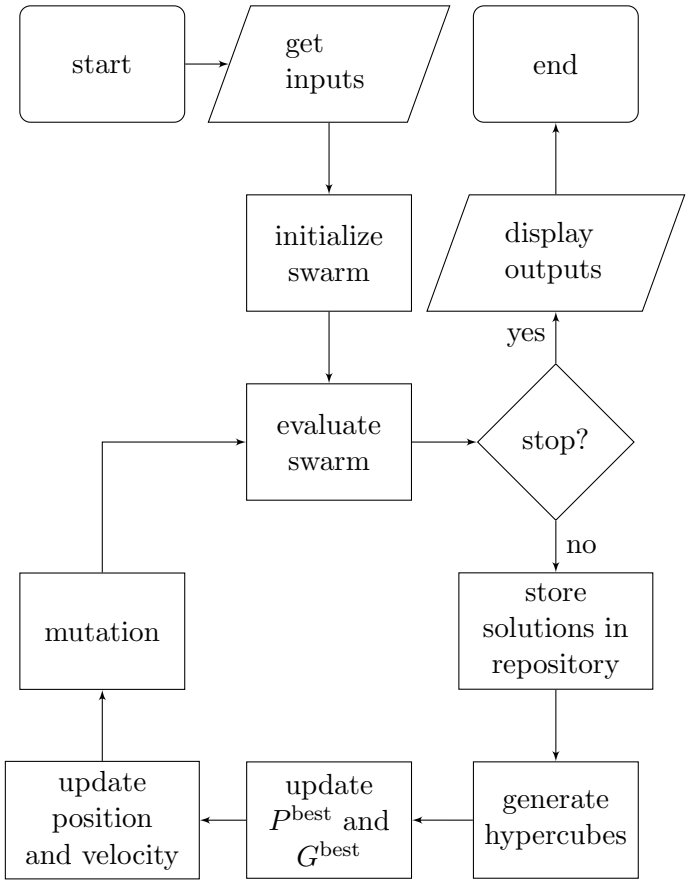

Figure 2.3: Flowchart of the MOPSO process

Other MOPSO versions

Since (Coello Coello et al., 2004), many other versions of the multi-objective particle swarm optimization algorithm have been proposed. The inertia weight and acceleration coefficients were decrease linearly though generations in (Tripathi et al., 2007). The leader selection was modified in (J. Yang et al., 2009) using the Sigma method to have a better trade-off between convergence and diversity. A comparison of some improving strategies for MOPSO was conducted in (Moslemi & Zandieh, 2011). A multi-swarm cooperative MOPSO was proposed in (Y. Zhang et al., 2011) to local multiple optima, and therefore increase diversity. To avoid premature convergence, a MOPSO using Gaussian distribution sequences to generate random numbers was presented in (Zeng & Sun, 2014). An adaptive MOPSO using parallel cell coordinate system was developed in (Hu & Yen, 2015) to overcome the main issues of the previous MOPSO versions.

Most of the research studies on MOPSO or other MOO algorithms focused only large population size. Little emphasis has been placed on micro-MOO algorithms, which use a small population of solution candidates. Such algorithms are suitable for optimization problems where evaluating objective functions is time-consuming, which is the case of many engineering applications such as aeronautical or building engineering problems (Fuentes Cabrera & Coello Coello, 2010). A micro-genetic algorithm for multi-objective optimization, named micro-GA, was proposed in (Coello Coello & Pulido, 2001), and then improved in (Pulido & Coello Coello, 2003). Another micro-MOO algorithm, called micro-MOPSO, was presented in (Fuentes Cabrera & Coello Coello, 2010), which was a micro version of the MOPSO algorithm. To the best knowledge of the author, none of them has been used in building engineering and no further research has been conducted on micro-MOO algorithms.

2.3 Summary of previous research studies

This literature review highlighted trends in both the solar combisystem and multi-objective optimization fields. Even if seven out of the 21 generic solar combisystem configurations considered by Task 26 implied more than one storage tank, most of the research studies involved only one. Using two storage tanks (i.e., one dedicated to DHW preparation and the other to space heating needs) appears more common nowadays based on recent studies (Asaee et al., 2014, 2016; Ng Cheng Hin

& Zmeureanu, 2014) as well as the Stiebel Eltron and Viessmann configurations. No conclusion can be drawn about using one or two thermal storage tanks based on (Home Performance Coalition, 2012). Most research studies used hot water within storage tanks for space heating needs (Ataei et al., 2009; Lund, 2005; Lundh et al., 2010). DHW preparation is therefore mainly done through an immersed heat exchanger. Nonetheless, some studies (Leckner & Zmeureanu, 2011; Raffenel et al., 2009) as well as the solar combisystem configurations proposed by Viessmann or Stiebel Eltron do not use a heat exchanger in the DHW loop (i.e., hot water within thermal storage tanks is dedicated to DHW needs), neither four out of five SCS configurations presented in (Home Performance Coalition, 2012). The most suitable type and operating mode of auxiliary heaters are difficult to determine. Based on the previous research studies as well as manufacturers configurations, an external water heater using a thermal storage tanks as a buffer seems to be preferred to an internal one (i.e., integrated within thermal storage tanks), based on the previous research studies as well as manufacturers configurations.

Solar combisystem designs have been analyzed over the past 20 years, but only a few studies focused on the impact of their possible configurations. Thus, most research studies focused on sizing a preselected solar combisystem configuration. Information collected from the literature review and manufacturers unveiled that many choices are available to select a solar combisystem configuration. However, to the best knowledge of the author, no studies have focused on the way of selecting a solar combisystem configuration. The emphasis was put on thermal storage tanks due to their key role in solar thermal combisystems; however, the use of stratifying devices or external heat exchangers also varies from one study to another.

The literature review showed that most of the solar thermal combisystem studies were simulation-based. TRNSYS was found to be the most widely used BPS software for solar combisystems. One of the main reasons of such a success around the world is its capability to solve complex problems by coupling subroutines that model subsystem components (Beckman et al., 1994). As a result, TRNSYS is selected in this thesis for evaluating the overall performance of solar thermal combisystems. BPS models reply on mathematical models, which must be validated by comparing with experimental data before drawing any conclusion. However, no model validation procedures were conducted in the previous experimental-based research studies. No uncertainty analyses were conducted. This literature review revealed a lack of methodology for studying solar combisystems

from data collection to simulation.

On the optimization side, no multi-objective optimizations of solar combisystems have been conducted to provide a set of Pareto solutions. The previous optimization research studies were performed using single-objective optimization algorithms. Many multi-objective optimization algorithms have however been developed in the specialized literature. Nevertheless, little emphasis was put on MOO algorithms using a small population size, referred to as micro-MOO algorithms. Such optimization algorithms are however of special interest in engineering where evaluating objective functions with an external program (such as TRNSYS) can be time-consuming.

In conclusion, this literature review unveiled research areas for improvement, either in solar combisystem or in optimization fields. Solar combisystems have been analyzed over the past 20 years, but only a few studies focused on their configurations. In the past, designing a solar combisystem was done by preselected a combisystem configuration, and then sizing its main components. No guideline is available to select the configuration of solar combisystems. Optimization methods were applied to enhance the performance of solar thermal combisystems; however, each objective was studied separately without taking into consideration that they are conflicting. Even though optimization methods become more and more popular, no multi-objective optimization frameworks have been proposed and used for solar thermal combisystems. As a result, the next section presents the main objectives of this thesis to overcome some of the aforementioned problems.

2.4 Objectives of this thesis

Designing a solar combisystem requires selecting a configuration, and then sizing all its components; however, previous research studies focused mainly on sizing solar combisystems. Attention has not been paid on the impact of configurations on the overall performance of solar thermal combisystems.

This literature review also revealed that few studies used optimization to enhance the whole performance of solar thermal combisystems. No multi-objective optimizations has been conducted to provide a set of optimized solar combisystem designs. Solar thermal combisystems were treated as single-objective optimization problems instead of multi-objective optimization ones.

Although different multi-objective optimization methods were developed, little emphasis has been placed on micro multi-objective optimization algorithms, which can be useful in building

engineering when evaluating objective functions is time-consuming.

Finally, no multi-objective optimization framework has been developed to solve problems where objective functions are evaluated by an external software. Consequently, the main research objectives of this thesis are to:

1. Develop a multi-objective optimization framework for optimizing solar combisystems;
2. Improve a micro multi-objective optimization algorithm to solve problems involving time-consuming objective function evaluations;
3. Apply the developments of items 1 to 2 to optimize the configuration and sizing of solar combisystems of two case studies;
4. Develop a methodology for optimizing solar combisystems: from data collection to optimization (through Case study no. 2).

Chapter 3

Preliminary study: comparison of multi-objective optimization methods[1]

The main advantages of non-classical optimization methods over classical ones are illustrated in this chapter with the equipment sizing of a residential solar thermal combisystem, which is treated as a two-objective optimization problem. The optimization problem is first defined, followed by an optimization with the classical and non-classical optimization method. A hybrid of the non-classical method is then introduced, which highlights a need of a multi-objective optimization framework, using an efficient micro multi-objective optimization algorithm, for optimizing solar combisystems.

3.1 Solar combisystem optimization problem

This preliminary study aims at reducing the life cycle cost (LCC) and life cycle energy (LCE) of a residential solar combisystem, whose model was developed in (Leckner, 2008) using the TRNSYS environment. Each of these objective functions was optimized, one at a time, in (Ng Cheng Hin & Zmeureanu, 2014) using a hybrid PSO/HJ algorithm. This previous research study approached the optimization of the residential solar combisystem as a single-objective problem, which led to only one solution per objective.

Multi-objective optimizations offer the advantage, over single-objective ones, of providing information to decision makers for better compromised decisions. Solar combisystems should therefore be approached as MOO problems where both the selection of a configuration and its sizing are

[1] This chapter is mainly based on the paper "Rey, A., & Zmeureanu, R. (2016). Multi-objective optimization of a residential solar thermal combisystem. *Solar Energy*, 139, 622-632. doi: `https://doi.org/10.1016/j.solener.2016.10.008`"

considered. For the sake of simplicity, the configuration of the residential solar combisystem is not taken into account in this preliminary study.

Figure 3.1 shows the scheme of the solar thermal combisystem used in this preliminary study. This residential solar combisystem, developed in (Leckner, 2008), will serve as an initial design solution in Chapter 8, where the multi-objective optimization framework proposed in this thesis is used for the selection of a configuration and its equipment sizing. More information about the residential solar combisystem is provided in Section 8.1, which enables emphasis to be placed on multi-objective optimization methods in this chapter.

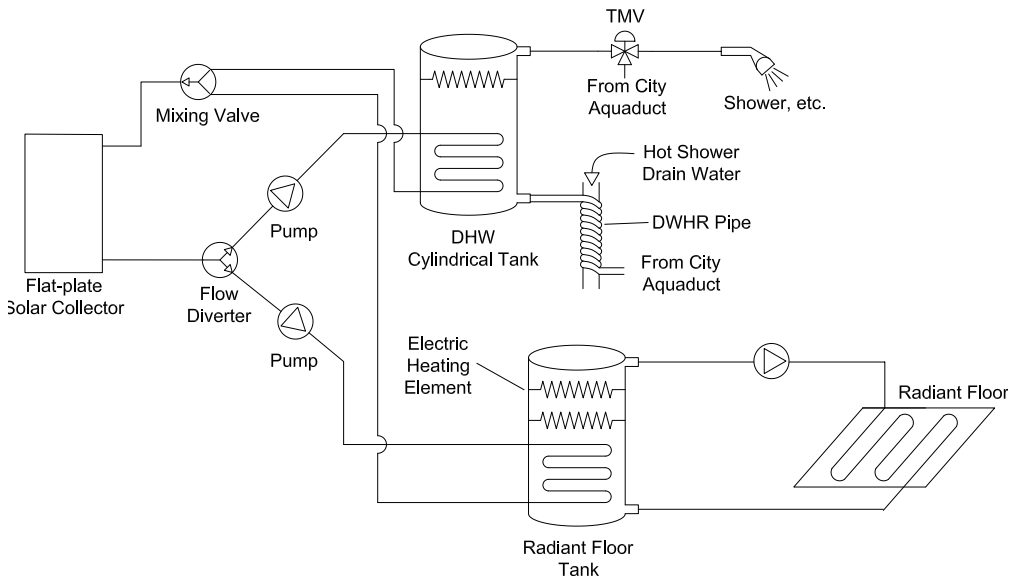

Figure 3.1: Scheme of the solar combisystem modeled in (Leckner, 2008)

Both the LCC and LCE objective functions are taken from (Ng Cheng Hin & Zmeureanu, 2014). The LCC objective function, expressed in present-value dollars, comprises three components: (i) the initial cost of all components, (ii) their replacement cost, and (iii) the operating cost during the entire life cycle, which is set to 40 years. The LCE objective function takes into account: (i) the embodied energy of different parts of the solar thermal combisystem, and (ii) the amount of electricity used for operation during the entire life cycle.

Each of these two objective functions depends on decision variables. Table 3.1 reports the eight decision variables of the residential solar combisystem selected for the optimization, along with their acceptable range of variation, which are taken from (Ng Cheng Hin & Zmeureanu, 2014).

Table 3.1: List of the main TRNSYS types used for the generic solar combisystem model

Decision variable	Acceptable range
Number of collectors [-]	1-22
Solar collector slop [degree]	0-90
Heat-transfer fluid mass flow rate per collector area [kg/(h·m$^2_{\text{coll}}$)]	10-115
DHW tank volume [L]	100-1,000
Radiant floor tank volume [L]	300-30,000
DHW heater auxiliary power [kW]	0.5-5
Radiant floor tank heater auxiliary power at high location [kW]	0.5-10
Radiant floor tank heater auxiliary power at low location [kW]	0.5-15

A penalty function is added to each objective function if the total number of hours under the heating set point, calculated for each thermal zone of the house, is greater than a maximum limit of 550 hours. Such an penalty function ensures acceptable comfortable indoor air temperature. More information about the optimization problem can be found in (Rey & Zmeureanu, 2016).

MOO problems can be optimized using classical or non-classical optimization methods. So far, the former has been preferred over the latter despite some disadvantages mentioned in Section 2.2.2. Benefits of using non-classical optimization methods for optimizing solar combisystems are shown here by comparing: (i) the weighted sum method (WSM) using a hybrid PSO/HJ algorithm, and (ii) the multi-objective optimization particle swarm optimization (MOPSO) algorithm.

3.2 Weighted sum method using a PSO/HJ algorithm

The two-objective optimization problem presented in Section 3.1 is first approached with the weighted sum method, whose general formulation is given in Equation 2.4. The weighted sum method (WSM) is one of the most widely used classical optimization methods, which turns the two-objective optimization problem into a single-objective one by using weights associated with each objective function. Each objective function is normalized so that all objectives have the same impact on the optimization. The normalized global objective function z is therefore expressed as follows:

$$z(x) = w_1 \cdot \frac{\text{LCC}(x) - \text{LCC}^{\text{U}}}{\text{LCC}^{\text{N}} - \text{LCC}^{\text{U}}} + w_2 \cdot \frac{\text{LCE}(x) - \text{LCE}^{\text{U}}}{\text{LCE}^{\text{N}} - \text{LCE}^{\text{U}}} \tag{3.1}$$

where x is the decision vector (composed of decision variables); w_1 and w_2, with $w_2 = 1 - w_1$, are the weights given by decision makers; LCC^{U} and LCC^{N} are the Utopia and Nadir points of the

LCC objective function [k$], respectively; LCE^U and LCE^N are the Utopia and Nadir points of the LCE objective function [MWh], respectively.

The Utopia and Nadir points correspond to the lower and upper bounds of the true Pareto front, in the case of minimization problems. Since the true Pareto front cannot be known without testing all the possible decision vectors, both the Utopia and Nadir points can be approximated only.

As mentioned in Section 2.2.2, one optimization run leads to only one Pareto solution. The weights w_1 and w_2 are varied from 0 to 1, with a step of 0.1, so several final values of z are obtained in order to approximate the true Pareto front. The weighted sum method requires an optimization algorithm. The hybrid PSO/HJ algorithm, available in GenOpt (Wetter, 2011), is used to solve this two-objective optimization problem. PSO/HJ already proved to be effective in several building engineering studies (Hasan et al., 2008; Ng Cheng Hin & Zmeureanu, 2014; Wetter & Wright, 2004) and offers a good trade-off between computing time and accuracy.

PSO is a population-based stochastic optimization algorithm from the swarm intelligence family whose update pattern is given in Equations 2.6 and 2.7. The Hooke and Jeeves algorithm (Hooke & Jeeves, 1961) is a deterministic algorithm that operates by changing iteratively the value of one variable at a time, examining the objective function value calculated at each iteration, and comparing that value to the minimum objective function value obtained so far; this is the exploratory move. When no decrease of the objective function is obtained, then the step size of each decision variable is reduced, and the process is repeated; this is the pattern move.

As shown in figure 3.2, HJ starts with the optimum solution found by PSO in order to enhance the local exploitation of the hybrid PSO/HJ algorithm. The spikes of the LCC objective function, after the PSO ending, during the HJ portion of the optimization, are due to the penalty function. When the algorithm searches for decreasing the LCC and LCE objective functions, the values of the decision variables are modified; some design solutions cannot satisfy space heating demand, which triggered the penalty function to avoid such design solutions.

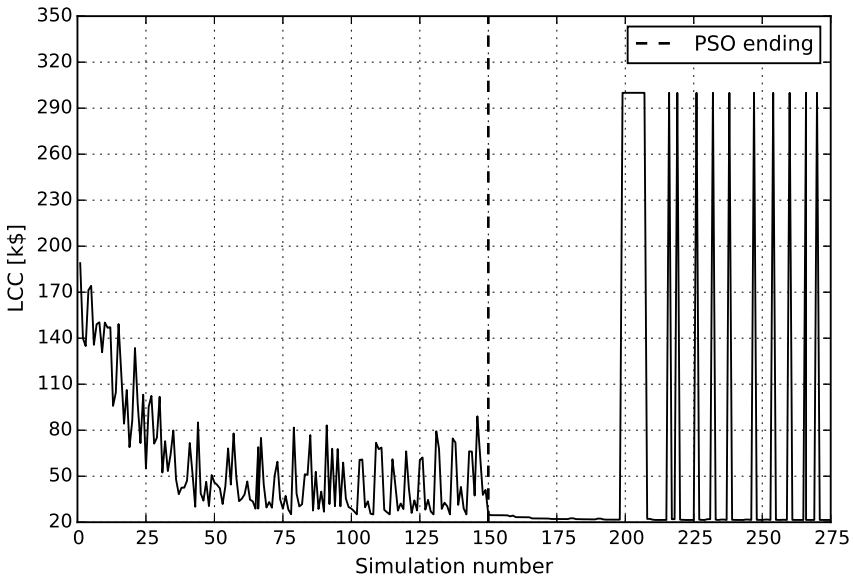

Figure 3.2: Evolution of the LCC value during the optimization using PSO/HJ

A population of six particles for PSO is selected since a computer with six cores is used for the optimization. Six TRNSYS simulations can therefore be launched in parallel, one for each particle. The number of particles should be a multiple of the number of cores, if not the computer performance is not fully utilized. For instance, let $N_{\text{particles}}$ and N_{cores} denote the number of particles and number of cores, respectively. The number of series per generation (i.e., the number of series to complete one generation), abbreviated N_{series}, is defined as:

$$N_{\text{series}} = \left\lceil \frac{N_{\text{particles}}}{N_{\text{cores}}} \right\rceil \tag{3.2}$$

where $\lceil x \rceil$ is the ceiling function, which returns the smallest integer greater than or equal to x.

For example, let Case no. 1 have a population size of six particles and Case no. 2 have a population of seven. All the simulations for each generation in the first case are completed in one single series. However, in the second case, two series of simulations are needed for each generation; the first series will run at full capacity of cores (i.e., with six particles), while the second series will run for only one particle. As a result, the computing time for each generation in Case no. 2 is twice as much as that in Case no. 1.

Before performing a multi-objective optimization of the residential solar combisystem with the WSM using PSO/HJ, the Nadir and Utopia values of each objective function have to be determined to compute z, as shown in Equation 3.1. The minimum value of LCC is obtained

when $w_1 = 1$ ($w_2 = 0$), and the minimum value of LCE is obtained when $w_1 = 0$ ($w_2 = 1$). A pre-optimization run is performed for each case (i.e., $w_1 = 1$ and $w_1 = 0$) to estimate the Nadir and Utopia values, which are listed in Table 3.2.

Table 3.2: Nadir and Utopia points of the LCC and LCE objective functions

	Nadir point	Utopia point
Life Cycle Cost [k$]	200	20
Life Cycle Energy [MWh]	375	120

For each combination of w_1 and w_2 (e.g., $w_1 = 0.2$ and $w_2 = 0.8$), PSO uses six particles during 25 generations, and for each particle one TRNSYS simulation is needed; hence, 150 TRNSYS simulations are performed to obtain the solution for each combination of w_1 and w_2. The HJ portion stops when no improvement of the global objective function can be achieved, so the number of TRNSYS simulations performed by the HJ algorithm varies from one optimization run to another. As reported in Table 3.3, the total number of TRNSYS simulations to approximate the Pareto front is 3,704.

Table 3.3: Results of the 11 optimization runs performed with the WSM using PSO/HJ

w_1	w_2	Number of TRNSYS simulations performed			LCC final value [k$]		LCE final value [MWh]	
		PSO	HJ	Total	After PSO	After HJ	After PSO	After HJ
0 1	1	150	155	305	24	21	316	307
0.1	0.9	150	113	263	25	23	259	228
0.2	**0.8**	**150**	**135**	**285**	**36**	**32**	**170**	**159**
0.3	0.7	150	144	294	33	32	172	158
0.4	0.6	150	131	281	53	37	149	130
0.5	0.5	150	109	259	39	38	174	127
0.6	0.4	150	263	413	80	37	171	132
0.7	0.3	150	230	380	121	41	157	123
0.8	0.2	150	240	390	112	45	179	127
0.9	0.1	150	267	417	117	41	172	123
1	0	150	267	417	117	41	172	123
Number of simulations		1,650	2,054	3,704	-	-	-	-

The average computing time for one optimization run is around 86 hours using 6-core Intel Xeon @ 2.40 GHz. More than 946 hours, or 39 days, were therefore necessary to approximate the true Pareto front. For instance, for the case of $w_1 = 0.2$ and $w_2 = 0.8$ (in bold), 150 TRNSYS

simulations are required for the PSO portion and 135 simulations for the HJ portion, for a total of 285 simulations. At the end of PSO portion, the LCC and LCE objective functions are equal to 36 k$ and 170 MWh, respectively, which change further to 32 k$ and 159 MWh at the end of HJ portion.

Although the WSM provides an approximation of the true Pareto front, as shown in Figure 3.3, this preliminary study shows that this method can be time consuming. If more non-dominated solutions are desired, the number of simulations would further increase. Less time-consuming multi-objective optimization algorithms are needed for such MOO problems.

3.3 Multi-objective particle swarm optimization algorithm

MOPSO needs only one optimization run to approximate the true Pareto front. Six particles and 150 generations are selected, which results in 900 TRNSYS simulations that lasted for 85 hours, or 3.5 days, compared with 3,704 TRNSYS simulations required by the WSM using PSO/HJ. Figure 3.3 presents the 18 non-dominated solutions found by MOPSO compared with the 11 non-dominated solutions found by the WSM. Most of the MOPSO solutions are dominated by those found by the WSM. This can be explained by a weak local search of MOPSO, while the WSM using PSO/HJ benefits from the local search of the HJ portion.

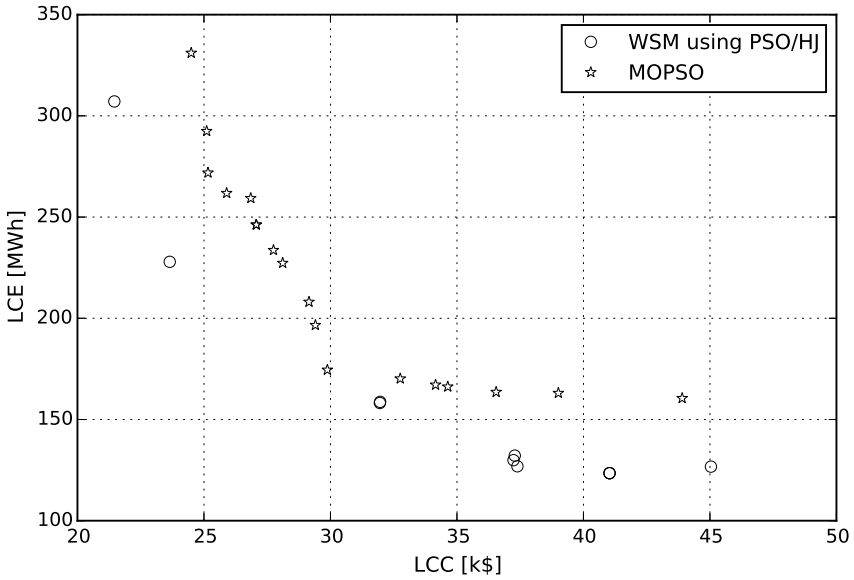

Figure 3.3: LCE vs. LCC from the WSM using PSO/HJ and MOPSO

As depicted in Figure 3.4, MOPSO converged quickly towards its final Pareto front (around the 75-th generation), then faced difficulties in finding new non-dominated solutions.

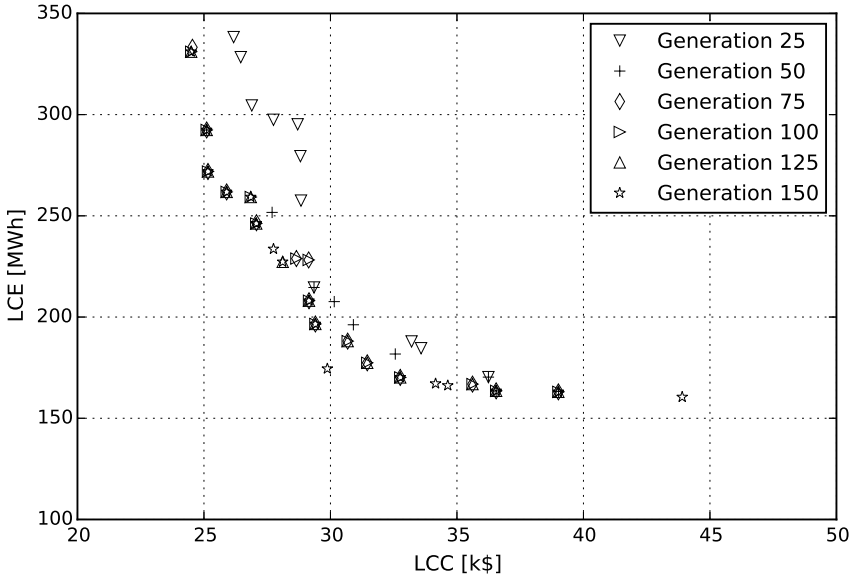

Figure 3.4: Evolution of the approximated true Pareto front with MOPSO

MOPSO outperforms the WSM using PSO/HJ in terms of computing time, but faces difficulties in approximating the true Pareto front. The weak local search of MOPSO can be overcome by using a hybrid MOPSO/HJ.

3.4 Hybrid MOPSO/HJ algorithm

Unlike population-based algorithms, HJ uses only one candidate solution at a time to evaluate one objective function. As a result, MOPSO/HJ requires several optimization runs of the HJ algorithm, each one being initialized by a different solution found by MOPSO. As mentioned in Section 2.2.2, MOPSO's repository is divided into hypercubes having a fitness value, inversely proportional to the number of particles that are within each hypercube. Diversity is then ensured using the roulette-wheel selection based on the calculated fitness values. This roulette-wheel selection is used for the selection of each non-dominated solution that will serve as an initial solution for the HJ portion of the hybrid MOPSO/HJ algorithm. Since HJ is a deterministic algorithm, the initialization of two HJ optimization runs with the same non-dominated solution from MOPSO's repository will lead to the same final non-dominated solution. Each selected non-dominated solution is therefore

temporarily removed from MOPSO's repository to avoid duplicate optimization search. Six HJ runs are launched in parallel using the six central processing units of the computer being used in order to speed up the optimization search.

As shown in figure 3.5, the hybridization of MOPSO with HJ improves the local search of the MOPSO algorithm. However, such an improvement comes with a higher computing time of 149 hours, compared with 85 hours for MOPSO. Both methods, the WSM using PSO/HJ and MOPSO/HJ, give close approximations of the Pareto front; however, MOPSO/HJ is more than six times faster than the WSM using PSO/HJ. In total, MOPSO/HJ performed 1,438 TRNSYS optimizations whereas the WSM required 3,704 to approximate their respective Pareto front. As a result, the WSM was found efficient, but time-consuming. As an alternative, MOPSO was faster, but was not able to approximate properly the true Pareto front. The hybrid MOPSO/HJ is a trade-off between the WSM and MOPSO. MOPSO/HJ was slower than MOPSO, but better at approximating the true Pareto front.

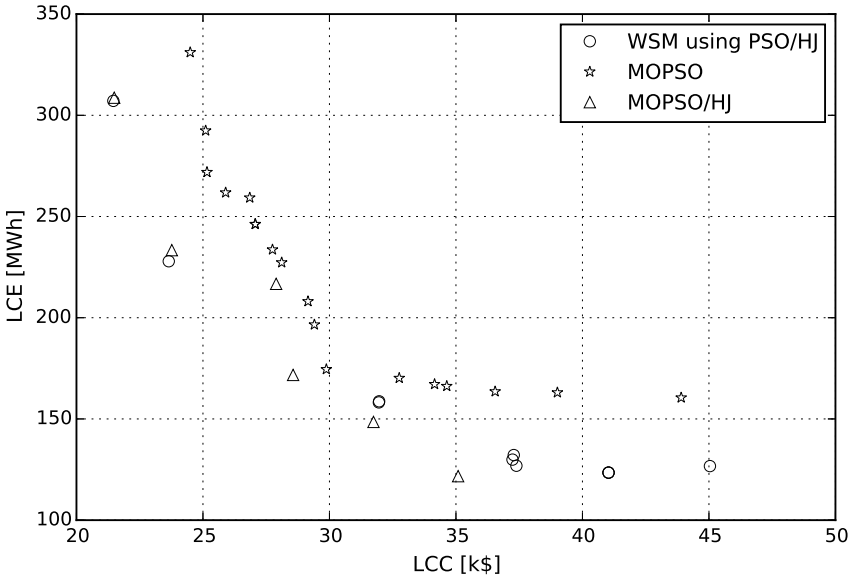

Figure 3.5: LCE vs. LCC from the WSM using PSO/HJ and MOPSO/HJ

This preliminary study shows that classical optimization methods, represented by the WSM, are not well-suited for multi-objective optimizations of solar thermal combisystems. Such MOO problems, where evaluating objective functions is time-consuming, should be optimized with non-classical methods. Non-classical methods, such as MOPSO and MOPSO/HJ, are less time-consuming

and do not require any previous knowledge about the selected objective functions. Although MOPSO/HJ has a better local search than MOPSO, an hybridization of MOPSO with HJ is not the most efficient way of optimizing MOO problems. A micro-MOO algorithm, which uses a small population of particles, will be an asset in the proposed multi-objective optimization framework.

Chapter 4

Method and applications

This chapter introduces the research method in order to provide a broad perspective of the development of this doctoral thesis. Searching for the optimum feasible solar combisystem designs requires: (i) a generic solar combisystem model, (ii) a multi-objective optimization framework, and (iii) a multi-objective optimization algorithm. Although each part is developed separately, they form together a coherent package. Afterwards, this package is applied to two different residential solar thermal combisystems located in Montreal, Quebec, Canada, and in Massachusetts, USA.

4.1 Generic solar combisystem model

A generic solar combisystem model is created to take into consideration different solar combisystem configurations. The TRNSYS environment is selected due to its capability to simulate complex thermal energy systems by coupling subroutines that model subsystem components. In addition, TRNSYS is found to be one of the most used BPS software from the literature review. Solar combisystem configurations are modeled one at a time within the same TRNSYS file to create a generic solar combisystem model at the end. The connection between each solar combisystem configuration is accomplished through TRNSYS equation blocks, which enable users to define their own mathematical equations. The selection of one configuration over another is achieved with Boolean variables inside these equation blocks. The value of these Boolean variables (for selecting equipment or technologies) as well as that of design variables (for sizing equipment) can then be selected by a multi-objective optimization algorithm to find the optimum feasible solar combisystem designs in terms of cost, energy use, and exergy destroyed.

4.2 Multi-objective optimization framework

A multi-objective optimization framework is developed to find the optimum feasible solar combisystem designs in terms of cost, energy use, and exergy destroyed. The life cycle analysis is found to be the most efficient way of comparing solutions, that is, solar combisystem designs. Three types of decision variables are used: (i) Boolean, (ii) discrete, and (iii) continuous. Discrete and continuous variables are design variables used for equipment sizing. Optimization constraints are added to ensure meaningfulness. The life cycle cost (LCC), life cycle energy use (LCE), and life cycle exergy destroyed (LCX) using the technical and physical boundary are the four objective functions used to compare solar combisystem designs. Two penalty functions are added to each objective function to ensure acceptable comfortable indoor air temperature.

4.3 Multi-objective optimization algorithm

Once the generic solar combisystem model and multi-objective optimization framework are developed, a multi-objective optimization algorithm is required to find the optimum feasible solar combisystem designs. As mentioned in the literature review, classical methods turn multi-objective optimization problems into single objective ones while non-classical methods can directly handle them. Non-classical methods are therefore more suitable for multi-objective optimization problems, as illustrated in Chapter 3. Based on the literature review, MOPSO was found to be a good compromise between effectiveness and simplicity. Like most of the non-classical methods, MOPSO has a large population size and requires a large number of objective function evaluations. However, building performance simulations can be time-consuming, which leads to high computational time in the search of optimum solutions. Algorithms with a small population size, known as micro-MOO algorithms, are therefore needed. The micro-MOPSO algorithm is improved in this doctoral thesis to overcome issues that have been mentioned but not solved. This new version, called micro-TVMOPSO, is compared to eight MOO algorithms on 24 benchmark problems to test its performance. The generic solar combisystem model, multi-objective optimization framework, and micro-TVMOPSO form together a package used to find optimum feasible solar combisystem designs for two case studies.

4.4 Applications to case studies

The multi-objective optimization package developed is then applied to two different residential solar thermal combisystems: one located in Montreal, Quebec, Canada, and the other in Massachusetts, USA. Each solar combisystem gives an initial design solution for the multi-objective optimization framework. The first case study is a simulation-based residential solar thermal combisystem initially modeled in (Leckner, 2008) using TNRSYS. The second case study is an actual solar thermal combisystem installed in Massachusetts, USA. Access to data collection for this experimental solar combisystem is the result of a collaboration with one of the leading international manufacturers of solar water heating technologies. Since no research studies have been published on model validation or uncertainty analysis of existing solar thermal combisystems, a methodology for validating solar thermal combisystem is proposed in Case study no. 2.

Chapter 5

Generic model for solar combisystems

A generic model for solar thermal combisystems is proposed in this chapter to take into consideration different configurations.

5.1 Description of the generic model

This section presents the different solar combisystem configurations covered in this doctoral thesis. Solar thermal combisystems can be divided into three sub-systems: (i) energy generation, (ii) energy storage, and (iii) energy distribution.

5.1.1 Energy generation

Solar thermal combisystems usually harvest solar energy through solar thermal collectors and transferred it as heat to be stored in one or several thermal storage tanks. Harvesting can be done by flat-plate collectors (FPCs) or evacuated tube collectors (ETCs), and therefore both are part of the generic solar combisystem model. Solar thermal collectors can be roof or wall-mounted. In some cases, solar combisystems can have both. Such combinations are taken into account in the generic model by using the tilt angle of solar collectors as a decision variable. Solar combisystems usually require additional energy to meet domestic hot water (DHW) and space heating (SH) needs. Electricity or natural gas are used as additional energy sources. Two cases are considered: (i) electrical resistances within one or several thermal storage tanks, and (ii) external water heaters. External water heaters can use electricity or natural gas to ensure that the DHW and SH supply temperatures are not below fixed set-point values.

5.1.2 Energy storage

Storage generation can be achieved through one or several thermal storage tanks. Although the use of one thermal storage is common practice, solar combisystems equipped with two thermal storage tanks were found in (Leckner & Zmeureanu, 2011; Ng Cheng Hin & Zmeureanu, 2014; Suter et al., 2000) as well as in manufacturers layout drawings (S. Royce, personal communication, March 2014; E. Wilson, personal communication, April 2014). Since domestic hot water and space heating needs are different in terms of supply temperature, the use of one thermal storage tank to DHW and another one to SH can allow a better thermal stratification within each tank. One and two thermal storage tanks (i.e., one dedicated to DHW and the other to SH) are taken into consideration in the generic solar combisystem model. More than two thermal storage tanks could be used, but such a configuration is not included herein.

Direct solar combisystems (i.e., the water within the thermal storage tank used as a heat-transfer fluid) are rather the exception than the rule, due to freezing temperatures in winter in cold climates. Heat is thus transferred to one or two thermal storage tanks through heat exchangers using an antifreeze heat-transfer fluid. Heat exchangers can be either internal or external. While the former is prevalent, the latter is used to increase thermal stratification within thermal storage tanks (Glembin & Rockendorf, 2012; Hugo et al., 2010; Pichler et al., 2014; Suter et al., 2000). Thermal stratification can also be enhanced using stratifying devices, also known as stratifiers, so they are included in the generic solar combisystem model. When a solar combisystem configuration has two thermal storage tanks, both will have on the solar collector loop either an internal heat exchanger or an external one along with stratifiers.

5.1.3 Energy distribution

When only one thermal storage tank is selected, an immersed heat exchanger is usually used for SH needs while the hot water within the tank is used for DHW preparation. When two thermal storage tanks are selected, one is dedicated to DHW and the other to SH. No internal heat exchanger is therefore required since the hot water within each tank is directly used. Instead of increasing the thermal storage tank size to reduce overheating, the thermal capacity of radiant floors could be used to store energy as heat. The concrete floor slab thickness is therefore set as a decision variable

in the optimization process. Solar energy harvested could be directly sent to the radiant floor for SH needs, but such a configuration is not included herein.

5.2 Modeling of the generic solar combisystem

This section provides a description of the numerical modeling of the generic solar combisystem. TRNSYS was selected due to its capability to solve complex problems by coupling subroutines that model subsystem components (Beckman et al., 1994) and the fact that it has been used in numerous studies for more than 30 years (Cao et al., 2014; Jordan & Vajen, 2000; Lin et al., 1997; Raffenel et al., 2009; Shariah & Shalabi, 1997). TRNSYS components, also referred to as types, are subroutines able to simulate physical phenomena as well as thermal energy systems. Each type requires one or several inputs and parameters to be able to supply one or several outputs. The main components used in the generic solar combisystem model are presented herein.

5.2.1 Solar combisystem configurations

The generic solar combisystem model takes into consideration the different configurations presented in Section 5.1, which requires the use of decision variables representing logical decisions (e.g., whether an equipment is selected or not). Such decision variables are Boolean variables that allows making choices. More details about these decision variables are given in Section 6.2, since they are part of the multi-objective optimization framework.

Choices can be made in the TRNSYS environment using an equation block. TRNSYS equation blocks allow users to define their own mathematical equations, which can be functions of outputs of TRNSYS types or constant numerical values. For instance, Type 1b (flat-plate collector) and Type 71 (evacuated-tube collector) are both used in TRNSYS. Both are connected with Type 15-2b (weather data) and have the same inlet temperature; however, the final outlet temperature of the array of solar thermal collectors depends on the selection between flat-plate or evacuated tube collectors, which can be illustrated as follows:

$$T_{\text{out,coll}} = B_1^1 \cdot T_{\text{out,FPC}} + B_1^2 \cdot T_{\text{out,ETC}} \tag{5.1}$$

where $T_{\text{out,coll}}$ is the temperature of the heat-transfer fluid leaving the array of solar thermal collectors [°C]; B_1^1 and B_1^2 are Boolean variables (equal to 0 or 1) associated with the flat-plate or

evacuated tube collectors [-], respectively; $T_{\text{out,FPC}}$ and $T_{\text{out,ETC}}$ are the temperatures of the heat-transfer fluid leaving the arrays of flat-plate and evacuated tube collectors [°C], respectively. When $B_1^1 = 1$ (and $B_1^2 = 0$), only the outlet temperature from Type 1b, which corresponds to an array of flat-plate collectors, is operational.

5.2.2 Component models

The generic model is composed of different TRNSYS components interconnected in a logical way to represent different solar thermal combisystem configurations. The key components of this generic model are presented in this section to better understand how they work.

Solar thermal collectors (Types 1b and 71)

Solar thermal collectors can be divided into two categories (Kalogirou, 2004b): (i) non-concentrating, and (ii) concentrating solar collectors. The former has the same area for intercepting and for absorbing solar radiation, whereas the latter uses reflective surfaces (e.g., mirrors or lenses) to concentrate solar radiation onto the absorber area. The concentrating systems reach therefore higher temperatures, which implies a lower efficiency. The higher the difference between the ambient and working fluid temperatures is, the lower the solar collector efficiency becomes. In view of the Canadian weather conditions, concentrating systems are not suitable. Accordingly, they are not taken into consideration in this doctoral thesis. The non-concentrating solar collectors can be classed into two categories:

1. Flat-plate collectors;
2. Evacuated tube collectors.

Evacuated tube collectors are more energetically efficient than flat-plate collectors; however, they were not cost-effective enough to be worth using some years ago. Both types are studied herein to know whether or not evacuated tube collectors are more suitable today.

Flat-plate collectors (Type 1b)

Type 1b uses the Cooper and Dunkle assumption applied to the Hottel-Whillier equation to estimate the thermal efficiency of a flat-plate solar collector as (Duffie & Beckman, 2006):

$$\eta_{\text{coll}} = a_0 - a_1 \cdot \frac{\Delta T}{G_{\text{tot,coll}}} - a_2 \cdot \frac{\Delta T^2}{G_{\text{tot,coll}}} \tag{5.2}$$

in which

$$\Delta T = T_{\text{in,coll}} - T_{\text{amb}}$$

where η_{coll} is the flat-plate solar collector thermal efficiency [-]; a_0 is the optical efficiency [-]; a_1 is the first order heat loss coefficient [W/(m^2·°C)]; a_2 is the second order heat loss coefficient [W/(m^2·°C^2)]; $G_{\text{tot,coll}}$ is the total solar irradiance incident on the solar collector [W/m^2]; $T_{\text{in,coll}}$ and T_{amb} are the inlet flat-plate collector and ambient temperatures [°C], respectively.

The general definition of the thermal efficiency of flat-plate collectors is expressed as follows (Duffie & Beckman, 2006):

$$\eta_{\text{coll}} = 100 \cdot \frac{\dot{Q}_{\text{harvested,coll}}}{\dot{Q}_{\text{received,coll}}} = 100 \cdot \frac{\dot{m}_{\text{coll}} \cdot c_{\text{p,coll}} \cdot (T_{\text{out,coll}} - T_{\text{in,coll}})}{A_{\text{coll}} \cdot G_{\text{tot,coll}}} \tag{5.3}$$

where $\dot{Q}_{\text{harvested,coll}}$ is the rate of heat harvested by the solar collector [W]; $\dot{Q}_{\text{received,coll}}$ is the rate of solar energy received by the solar collector [W]; $\dot{m}_{\text{coll}}$ is the heat-transfer fluid mass flow rate [kg/s]; $c_{\text{p,coll}}$ is the specific heat capacity at constant pressure of the heat-transfer fluid [J/(kg·°C)]; $T_{\text{out,coll}}$ is the outlet solar collector temperature [°C]; A_{coll} is the solar collector area [m^2].

The thermal efficiency of flat-plate solar collectors can therefore be determined from Equation 5.2, which can then be used in Equation 5.3 to estimate the rate of harvested solar energy and outlet flat-plate collector temperature. Different corrections are also applied to account for operation at flow rates other than the value at test conditions, identical collectors mounted in series, and non-normal solar incidence by using an incidence angle modifier (IAM).

Evacuated tube collectors (Type 71)

Type 71 uses the same subroutine as the one used in the TRNSYS Type 71 (i.e., for flat-plate collectors), but the user-defined parameters a_0, a_1, and a_2 are different since heat loss by convection are reduced in ETCs. Type 71 also requires biaxial IAM data from an external file.

External heat exchanger (Type 5e)

Type 5e models external steady-state cross-flow heat exchangers with unmixed fluids, where their overall heat transfer coefficient is given as an input. The overall heat transfer coefficient of such heat exchangers can be estimated using the correlation used in (Heimrath & Haller, 2007; Hugo et al., 2010):

$$U_{\mathrm{HX}} = 3.6 \cdot (88.561 \cdot A_{\mathrm{tot,coll}} + 328.19) \tag{5.4}$$

where U_{HX} is the overall heat transfer coefficient of the heat exchanger [W/°C]; $A_{\mathrm{tot,coll}}$ is the total area of the solar collector array [m^2].

Thermal storage tanks (Type 534)

Some TRNSYS subroutines (i.e., components) have been developed by Thermal Energy Systems Specialists (TESS), which is an engineering consulting company (TESS, 2014). The TESS Type 534 models a vertically cylindrical thermal storage tank with immersed heat exchangers. This component can also represent a storage tank with no heat exchanger if desired. Either with or without heat exchangers, Type 534 is a multi-node approach; it means that the storage tank is divided into constant volume sections, called nodes.

Each node is assumed to be fully mixed and at a uniform temperature. Thus, the temperature of a node can be predicted by performing an energy balance on each storage section, accounting for thermal losses to the surroundings and energy flows between adjacent nodes as shown in Figure 5.1. The energy balance of any node i (where auxiliary electric and gas heaters are not taken into account) is expressed as:

$$\begin{aligned} m_{\mathrm{fluid},i} \cdot c_{\mathrm{p,fluid}} \cdot \frac{dT_i}{dt} = {} & \frac{(\lambda + \Delta\lambda) \cdot A_{\mathrm{cross},i}}{\Delta D_{i+1 \to i}} \cdot (T_{i+1} - T_i) + \frac{(\lambda + \Delta\lambda) \cdot A_{\mathrm{cross},i}}{\Delta D_{i-1 \to i}} \cdot (T_{i-1} - T_i) \\ & + U_{\mathrm{tank},i} \cdot (T_{\mathrm{env}} - T_i) + \dot{m}_{\mathrm{down}} \cdot c_{\mathrm{p,fluid}} \cdot T_{i-1} \\ & + \dot{m}_{\mathrm{up}} \cdot c_{\mathrm{p,fluid}} \cdot T_i - \dot{m}_{\mathrm{down}} \cdot c_{\mathrm{p,fluid}} \cdot T_i + \dot{m}_{\mathrm{up}} \cdot c_{\mathrm{p,fluid}} \cdot T_{i+1} \\ & + \dot{m}_{1,\mathrm{in}} \cdot c_{\mathrm{p,fluid}} \cdot T_{1,\mathrm{in}} - \dot{m}_{1,\mathrm{out}} \cdot c_{\mathrm{p,fluid}} \cdot T_{1,\mathrm{out}} \\ & + \dot{m}_{2,\mathrm{in}} \cdot c_{\mathrm{p,fluid}} \cdot T_{2,\mathrm{in}} - \dot{m}_{2,\mathrm{out}} \cdot c_{\mathrm{p,fluid}} \cdot T_{2,\mathrm{out}} \end{aligned} \tag{5.5}$$

where $m_{\mathrm{fluid},i}$ is the mass of the fluid within the i-th node [kg]; $c_{\mathrm{p,fluid}}$ is the specific heat capacity

at constant pressure of the fluid within the i-th node [J/(kg·°C)]; $\Delta D_{i+1\to i}$ and $\Delta D_{i-1\to i}$ are the center-to-center distance between the i-th node and the node below and above it [m], respectively; λ and $\Delta\lambda$ are the fluid thermal conductivity and the de-stratification conductivity [W/(m·°C)], respectively; $A_{\text{cross},i}$ is the cross-sectional area of i-th node [m^2], respectively; $U_{\text{tank},i}$ is the tank heat loss coefficient of i-th node [W/°C]; $\dot{m}_{\text{up}}$ and $\dot{m}_{\text{down}}$ are the fluid mass flow rates up and down the i-th node [kg/s], respectively; $\dot{m}_{1,\text{in}}$, $\dot{m}_{1,\text{out}}$, $\dot{m}_{2,\text{in}}$ and $\dot{m}_{2,\text{out}}$ are the mass flow rates of the entering and exiting fluids 1 and 2 [kg/s], respectively; T_{i+1}, T_i, T_{i-1}, $T_{1,\text{in}}$, $T_{2,\text{in}}$, and T_{env} are the temperatures located below, at and above node i, the temperature of the entering fluid 1 and the entering fluid 2, and the temperature of the environment [°C], respectively;

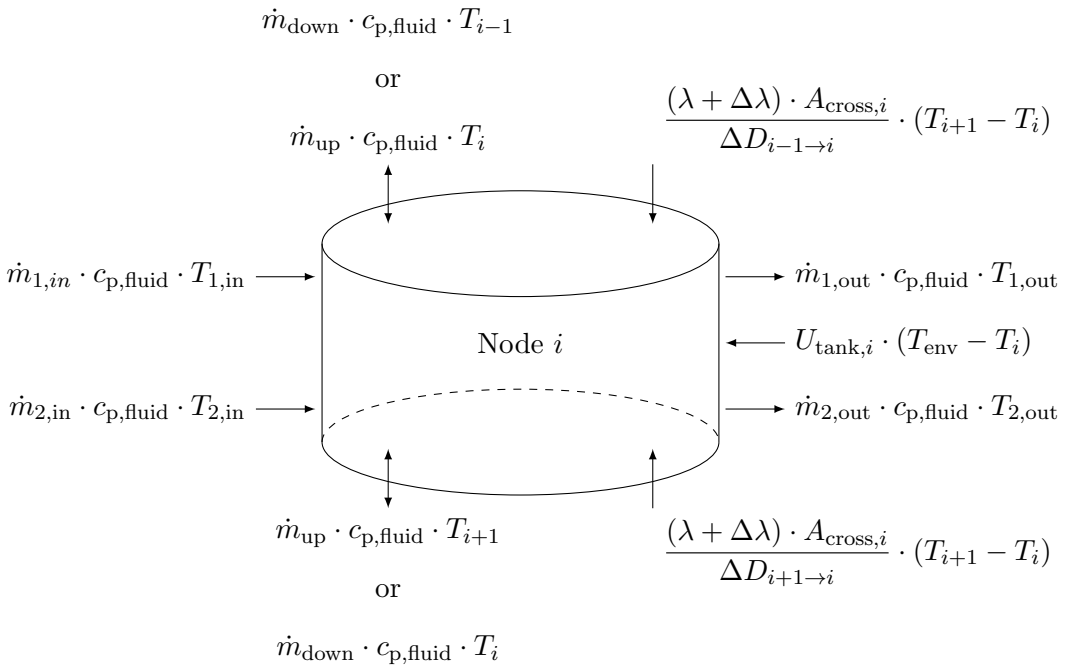

Figure 5.1: Energy flows of the i-th node of Type 534

Type 531 can contain multiple immersed heat exchangers, inlets and outlets, as well as external heating elements. It also has different options, which gives the ability to model stratifying devices. Two options are used: (i) fixed inlet and outlet, and (ii) temperature seeking inlets with fixed outlets. The position of inlets and outlets is user-defined in the former, while the latter automatically directs the entering water into the closest temperature layer to simulate the effect of stratifying devices.

Multi-zone building (Type 56a)

Type 56a simulates a multi-zone building, based on an energy balance model. Each thermal zone uses one air node representing the thermal capacity of the entire air volume of the zone as well as that of other closely connected objects, such as furniture. The net heat gain for the i-th air node is defined as (Klein et al., 2017):

$$\dot{Q}_{\text{net},i} = \dot{Q}_{\text{surface},i} + \dot{Q}_{\text{infiltration},i} + \dot{Q}_{\text{ventilation},i} + \dot{Q}_{\text{g,c},i} + \dot{Q}_{\text{cplg},i} \tag{5.6}$$

where $\dot{Q}_{\text{surface},i}$ is the convective gain from surfaces [W]; $\dot{Q}_{\text{infiltration},i}$ is the infiltration gains [W]; $\dot{Q}_{\text{ventilation}}$ is the ventilation gains [W]; $\dot{Q}_{\text{g,c},i}$ is the internal convective gains [W]; $\dot{Q}_{\text{cplg},i}$ is the internal convective gains due to air flow from adjacent zones [W].

Type 56a allows users to insert *active layer* in any floor to model an embedded-tube radiant heating floor, where the supply water temperature is an input of the multi-zone building model. An active layer contains fluid filled pipes, which are characterized by the pipe spacing, pipe outside diameter, pipe wall thickness, and pipe wall conductivity. TRNSYS uses a thermal resistance network to calculate the heat transfer between the fluid in the tube and the active layer and requires the following criteria to be met (Klein et al., 2017):

$$\frac{D_{\text{above}}}{D_{\text{spacing}}} \geq 0.3 \tag{5.7}$$

$$\frac{\lambda_{\text{below}}}{D_{\text{below}}} < 1.212 \ \ \text{W/(m}^2\cdot^\circ\text{C)} \tag{5.8}$$

where D_{above} and D_{below} are the thickness of the slab above the tubes and that of the layer directly below the slab [m], respectively; D_{spacing} is the tube spacing [m]; λ_{below} is the thermal conductivity of the layer directly below the slab [W/(m·°C)].

The slab thickness above the embedded-tubes is used as a decision variable in Chapter 8 to increase thermal storage. As mentioned in (Brideau et al., 2016), Type 56a cannot simulate thin slab embedded-tube radiant floor. The lower boundary of the decision variable associated with the slab thickness will therefore ensure a minimum slab thickness that prevents simulating a thin slab.

Main types

The main TRNSYS types used to develop the generic solar thermal combisystem model are reported in Table 5.1. More details about each type are provided in (Klein et al., 2017).

Table 5.1: List of the main TRNSYS types used for the generic solar combisystem model

Description	Type
Weather data reading and processing – TMY2	15-2b
Flat-plate collector	1b
Evacuated tube collector	71
Flow diverter	11f
Mixing valve (TESS library)	649
Pumps variable speed (TESS library)	742
Differential controller with hysteresis	2b
3-stage room thermostat with heating set back and temperature deadband	8b
External cross flow heat exchanger	5e
Vertical cylindrical tank (TESS library)	534
Heating and cooling season scheduler (TESS Library)	515
Hourly forcing function scheduler weekdays and weekends (TESS Library)	516
Hourly forcing function scheduler identical days (TESS Library)	517
Basement conduction heat losses (TESS Library)	701a
Multi-zone building	56a
Input value recall	93
Auxiliary heater	659

Chapter 6

Multi-objective optimization framework

This chapter presents the multi-objective optimization framework for optimizing the configuration and sizing of solar thermal combisystems. The proposed framework includes: (i) decision variables, (ii) optimization constraints, and (iii) objective functions.

6.1 Mixed integer nonlinear programming model

The multi-objective optimization framework for solar thermal combisystems aims at being used in optimization searches to find the most suitable design (i.e., configuration and sizing), from a set of equipment, given particular space heating and domestic hot water loads and external conditions. Mixed integer nonlinear programming (MINLP) refers to optimization problems consisting of nonlinear objective functions in which some decision variables are discrete variables, while others are allowed to be continuous. Discrete variables can represent physical variables as well as logical decisions, such as selecting or not an equipment. Such logical decisions are made using Boolean decision variables. Choosing a configuration for a solar thermal combisystem and then sizing its components implies both discrete and continuous variables. A MINLP model for the optimum design of solar thermal combisystems is presented in this section.

6.1.1 Description of the optimization model

An optimization model for solar thermal combisystems is presented in this section using mixed integer nonlinear programming. The proposed approach presented in this doctoral thesis is limited to a set of feasible solar combisystem configurations, which were discussed in Section 5.1. This optimization model could be also expanded to many other solar or non-solar systems. The generic

optimization configuration can be illustrated by nodes representing equipment or technologies for energy generation, storage, and distribution, as well as by arcs symbolizing mass and energy flows between them, as shown in Figure 6.1.

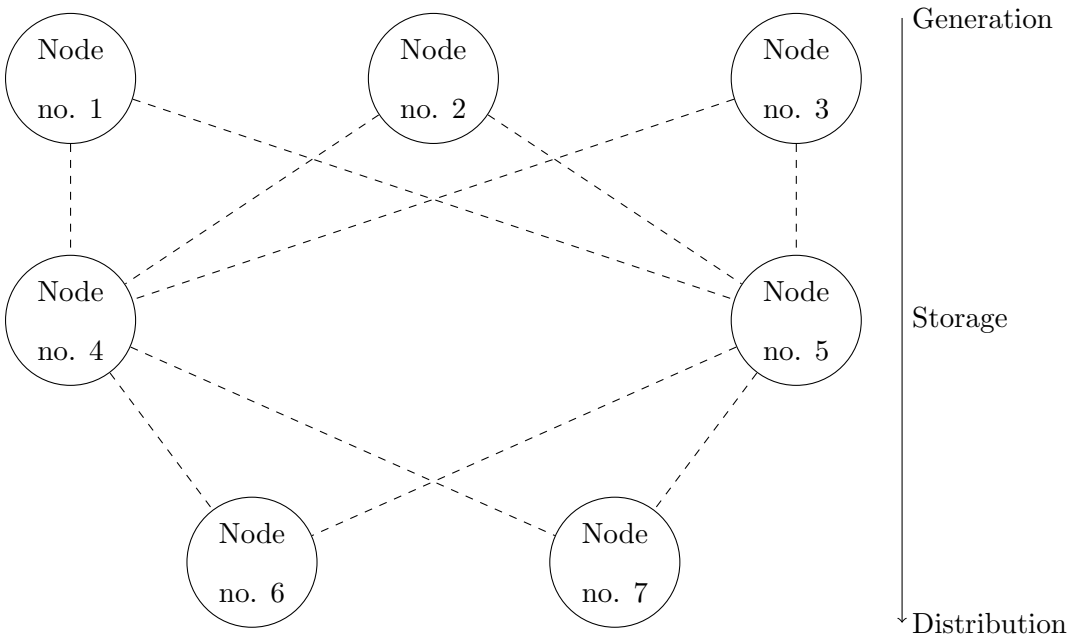

Figure 6.1: Network flow diagram of the optimization model for solar thermal combisystems

Node no. 1 corresponds to one array of flat-plate or evacuated tube collectors. Node no. 2 corresponds to two distinct arrays of flat-plate or evacuated tube collectors, each one having its own tilt angle (to take into account the case of both roof-mounted and wall-mounted solar thermal collectors). Solar thermal collectors in nodes no. 1 and no. 2 are facing south, which means an azimuth angle of zero. Node no. 3 is dedicated to auxiliary energy supplied from immersed electrical resistances or water heaters using either electricity or natural gas. Node no. 4 is used to select one thermal storage tank equipped with an internal or an external heat exchanger on the solar loop side, where the latter comes with a stratifying device installed inside the storage tank. Node no. 5 allows for two thermal storage tanks with either an internal or an external heat exchanger on the solar loop side to be chosen. One tank is dedicated to DHW and the other to SH. Finally, node no. 6 corresponds to the demand for DHW that is satisfied by the solar combisystem, and node no. 7 corresponds to the radiant floor heating system that covers the SH needs.

6.1.2 Description of the nodes and arcs

The mathematical formulation contains: (i) decision variables associated with each node and arc, (ii) optimization constraints applied to the decision variables, and (iii) objective functions. Constraints associated with the control strategy are presented for each case study in their respective chapter.

Any connection between two nodes i and j is controlled by a Boolean decision variable $B_{i,j}$. Setting $B_{i,j}$ equal to one means that the arc connecting the nodes i and j is operational. The final solar combisystem configuration depends on the arcs; for instance, if the arcs connecting the node no. 5 to the other nodes are not operational (i.e., only the node no. 4 is selected), the solar thermal combisystem has only one thermal storage tank. Nodes have also Boolean decision variables to select an equipment or a technology over another. These Boolean decision variables are denoted by B_i^k, where i represents a node and k represents its available technology. For example, the node no. 1 (i.e., $i = 1$) can have either flat-plate ($k = 1, B_1^1 = 1$) or evacuated tube collectors ($k = 2, B_1^2 = 1$), with the constraint $B_1^1 + B_1^2 = 1$, as illustrated in Figure 6.2 .

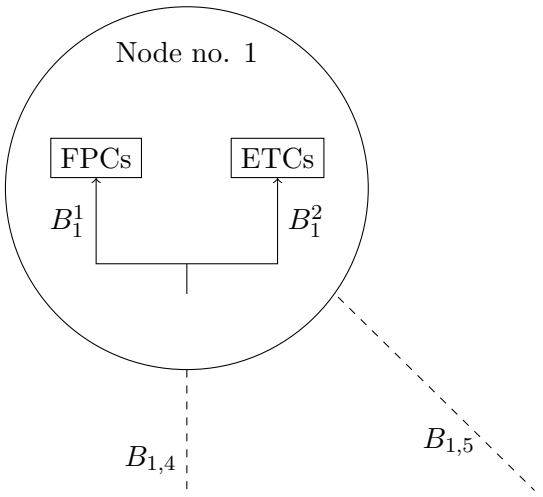

Figure 6.2: Detailed representation of node no. 1

The Boolean variables $B_{1,4}$ and $B_{1,5}$ are associated with the arcs connecting node no. 1 to nodes no. 4 and no. 5, respectively. If the solar combisystem has only one thermal storage tank, $B_{1,4}$ is equal to 1 and $B_{1,5}$ is equal to zero, hence the constraint $B_{1,4} + B_{1,5} = 1$.

6.2 Decision variables

Decision variables are altered in the design space during optimization searches to minimize the value of each objective function. As mentioned in (Bravo & Flocker, 2012), engineering problems usually imply discrete variables instead of continuous ones (e.g., standard dimensions of a specific equipment). The proposed MINLP model is therefore composed of continuous and discrete decision variables which are listed in Table 6.1. The range of values for some decision variables is taken from (Ng Chen Hin, 2013). For instance, the number of solar collectors is limited by the available area on the south facing roof of the house presented in Case study no. 1 (see Chapter 8). The upper limit of the tank volume is determined based on the height in the basement of the house – assuming a linear correlation between tank height and volume. Since solar thermal collectors can be roof-mounted or wall-mounted, the tilt angle can take values between 0 and 90 degrees.

Table 6.1: List of the selected decision variables

Decision variable	Type	Range	Step size	Unit
Arc				
$B_{1,4}$	Boolean	0/1	1	-
$B_{1,5}$	Boolean	0/1	1	-
$B_{2,4}$	Boolean	0/1	1	-
$B_{2,5}$	Boolean	0/1	1	-
$B_{3,4}$	Boolean	0/1	1	-
$B_{3,5}$	Boolean	0/1	1	-
$B_{4,6}$	Boolean	0/1	1	-
$B_{4,7}$	Boolean	0/1	1	-
$B_{5,6}$	Boolean	0/1	1	-
$B_{5,7}$	Boolean	0/1	1	-
Node				
B_1^1	Boolean	0/1	1	-
B_1^2	Boolean	0/1	1	-
B_2^1	Boolean	0/1	1	-
B_2^2	Boolean	0/1	1	-
B_3^1	Boolean	0/1	1	-
B_3^2	Boolean	0/1	1	-
B_3^3	Boolean	0/1	1	-
B_4^1	Boolean	0/1	1	-
B_4^2	Boolean	0/1	1	-
B_5^1	Boolean	0/1	1	-
B_5^2	Boolean	0/1	1	-
Number of flat-plate collectors	Discrete	1-22	1	-
Number of evacuated-tube collectors	Discrete	1-22	1	-
Tilt angle of array A1	Discrete	0-90	5	degree
Tilt angle of array A2	Discrete	0-90	5	degree
Flow rate per collector area	Continuous	10-115	-	$kg/(h \cdot m^2_{coll})$
Volume of tank no. 1 (DHW or both)	Discrete	100-30,000	100	L
Volume of tank no. 2 (SH)	Discrete	100-30,000	100	L
Tank no. 1 auxiliary power at high location	Discrete	0.5-15	0.5	kW
Tank no. 1 auxiliary power at low location	Discrete	0.5-15	0.5	kW
Tank no. 2 auxiliary power at high location	Discrete	0.5-15	0.5	kW
Tank no. 2 auxiliary power at low location	Discrete	0.5-15	0.5	kW
DHW heater auxiliary power	Discrete	0.5-15	0.5	kW
SH heater auxiliary power	Discrete	0.5-15	0.5	kW
Floor slab thickness	Discrete	0.06-0.26	0.01	m

B_1^1 and B_1^2 decide whether one array of FPCs or one array of ETCs is selected. B_2^1 and B_2^2 decide whether the two arrays of solar collectors, each having its own tilt angle, are composed of FPCs or ETCs. B_3^1, B_3^2, and B_3^3 are Boolean decision variables deciding whether the solar thermal combisystem is equipped with electric resistances ($k = 1$), electrical water heaters ($k = 2$), or

natural gas water heaters ($k = 3$). B_4^1 and B_4^2 decide whether the thermal storage tank is equipped with an immersed heat exchanger on the solar loop side ($k = 1$) or with an external one along with the use of a stratifying device ($k = 2$). B_5^1 and B_5^2 decide whether the two thermal storage tanks are equipped with an internal heat exchanger on the solar loop side ($k = 1$) or with an external one along with the use of a stratifying device ($k = 2$).

6.3 Optimization constraints

Optimization constraints ensure meaningfulness. Any decision vector found by a multi-objective optimization algorithm must provide a feasible solar combisystem design. Thus, this section focuses on optimization constraints applied to the decision variables. In order to generate a feasible solar combisystem configuration, the Boolean decision variables are subject to constraints as follows:

6.3.1 Energy generation and storage

The relationship between the energy generation and energy storage is defined as follows:

$$B_{1,4} + B_{1,5} + B_{2,4} + B_{2,5} + B_{3,4} + B_{3,5} \leq 2 \tag{6.1}$$

with

$$B_{1,4} + B_{1,5} + B_{2,4} + B_{2,5} = 1 \tag{6.2}$$

$$B_{1,4} + B_{1,5} \leq 1 \tag{6.3}$$

$$B_{2,4} + B_{2,5} \leq 1 \tag{6.4}$$

$$B_{3,4} + B_{3,5} \leq 1 \tag{6.5}$$

Thermal storage tanks are connected to the solar thermal collectors and auxiliary heaters. Since the solar combisystem configuration should involve either one or two arrays of solar thermal collectors, the arcs associated with nodes no. 1 and no. 2 cannot be operational at the same time, as shown in Equation 6.2. Auxiliary heaters might or might not be involved in the solar combisystem configuration, as reported by the last inequality.

6.3.2 Energy storage and distribution

Domestic hot water and space heating are always supplied by either one or two thermal storage tanks, according to the definition of solar thermal combisystems. The arcs associated nodes no. 4 with nodes no. 6 and no. 7 cannot be operational at the same time as those associated node no. 5 with nodes no. 6 and no. 7, as reported in Equations no. 6.6 and 6.8.

$$B_{4,6} + B_{5,6} = 1 \tag{6.6}$$

$$B_{4,7} + B_{5,7} = 1 \tag{6.7}$$

$$B_{4,6} + B_{5,6} + B_{4,7} + B_{5,7} = 1 \tag{6.8}$$

6.3.3 Technologies

Equations 6.9 and 6.10 decide whether flat-plate or evacuated tube collectors are selected. The Boolean decision variables related to node no. 3 select either electrical resistances (B_3^1) or water heaters using electricity (B_3^2) or natural gas (B_3^3). The selection is governed by the following two inequalities, where the last one prevents both electrical and natural gas water heaters to be selected at the same time.

$$B_1^1 + B_1^2 = 1 \tag{6.9}$$

$$B_2^1 + B_2^2 = 1 \tag{6.10}$$

$$B_3^1 + B_3^2 + B_3^3 \leq 1 \tag{6.11}$$

with

$$B_3^2 + B_3^3 = 1 \tag{6.12}$$

Equations 6.13 and 6.14 decide whether thermal storage tanks are equipped with immersed heat exchangers or external ones along with the use of stratifying devices.

$$B_4^1 + B_4^2 = 1 \tag{6.13}$$

$$B_5^1 + B_5^2 = 1 \tag{6.14}$$

6.4 Objective functions

Objective functions aims at evaluating the performance of solar combisystems. Three objective functions are selected (whose last one is divided into two parts):

1. Life cycle cost (LCC);
2. Life cycle energy use (LCE);
3. Life cycle exergy destroyed (LCX).

Additional penalty functions are added to each of the three aforementioned objective functions to ensure that the selected solar combisystem design is able to ensure the thermal comfort of occupants.

6.4.1 Life cycle cost analysis

A life cycle cost analysis accounts for present and future costs of an energy-conservation project over its life cycle. Design alternatives can therefore be compared by using their respective LCC value, which must be computed with the same assumptions. All costs are expressed in Canadian dollar, before taxes.

For case study no. 1, the Quebec sales tax is set as 9.975%, which is compounded on top of the 5% for the goods and services tax (Revenu Québec, 2016). For case study no. 2, the Massachusetts sales tax is 6.25% (Department of Revenue, 2016).

The service period for each case study, which is the expected life of the house before major renovations, is set at 40 years. As mentioned in (Islam et al., 2015), the assumption related to the building lifespan varies significantly between life cycle cost analysis studies, ranging from 40 to 100 years, with a median value of 50 years. For example, a service period of 30 years was selected in (Tokarik & Richman, 2016), 50 years in (Stephan & Stephan, 2016), and 60 years in (Schwartz et al., 2016). A period of 40 years is therefore a reasonable assumption.

Cost categories

The life cycle cost objective function of solar combisystems should take into consideration the different costs associated with acquiring, operating, maintaining, and disposing such system. Since costs occurring at different points in time cannot be directly added, because they do not have the same values, all costs must be converted to their present-value before being summed. To better estimate the costs, a distinction is required between:

1. Initial investment costs;

2. Operating costs;
3. Replacement costs.

Initial costs correspond to all costs that occur before the solar combisystem is put into service; all costs occurring after that moment are referred to future costs (e.g., operating and replacement costs). Operating costs are costs taking place every year in the service period, whereas replacement costs occur one or more times but irregularly, for instance the thermal storage tanks are expected to be changed after 15 years of operation.

Interest and inflation rates

Earning money from money, and therefore increasing its amount over time is known as the time value of money (Fuller et al., 1995). The value or cost of money is a function of the interest and inflation rates. The present worth (PW), also known as present value, of an amount of cash has a lower value than its future worth (FW). Analyzing the present worth of a solar combisystem allows determining whether or not such an investment is cost-effective.

Interest and discount rates

The present worth PW of an interest-earning amount of money after n years is given by:

$$\mathrm{PW} = \frac{\mathrm{FW}}{(1+d_\mathrm{r})^N} \tag{6.15}$$

where d_r is the real discount rate [-], which is assumed to be constant over the N years.

Estimating the present worth of a future sum of money, as described by Equation 6.15, is known as discounting. As mentioned in (Fuller & Petersen, 1996), the real discount rate is a special type of interest rate used in discounted cash flow analysis. Discount rates are separated into two categories: (i) nominal, or (ii) real. The nominal discount rate d_n includes the inflation, whereas the real discount d_r rate does not. Thus, one can be estimated from the other as follows:

$$1 + d_\mathrm{r} = \frac{1+d_\mathrm{n}}{1+I} \tag{6.16}$$

where d_r and d_n are the real and nominal discount rates [-], respectively; I is the inflation rate [-].

Inflation rate

Inflation is an increase in the price of goods or services over time without changing their intrinsic value. While inflation reduces the purchasing power, deflation increases it. Since goods or services may inflate at different rates, inflation must be taken into account in any life cycle cost analysis. Inflation is what makes a distinction between current and constant dollars. Current dollars, which account for inflation, represent the amount of dollars required to purchase goods or services at a specific time. Constant dollars refer to dollars of constant purchasing power. As explained in (Fuller & Petersen, 1996), a life cycle cost analysis can be performed using constant or current dollars; however, the use of constant dollars is usually preferred. Future costs and savings are estimated in constant dollars, then discounted with an real discount rate (i.e., exclusive of inflation).

LCC objective function

The maintenance and repair costs associated with solar thermal combisystems are not taken into account. Costs related to insurances and subsidies are also neglected. Thus, the LCC objective function given in (Fuller & Petersen, 1996), expressed in present-value dollars, can be simplified as follows:

$$\mathrm{LCC} = \mathrm{PW_{inv}} + \mathrm{PW_{rep}} + \mathrm{PW_{op}} \tag{6.17}$$

where $\mathrm{PW_{inv}}$, $\mathrm{PW_{rep}}$, and $\mathrm{PW_{op}}$ are the initial investment, replacement, and operating costs [$], respectively.

Initial investment costs

The initial investment costs do not need to be discounted, since they are already in present-value dollars. The initial investment costs are calculated as:

$$\begin{aligned}\mathrm{PW_{inv}} = {} & \mathrm{PW_{inv,coll}} + \mathrm{PW_{inv,gly}} + \mathrm{PW_{inv,ctr}} + \mathrm{PW_{inv,pipe}} \\ & + \mathrm{PW_{inv,pump}} + \mathrm{PW_{inv,aux}} + \mathrm{PW_{inv,tank}} + \mathrm{PW_{inv,slab}}\end{aligned} \tag{6.18}$$

where $\mathrm{PW_{inv,coll}}$, $\mathrm{PW_{inv,gly}}$, $\mathrm{PW_{inv,ctrl}}$, $\mathrm{PW_{inv,pipe}}$, $\mathrm{PW_{inv,pump}}$, $\mathrm{PW_{inv,aux}}$, $\mathrm{PW_{inv,tank}}$, and $\mathrm{PW_{inv,slab}}$, are the initial investment costs associated with the solar thermal collectors, glycol-water mixture,

controller, piping, pumps, auxiliary heaters, tanks, and additional concrete slab [$], respectively. All the components are defined as follows:

$$\begin{aligned} \mathrm{PW}_{\mathrm{inv,coll}} = (B_{1,4} + B_{1,5}) \cdot \left[B_1^1 \cdot C_{\mathrm{coll},1,1} + B_1^2 \cdot C_{\mathrm{coll},1,2}\right] \\ + (B_{2,4} + B_{2,5}) \cdot \left[B_2^1 \cdot C_{\mathrm{coll},2,1} + B_2^2 \cdot C_{\mathrm{coll},2,2}\right] \end{aligned} \tag{6.19}$$

$$\begin{aligned} \mathrm{PW}_{\mathrm{inv,gly}} = (B_{1,4} + B_{1,5}) \cdot \left[B_1^1 \cdot C_{\mathrm{gly},1,1} + B_1^2 \cdot C_{\mathrm{gly},1,2}\right] \\ + (B_{1,4} + B_{1,5}) \cdot \left[B_2^1 \cdot C_{\mathrm{gly},2,1} + B_2^2 \cdot C_{\mathrm{gly},2,2}\right] \end{aligned} \tag{6.20}$$

$$\mathrm{PW}_{\mathrm{inv,ctrl}} = C_{\mathrm{ctrl}} \tag{6.21}$$

$$\begin{aligned} \mathrm{PW}_{\mathrm{inv,pipe}} = (B_{1,4} + B_{1,5}) \cdot \left[B_1^1 \cdot C_{\mathrm{pipe},1,1} + B_1^2 \cdot C_{\mathrm{pipe},1,2}\right] \\ + (B_{1,4} + B_{1,5}) \cdot \left[B_2^1 \cdot C_{\mathrm{pipe},2,1} + B_2^2 \cdot C_{\mathrm{pipe},2,2}\right] \end{aligned} \tag{6.22}$$

$$\begin{aligned} \mathrm{PW}_{\mathrm{inv,pump}} &= C_{\mathrm{pump},1} \cdot \left[(B_{1,4} + B_{1,5}) \cdot \left(B_1^1 + B_1^2\right) + 2\,(B_{2,4} + B_{2,5}) \cdot \left(B_2^1 + B_2^2\right)\right] \\ &= C_{\mathrm{pump},2} \cdot \left[(B_{1,4} + B_{2,4}) \cdot B_4^2 + (B_{1,5} + B_{2,5}) \cdot B_5^2\right] \end{aligned} \tag{6.23}$$

$$\mathrm{PW}_{\mathrm{inv,aux}} = (B_{3,4} + B_{3,5}) \cdot \left[B_3^1 \cdot C_{\mathrm{aux},1} + B_3^2 \cdot C_{\mathrm{aux},2} + B_3^3 \cdot C_{\mathrm{aux},3}\right] \tag{6.24}$$

$$\mathrm{PW}_{\mathrm{inv,tank}} = \left(B_4^1 + 2B_5^1\right) \cdot C_{\mathrm{tank},1} + \left(B_4^2 + 2B_5^2\right) \cdot C_{\mathrm{tank},2} \tag{6.25}$$

$$\mathrm{PW}_{\mathrm{inv,slab}} = C_{\mathrm{slab}} \tag{6.26}$$

in which $C_{\mathrm{coll},1,1}$ and $C_{\mathrm{coll},2,1}$ are the costs of solar flat-plate collectors [$]; $C_{\mathrm{coll},1,2}$ and $C_{\mathrm{coll},2,2}$ are the costs of solar evacuated tube collectors [$]; $C_{\mathrm{gly},1,1}$, $C_{\mathrm{gly},1,2}$, $C_{\mathrm{gly},2,1}$, and $C_{\mathrm{gly},2,2}$ are the costs associated with the quantity of glycol-water mixture needed for node no. 1 technologies no. 1 and no. 2 and for node no. 2 technologies no. 1 and no. 2 [$], respectively; C_{ctrl} is the cost of a controller [$]; $C_{\mathrm{pipe},2}$ and $C_{\mathrm{pipe},2}$ are the costs of the piping for one or two arrays of solar thermal collectors, respectively [$]; $C_{\mathrm{pump},2}$ and $C_{\mathrm{pump},2}$ are the costs of pumps on the solar side and on the tank side, respectively [$]; $C_{\mathrm{aux},1}$ is the cost of an immersed electrical heating element [$]; $C_{\mathrm{aux},2}$ and $C_{\mathrm{aux},3}$ are the costs of external water heaters using electricity or natural gas, respectively [$]; $C_{\mathrm{tank},1}$ and $C_{\mathrm{tank},2}$ are the costs of thermal storage tanks without or with stratifying devices [$], respectively; C_{slab} is the cost of the additional concrete to increase the slab thickness over 0.06 m [$].

Table 6.2 shows the selected initial costs associated with the flat-pate and evacuated-tube collectors, highlighted in light gray, among other costs. Models 100F SV18 / SH1B and 2000T SPE (28 tubes) are selected, since they are the closest to the average values. Model SOL27 S is

however used in Case study no. 2 instead of 100F SV18 / SH1B, since the existing solar combisystem is equipped with such solar collectors.

Table 6.2: Solar thermal collector costs

Model	Area	Price	Price	Reference
Flat-plate collector	[m^2]	[$]	[$/$m^2$]	
100F SV1B / SH1B	2.51	890	355	(S. Royce, personal communication, March 2014)
200F SV2C / SH 2C	2.51	1,014	404	(S. Royce, personal communication, March 2014)
SOL27 S	2.54	624	246	(E. Wilson, personal communication, April 2014)
G32-P	2.98	1,099	369	(Thermo Dynamics Ltd., 2016)
S-32A P	2.97	1,099	370	(Thermo Dynamics Ltd., 2016)
TitanPower ALH26	2.35	910	387	(Silicon Solar, 2016)
TitanPower ALH32	2.90	897	310	(Silicon Solar, 2016)
Average	-	-	349	-
Evacuated-tube collector	[m^2]	[$]	[$/$m^2$]	
200T SPE (9 tubes)	1.63	1,499	920	(S. Royce, personal communication, March 2014)
200T SPE (28 tubes)	3.26	2,943	903	(S. Royce, personal communication, March 2014)
200T SP2A (12 tubes)	1.51	1,518	1,005	(S. Royce, personal communication, March 2014)
200T SP2A (24 tubes)	3.03	3,035	1,002	(S. Royce, personal communication, March 2014)
VHP30 (30 tubes)	5.24	3,113	594	(Silicon Solar, 2016)
Average	-	-	885	-

The glycol-water mixture initial cost is calculated using the relationship between the number of solar thermal collectors and the glycol-water mixture volume required developed in (Leckner, 2008) and the glycol-mixture price per liter from (E. Wilson, personal communication, April 2014). The initial cost of the differential controller is taken from (RSMeans, 2014). As the initial cost of a pump depends on its capacity, a linear correlation between the flow rate and initial cost is used based on data from (RSMeans, 2014). The initial cost associated with the piping, including insulation and fittings, is the same as the one used in (Leckner, 2008). Although the initial piping cost does not have a significant impact on the LCC objective function, a 10% increase is used to take into consideration the additional piping due to two arrays of solar collectors. The initial cost of a storage tank without a stratifier depends on its volume, the number of internal heat exchangers, and the power input of each heating element (i.e., immersed electrical resistance). The initial cost of a storage tank is a function of its volume and its number of heat exchangers, which was derived from a linear fit of several tank prices for volumes going from 85 liters up to 8,000 liters (RSMeans, 2014; Silicon Solar, 2016; Thermo Dynamics Ltd., 2016). The additional cost due to the power

input of each heating element is derived from a linear fit of several prices from (The Home Depot, 2016). A linear correlation between the flow rate and initial cost associated with the external heat exchanger required for a stratifying device is developed based on data from (RSMeans, 2014). The initial cost associated with the external heat exchanger is directly included in the thermal storage tank initial cost using stratifying device. An additional 5% of the heat exchanger cost is added to the thermal storage tank initial cost to take into account the stratifying device. The initial costs of the electrical and natural gas water heaters are a function of the power input, which was derived from several water heater prices (RSMeans, 2014). The initial cost of the additional concrete for the slab floor is calculated based on the concrete price per cubic meter from (RSMeans, 2016).

The initial cost of each solar combisystem component and its expected life span, taken from (Leckner, 2008), are reported in Table 6.3.

Table 6.3: Initial cost and replacement time for solar combisystem components

Component	Replacement time [years]	Initial cost C [$]	Reference
Flat-plate collectors (Case study no. 1)	25	$355 \cdot A_{\text{FPC},1} \cdot N_{\text{FPC}}$	(S. Royce, personal communication, March 2014)
Flat-plate collectors (Case study no. 2)	25	$246 \cdot A_{\text{FPC},2} \cdot N_{\text{FPC}}$	(E. Wilson, personal communication, April 2014)
Evacuated-tube collectors	25	$903 \cdot A_{\text{ETC}} \cdot N_{\text{ETC}}$	(S. Royce, personal communication, March 2014)
Storage tank without stratifiers	15	$(1.544 + 0.176 \cdot N_{\text{hx}}) \cdot V_{\text{tank}} + (1,686.2 + 653.9 \cdot N_{\text{hx}})$	(RSMeans, 2014; Silicon Solar, 2016; Thermo Dynamics Ltd., 2016)
Storage tank with stratifiers	15	$(1.544 + 0.176 \cdot N_{\text{hx}}) \cdot V_{\text{tank}} + (1,686.2 + 653.9 \cdot N_{\text{hx}}) + 0.8 \cdot \dot{m}_{\text{coll,hx}} \cdot A_{\text{tot,coll}} \cdot N_{\text{tot,coll}} + 1,602.9$	(RSMeans, 2014; Silicon Solar, 2016; The Home Depot, 2016; Thermo Dynamics Ltd., 2016)
Glycol-water mixture	3	$3.1 \cdot A_{\text{tot,coll}} \cdot N_{\text{tot,coll}} + 80.4$	(E. Wilson, personal communication, April 2014)
Pump (no external HX)	10	$0.0156 \cdot \dot{m}_{\text{coll}} \cdot A_{\text{tot,coll}} \cdot N_{\text{tot,coll}} + 155$	(RSMeans, 2014)
Pump (with external HX)	10	$0.0156 \cdot \dot{m}_{\text{coll,hx}} \cdot A_{\text{tot,coll}} \cdot N_{\text{tot,coll}} + 155$	(RSMeans, 2014)
Controller	15	129	(RSMeans, 2014)
Electrical heating element	15	$0.0034 \cdot P_{\text{aux}} + 4.6$	(The Home Depot, 2016)
Electrical water heater	15	$1.1 \cdot P_{\text{aux}} + 436$	(RSMeans, 2014)
Natural gas water heater	15	$0.9 \cdot P_{\text{aux}} + 574$	(RSMeans, 2014)
Pipes	-	277	(Leckner, 2008)
Pipes (two arrays of solar collectors)	-	291	(Leckner, 2008)
Additional concrete	-	$129 \cdot A_{\text{slab}} \cdot D_{\text{above}}$	(RSMeans, 2016)

Replacement costs

The replacement costs must be discounted using Equation 6.15 to be in present-value dollars, so as to take into consideration the time value of money. The replacement costs are calculated as:

$$\begin{aligned} \mathrm{PW_{rep}} = \mathrm{PW_{rep,coll}} + \mathrm{PW_{rep,gly}} + \mathrm{PW_{rep,ctrl}} \\ + \mathrm{PW_{rep,pump}} + \mathrm{PW_{rep,aux}} + \mathrm{PW_{rep,tank}} \end{aligned} \tag{6.27}$$

where $\mathrm{PW_{rep,coll}}$, $\mathrm{PW_{rep,gly}}$, $\mathrm{PW_{rep,ctrl}}$, $\mathrm{PW_{rep,pump}}$, $\mathrm{PW_{rep,aux}}$, and $\mathrm{PW_{rep,tank}}$ are the replacement costs associated with the solar thermal collectors, glycol, controllers, pumps, auxiliary heaters, and tanks [$], respectively, and are defined as:

$$\mathrm{PW_{rep,coll}} = \mathrm{PW_{inv,coll}} \cdot \left(\frac{1+I}{1+d_\mathrm{n}}\right)^{25} \tag{6.28}$$

$$PW_\mathrm{rep,gly} = \sum_{t=1}^{13} PW_\mathrm{inv,gly} \cdot \left(\frac{1+I}{1+d_\mathrm{n}}\right)^{3\cdot t} \tag{6.29}$$

$$PW_\mathrm{rep,ctrl} = \sum_{t=1}^{2} PW_\mathrm{inv,ctrl} \cdot \left(\frac{1+I}{1+d_\mathrm{n}}\right)^{15\cdot t} \tag{6.30}$$

$$PW_\mathrm{rep,pump} = \sum_{t=1}^{3} PW_\mathrm{inv,pump} \cdot \left(\frac{1+I}{1+d_\mathrm{n}}\right)^{10\cdot t} \tag{6.31}$$

$$PW_\mathrm{rep,aux} = \sum_{t=1}^{13} PW_\mathrm{inv,aux} \cdot \left(\frac{1+I}{1+d_\mathrm{n}}\right)^{3\cdot t} \tag{6.32}$$

$$PW_\mathrm{rep,tank} = \sum_{t=1}^{2} PW_\mathrm{inv,tank} \cdot \left(\frac{1+I}{1+d_\mathrm{n}}\right)^{15\cdot t} \tag{6.33}$$

Operating costs

The operating costs correspond to the energy used by the pumps and auxiliary water heaters. Unlike the replacement costs, the operating costs are annually recurring costs, which can be calculated as follows (Fuller & Petersen, 1996):

$$\mathrm{PW_{op}} = A_0 \cdot \sum_{t=1}^{N} \left(\frac{1+e_\mathrm{r}}{1+d_\mathrm{r}}\right)^{t} = A_0 \cdot \frac{1+e_\mathrm{r}}{d_\mathrm{r}-e_\mathrm{r}} \cdot \left[1 - \left(\frac{1+e_\mathrm{r}}{1+d_\mathrm{r}}\right)^{N}\right] \tag{6.34}$$

where A_0 is the annual energy cost during the first year of the study period [$]; d_r is the real discount rate [-]; e_r is the constant real escalation rate (i.e., exclusive of inflation) [-]; N is the number of years [-].

Few commodities, such as energy sources, have prices that change at a rate higher or lower than that of general inflation. A real escalation rate, which is assumed to be constant, is used to take into account the rate difference between energy sources and general inflation. The annual energy cost during the first year of the study period is calculated as the total electricity and natural gas used by the solar combisystem times their respective price. As a result, the operating costs are computed as follows:

$$\mathrm{PW}_{\mathrm{op}} = A_{0,\mathrm{elec}} \cdot \frac{1+e_{\mathrm{r,elec}}}{d_{\mathrm{r}}-e_{\mathrm{r,elec}}} \cdot \left[1-\left(\frac{1+e_{\mathrm{r,elec}}}{1+d_{\mathrm{r}}}\right)^{N}\right] + A_{0,\mathrm{gas}} \cdot \frac{1+e_{\mathrm{r,gas}}}{d_{\mathrm{r}}-e_{\mathrm{r,gas}}} \cdot \left[1-\left(\frac{1+e_{\mathrm{r,gas}}}{1+d_{\mathrm{r}}}\right)^{N}\right] \quad (6.35)$$

Assumptions

For case study no. 1, the electricity and natural gas prices are the 2015 estimations for a residential home in Montreal having a monthly consumption of 1,000 kWh. Their prices are equal to 0.0719 $/kWh (Hydro Québec, 2016) and 0.0289 $/kWh (Gaz Métro, 2016), respectively. An inflation rate of 2% is used to take into account the inflation-control target adopted by the Bank and the Government of Canada (Bank of Canada, 2016). The real escalation rates for electricity and natural gas in Quebec are set equal to -0.35% and -3.20% (Hydro Québec, 2016), respectively. Both are average values based on the evolution of their respective price between 2006 and 2016, that is, a period of 10 years. The real escalation rate of electricity is close to zero, which means that the electricity price increases almost at the same rate as the general inflation. The real escalation rate of natural gas is negative because of a significant decrease of its price since 2008 whereas the general inflation has continued increasing. The real discount rate is set to 5%, based on (Government of Canada, 2016).

For case study no. 2, the electricity price is 0.3003 $/kWh, which is an average of the price in 2014 for different cities in Massachusetts (U.S. Energy Information Administration, 2016). The natural gas price for the state of Massachusetts is taken equal to 0.0535 $/kWh from (U.S. Energy Information Administration, 2016), based on the year 2015. The inflation rate is equal to 1.95% (United States Department of Labor, 2016). The real escalation rates for electricity and natural gas in Massachusetts, which are averaged over the same period of 10 years, are fixed to 2.57% and -3.87% (U.S. Energy Information Administration, 2016), respectively. The real discount rate is

taken from (Lavappa & Kneifel, 2015) equal to 3%.

6.4.2 Life cycle energy analysis

Life cycle energy analysis is defined for the buildings sector in (Cabeza et al., 2014) as an approach that takes into account all energy inputs of a system over its entire life cycle. Thus, LCEA includes the energy use related to: (i) manufacturing, (ii) operating, and (iii) demolition. The manufacturing phase involves the construction, transportation, and installation of each solar combisystem component. The operating phase covers the amount of energy required to make the solar thermal combisystem operate, while the demolition phase includes the destruction and transportation of the solar combisystem. These three phases imply two types of energy uses:

1. Embodied energy;
2. Operating energy.

Embodied energy

Any energy used during the manufacturing and demolition phases is referred to as embodied energy. Either material manufacturing, including resource extraction, or transportation is included in embodied energy. As a result, the embodied energy associated with a solar combisystem is difficult to estimate. As mentioned in (Ng Cheng Hin & Zmeureanu, 2014), manufacturing and transportation methods, as well as material types and quantities, are hard to obtain with high accuracy. Average values of previous research studies are therefore used herein to assess the embodied energy of each solar combisystem component. When no information can be retrieved from the literature, an estimation of the embodied energy is made based on the quantity of the materials used to fabricate the solar combisystem components. The demolition phase is disregarded from the life cycle energy analysis, since no information is available from the literature.

Solar thermal collectors

The embodied energy of solar thermal collectors is determined based on previous research studies, which are listed in Table 6.4. Since different flat-plate collectors were used in different countries, the embodied energy of solar thermal collectors is averaged. Only one research study reported the

embodied energy of evacuated solar collectors.

Table 6.4: Embodied energy of flat-plate and evacuated collectors

Area [m^2]	Embodied energy [kWh/m^2]	Country	Reference
Flat-plate collectors			
2.00	500	India	(Gürzenich & Mathur, 1998)
6.15	517	Germany	(Gürzenich & Mathur, 1998)
5.76	472	Germany	(Gürzenich & Mathur, 1998)
5.00	356	Germany	(Stricher et al., 2004)
5.00	480	Germany	(Stricher et al., 2004)
1.90	518	Cyprus	(Kalogirou, 2004a)
2.13	458	Italy	(Ardente et al., 2005)
1.35	548	Cyprus	(Kalogirou, 2009)
Average	481		
Evacuated tube collectors			
5.00	439	Germany	(Gürzenich & Mathur, 1998)
Average	439		

As a result, the average embodied energy of flat-plate and evacuated solar collectors are calculated as follows:

$$\mathrm{EE_{FPC}} = 481 \cdot A_{\mathrm{FPC}} \cdot N_{\mathrm{FPC}} \tag{6.36}$$

$$\mathrm{EE_{ETC}} = 439 \cdot A_{\mathrm{ETC}} \cdot N_{\mathrm{ETC}} \tag{6.37}$$

where $\mathrm{EE_{FPC}}$ and $\mathrm{EE_{ETC}}$ are the embodied energies of flat-plate and evacuated tube collectors [kWh], respectively; A_{FPC} and A_{ETC} are the surface areas of flat-plate and evacuated tube collectors [m^2], respectively; N_{FPC} and N_{ETC} are the number of flat-plate and evacuated solar collectors [-], respectively.

Glycol-water mixture

The embodied energy value for the glycol-water mixture of 21.5 kWh/kg is taken from (Ardente et al., 2005). Using the same relationship between the number of solar thermal collectors and the glycol-water mixture volume developed in (Leckner, 2008), the embodied energy value for the glycol-water mixture is:

$$\mathrm{EE_{gly}} = 409.15 + 42.78 \cdot (N_{\mathrm{FPC}} \cdot A_{\mathrm{FPC}} + N_{\mathrm{ETC}} \cdot A_{\mathrm{ETC}}) \tag{6.38}$$

Pipes

The embodied energy of the pipes connecting the solar collectors to thermal storage tanks is equal to 27 kWh/m (Leckner, 2008). The embodied energy of the pipes, assumed to be composed of 25 m of piping between the solar collectors and thermal storage tanks for one array and 27.5 m for two arrays (that is, a 10% increase), to which was added 0.5 m per collector (Leckner, 2008), is calculated as:

$$\mathrm{EE}_{\mathrm{pipe,one,array}} = 675 + 13.5 \cdot (N_{\mathrm{FPC}} + N_{\mathrm{ETC}}) \tag{6.39}$$

$$\mathrm{EE}_{\mathrm{pipe,two,arrays}} = 742 + 13.5 \cdot (N_{\mathrm{FPC}} + N_{\mathrm{ETC}}) \tag{6.40}$$

where $\mathrm{EE}_{\mathrm{pipe}}$ is the embodied energy of the pipes connecting solar collectors to thermal storage tanks [kWh].

Thermal storage tanks

The embodied energy of thermal storage tanks was taken from (Ng Chen Hin, 2013), where a correlation for embodied energy versus tank volume was developed. As stated, different materials or manufacturing techniques can be used for thermal storage tanks depending on their size. Therefore, the correlation provides a way of evaluating, on average, the effects of different tank sizes. The embodied energy of thermal storage tanks is computed as follows (Ng Chen Hin, 2013):

$$\mathrm{EE}_{\mathrm{tank}} = 31.08 \cdot {V_{\mathrm{tank}}}^{0.61} \tag{6.41}$$

where $\mathrm{EE}_{\mathrm{tank}}$ is the embodied energy of thermal storage tanks [kWh].

Concrete slab

The embodied energy value for the additional concrete to increase the slab thickness over 0.06 m is taken from (Harvey, 2006), where a compressive strength of 20 MPa is selected [427.78 kWh/m^3]:

$$\mathrm{EE}_{\mathrm{slab}} = 427.78 \cdot A_{\mathrm{slab}} \cdot D_{\mathrm{above}} \tag{6.42}$$

Others

The embodied energy associated with the controller, the pumps, and the external auxiliary heater are not taken into consideration, because there is no sufficient information and in product specifi-

cations for these components to be estimated properly.

Replacement

The embodied energy of the generic solar thermal combisystem takes into account the embodied energy of the initial installation as well as that of the replacement of equipment. The expected service life of each component is the same as the one used in Table 6.3. The embodied energy is assumed not to change, so the replacement embodied energy of each equipment is equal to its initial embodied energy multiplied by the number of times it must be replaced over the 40 year life of the house.

Operating energy

Solar thermal combisystems require energy to operate and maintain the temperature set point conditions for thermal comfort. The amount of auxiliary energy used (i.e., any additional energy except solar energy) by solar thermal combisystems through pumps or auxiliary water heaters is referred to as operating energy. The operating energy, expressed in kWh, is thus calculated as follows:

$$\mathrm{OE} = 40 \cdot (E_{0,\mathrm{pump}} + E_{0,\mathrm{aux,elec}} + E_{0,\mathrm{aux,gas}}) \tag{6.43}$$

where $E_{0,\mathrm{pump}}$ is the annual energy consumption of the electric pumps during the first year of the study period [kWh]; $E_{0,\mathrm{aux,elec}}$ and $E_{0,\mathrm{aux,gas}}$ are the annual energy consumptions of the auxiliary water heaters powered by electricity or natural gas during the first year of the study period [kWh], respectively.

The factor 40 comes from the service period, which is set as 40 years (see Section 6.4.1).

Life cycle energy objective function

The life cycle energy use (LCE) by the generic solar combisystem comprises the initial and replacement embodied energies as well as the operating energy. As a result, the LCE objective function for the generic solar thermal combisystem is calculated as follows:

$$\mathrm{LCE} = \mathrm{EE_{ini}} + \mathrm{EE_{rep}} + \mathrm{OE} \tag{6.44}$$

where EE_{ini}, EE_{rep}, and OE are the initial embodied energy, replacement embodied energy, and operating energy [kWh], respectively.

6.4.3 Life cycle exergy analysis

Exergy, also known as availability, is defined as the maximum theoretical work obtainable as a system is brought into equilibrium with its environment (Moran & Shapiro, 2004). Exergy is therefore a thermodynamic property of the system-environment combination (Çengel & Boles, 2006), which is useful for revealing whether or not and by how much systems can be made more energy efficient. As a result, exergy analysis in addition to or in place of energy analysis provides more indication of where system inefficiencies occur (Dincer, 2002). For instance, electricity generated from burning fossil fuels at very high temperatures represents a poor process for space heating applications, where the environment being heated is close to ambient conditions (Hepbasli, 2012).

Exergy evaluation

The exergy content of energy sources may be defined as the energy content of the sources multiplied by a quality factor (Dincer & Rosen, 2006), where thermal energy has the lowest quality factor. The exergy consumption during a process is proportional to the entropy created due to irreversibilities associated with the process. Irreversibility, equivalent to the exergy destroyed, can be viewed as the wasted work potential. The rate of exergy of a control volume is expressed as (Çengel & Boles, 2006):

$$\frac{dX}{dt} = \dot{X} = \dot{m} \cdot [(h - h_0) - T_0 \cdot (s - s_0)] + \dot{E}_{\mathrm{KE}} + \dot{E}_{\mathrm{PE}} \tag{6.45}$$

where $\dot{m}$ is the mass flow rate entering the system [kg/s]; h and h_0 are the total specific enthalpies of the system and reference environment [kJ/kg], respectively; T_0 is the temperature of the reference environment [K]; s and s_0 are the total specific entropies of the system and reference environment [kJ/(kg·K)], respectively; $\dot{E}_{\mathrm{KE}}$ and $\dot{E}_{\mathrm{PE}}$ are the rates of kinetic and potential energy [kW], respectively.

Kinetic and potential energies are forms of mechanical energy, and therefore they can be converted to useful work entirely. On the contrary, only a portion of heat transfer at a temperature higher than that of the environment can be converted into useful work. This portion is calculated

using a quality factor (or exergy factor) equal to the efficiency of a Carnot engine. As a result, the rate of exergy associated with heat transfer is defined as follows (Çengel & Boles, 2006):

$$\dot{X}_{\text{heat}} = \left(1 - \frac{T_0}{T}\right) \cdot \dot{Q} \tag{6.46}$$

where T is the hot source temperature [K]; $\dot{Q}$ is the heat transfer rate [kW].

Exergy balance of solar combisystems

The rate form of the exergy balance of the residential solar combisystem can be expressed as follows (Suzuki, 1988):

$$\dot{X}_{\text{d}} = \dot{X}_{\text{in}} - \dot{X}_{\text{out}} - \dot{X}_{\text{s}} - \dot{X}_{\text{L}} \tag{6.47}$$

where $\dot{X}_{\text{d}}$, $\dot{X}_{\text{in}}$, $\dot{X}_{\text{out}}$, $\dot{X}_{\text{s}}$, and $\dot{X}_{\text{L}}$ are the rates of exergy destroyed, exergy flow into the system, exergy flow out from the system, exergy stored in the system, and exergy leaked from the system [kW], respectively.

Technical and physical boundaries

As mentioned in (Torío et al., 2009), two different approaches have been used for calculating exergy losses in solar thermal systems: (i) technical boundary, and (ii) physical boundary.

The difference between the former and the latter consists on whether the conversion of solar radiation into heat should be taken into consideration or not. A more thorough discussion about these two boundaries for exergy analysis can be found in (Torío & Schmidt, 2010). Since the technical boundary takes into account the conversion of high quality solar radiation into low temperature heat, the greatest exergy losses occur in solar thermal collectors. As a result, systems making a direct use of solar radiation are penalized compared to indirect-solar systems, because exergy losses related to solar radiation are ignored. Consequently, both boundaries are used in this doctoral thesis to evaluate the exergy performance of solar thermal combisystems.

Solar thermal collectors

The rate of exergy flowing into a solar thermal collector is made of two components:

1. The rate of exergy associated with the heat-transfer fluid entering;

2. The rate of exergy gained from solar radiation.

The rate of exergy associated with the heat-transfer fluid entering is calculated using Equation 6.48, assuming that the kinetic and potential energies can be neglected and that the heat-transfer fluid is incompressible, as follows (Çengel & Boles, 2006):

$$\dot{X}_{\text{in,coll}} = \dot{m}_{\text{in,coll}} \cdot c_{\text{p,coll}} \cdot \left[T_{\text{in,coll}} - T_0 - T_0 \cdot \ln\left(\frac{T_{\text{in,coll}}}{T_0}\right) \right] \tag{6.48}$$

where $\dot{m}_{\text{in,coll}}$ is the mass flow rate of the heat-transfer fluid entering the solar collectors [kg/s]; $c_{\text{p,coll}}$ is the specific heat of the heat-transfer fluid [kJ/(kg·K)]; $T_{\text{in,coll}}$ is the temperature of the heat-transfer fluid entering the solar collector [K].

The rate of exergy gained from solar radiation depends on the boundary being used. When the technical boundary is considered, three approaches are usually used for assessing the exergy of solar radiation. The first one, developed in (Patela, 1964), is defined as follows:

$$\dot{X}_{\text{solar}} = A_{\text{coll}} \cdot G_{\text{tot,coll}} \cdot \left[1 + \frac{1}{3} \cdot \left(\frac{T_0}{T_{\text{sun}}}\right) - \frac{4}{3} \cdot \ln\left(\frac{T_0}{T_{\text{sun}}}\right) \right] \tag{6.49}$$

The second one, developed in (Jetler, 1981), is formulated as follows:

$$\dot{X}_{\text{solar}} = A_{\text{coll}} \cdot G_{\text{tot,coll}} \cdot \left[1 + \frac{T_0}{T_{\text{sun}}} \right] \tag{6.50}$$

where A_{coll} is the solar collector area [m^2]; $G_{\text{tot,coll}}$ is the total solar irradiance incident on the solar collector [kW/m^2]; T_{sun} is the sun temperature, which is taken equal to 6,000K.

As observed in (Agudelo & Cortés, 2010), the first expression is the most commonly used formula to assess exergy from solar radiation; thus, it is used in this study when the technical boundary is taken into consideration. Besides, as mentioned in (Chow et al., 2009), the results from these three equations do not have more than a 2% difference.

When the physical boundary is considered, the exergy gained from solar radiation is determined using the collector absorber plate temperature as heat source. As a result, the rate of exergy gained from solar radiation is expressed as follows (Ng Cheng Hin & Zmeureanu, 2014):

$$\dot{X}_{\text{plate}} = \dot{m}_{\text{in,coll}} \cdot c_{\text{p,coll}} \cdot \left[T_{\text{plate}} - T_0 - T_0 \cdot \ln\left(\frac{T_{\text{plate}}}{T_0}\right) \right] \tag{6.51}$$

where T_{plate} is the collector absorber plate temperature defined as follows:

$$T_{\text{plate}} = \frac{T_{\text{out,coll}} - T_{\text{in,coll}}}{\eta_{\text{coll}}} + T_{\text{in,coll}} \tag{6.52}$$

The rate of exergy associated with the heat-transfer fluid leaving the collector is similar to Equation 6.48, but involves the temperature of the heat-transfer fluid leaving the solar collector as follows:

$$\dot{X}_{\text{out,coll}} = \dot{m}_{\text{out,coll}} \cdot c_{\text{p,coll}} \cdot \left[T_{\text{out,coll}} - T_0 - T_0 \cdot \ln\left(\frac{T_{\text{out,coll}}}{T_0} \right) \right] \tag{6.53}$$

Assuming that the exergy stored in and leaked from the solar thermal collector are negligible compared to the other terms (Suzuki, 1988), the exergy destroyed in solar collectors can be calculated using the technical or physical boundary as follows:

$$X_{\text{d,coll,tech}} = \Delta t \cdot \dot{X}_{\text{d,coll,tech}} = \Delta t \cdot \left(\dot{X}_{\text{solar}} + \dot{X}_{\text{in,coll}} - \dot{X}_{\text{out,coll}} \right) \tag{6.54}$$

$$X_{\text{d,coll,phys}} = \Delta t \cdot \dot{X}_{\text{d,coll,phys}} = \Delta t \cdot \left(\dot{X}_{\text{plate}} - \dot{X}_{\text{out,coll}} \right) \tag{6.55}$$

where Δt is the simulation time step [h], which is equal to ten minutes (i.e., 10/60 hours).

External heat exchangers

The rate of exergy following in and out of an external heat exchanger is similar to that of a solar collector, which is expressed as follows:

$$\dot{X}_{\text{in,hx,hot}} = \dot{m}_{\text{in,hx,hot}} \cdot c_{\text{p,hx,hot}} \cdot \left[T_{\text{in,hx,hot}} - T_0 - T_0 \cdot \ln\left(\frac{T_{\text{in,hx,hot}}}{T_0} \right) \right] \tag{6.56}$$

$$\dot{X}_{\text{out,hx,hot}} = \dot{m}_{\text{out,hx,hot}} \cdot c_{\text{p,hx,hot}} \cdot \left[T_{\text{out,hx,hot}} - T_0 - T_0 \cdot \ln\left(\frac{T_{\text{out,hx,hot}}}{T_0} \right) \right] \tag{6.57}$$

$$\dot{X}_{\text{in,hx,cold}} = \dot{m}_{\text{in,hx,cold}} \cdot c_{\text{p,hx,cold}} \cdot \left[T_{\text{in,hx,cold}} - T_0 - T_0 \cdot \ln\left(\frac{T_{\text{in,hx,cold}}}{T_0} \right) \right] \tag{6.58}$$

$$\dot{X}_{\text{out,hx,cold}} = \dot{m}_{\text{out,hx,cold}} \cdot c_{\text{p,hx,cold}} \cdot \left[T_{\text{out,hx,cold}} - T_0 - T_0 \cdot \ln\left(\frac{T_{\text{out,hx,cold}}}{T_0} \right) \right] \tag{6.59}$$

where $\dot{m}_{\text{in,hx}}$ and $\dot{m}_{\text{out,hx}}$ are the mass flow rates of the fluid flowing in and flowing out of the external heat exchanger [kg/s], respectively; $c_{\text{p,hx}}$ is the specific heat capacity at constant pressure of the fluid going through the external heat exchanger [kJ/(kg·K)]; $T_{\text{in,hx}}$ and $T_{\text{out,hx}}$ are the temperatures of the fluid entering and leaving the external heat exchanger [K], respectively.

Therefore, the exergy destroyed in external heat exchangers is calculated as follows:

$$X_{\text{d,hx}} = \Delta t \cdot \left(\dot{X}_{\text{in,hx,hot}} - \dot{X}_{\text{out,hx,hot}} + \dot{X}_{\text{in,hx,cold}} - \dot{X}_{\text{out,hx,cold}} \right) \tag{6.60}$$

Pumps

Since exergy is the useful work potential, the rate of exergy transfer by electric work is equal to the rate of electric work itself. In order to take into account the inefficiencies of electricity production and transmission, a primary electricity conversion factor is added. Thus, the exergy destroyed by a pump is calculated as follows:

$$X_{\mathrm{d,pump}} = \Delta t \cdot \dot{W}_{\mathrm{pump}} \tag{6.61}$$

where $\dot{W}_{\mathrm{pump}}$ is the rate of electricity supplied to the pump [kW]. The increase of the physical exergy of the pumped fluid to increase the pressure and temperature of the fluid is neglected in this study.

Auxiliary heaters

The exergy balance of an external auxiliary heater is composed of the exergy of the fluid flowing into the auxiliary heater, exergy of the fluid flowing out from the auxiliary heater, and exergy gained by electricity or by natural gas. As mentioned in (Dincer & Rosen, 2006), exergy gained can be simplified as exergy = energy × exergy/energy ratio. The exergy/energy ratio τ is equal to 1.00 for electricity and 0.94 for natural gas. The exergy destroyed by an external auxiliary heater is therefore calculated as follows:

$$X_{\mathrm{d,aux}} = E_{\mathrm{aux}} \cdot \tau + X_{\mathrm{in,aux}} - X_{\mathrm{out,aux}} \tag{6.62}$$

in which

$$X_{\mathrm{in,aux}} = \Delta t \cdot \dot{m}_{\mathrm{out,aux}} \cdot c_{\mathrm{p,water,aux}} \cdot \left[T_{\mathrm{out,aux}} - T_0 - T_0 \cdot \ln\left(\frac{T_{\mathrm{out,aux}}}{T_0} \right) \right] \tag{6.63}$$

$$X_{\mathrm{out,aux}} = \Delta t \cdot \dot{m}_{\mathrm{out,aux}} \cdot c_{\mathrm{p,water,aux}} \cdot \left[T_{\mathrm{out,aux}} - T_0 - T_0 \cdot \ln\left(\frac{T_{\mathrm{out,aux}}}{T_0} \right) \right] \tag{6.64}$$

Thermal storage tanks

Unlike solar thermal collectors, the exergy stored in $X_{\mathrm{s,tank}}$ and leaked from the thermal storage tank $X_{\mathrm{L,tank}}$ must be taken into consideration. A thermal storage tank can be equipped with inlets, outlets, electrical resistances, and immersed heat exchangers, and therefore its exergy destroyed is expressed as follows:

$$
\begin{aligned}
X_{\mathrm{d,tank}} = {} & \Delta t \cdot \sum_i \left(\dot{X}_{\mathrm{in,tank},i} - \dot{X}_{\mathrm{out,tank},i} \right) \\
& + \Delta t \cdot \sum_j \left(\dot{X}_{\mathrm{in,hx},j} - \dot{X}_{\mathrm{out,hx},j} \right) \\
& + \Delta t \cdot \left(\sum_k \dot{W}_{\mathrm{elec},k} - \dot{X}_{\mathrm{L,tank}} \right) + X_{\mathrm{s,tank}}
\end{aligned}
\tag{6.65}
$$

where $\dot{X}_{\mathrm{in,tank},i}$ and $\dot{X}_{\mathrm{out,tank},i}$ are the exergy rate flowing in and out of the storage tank through the i-th inlet and outlet [kW], respectively; $\dot{X}_{\mathrm{in,hx},j}$ and $\dot{X}_{\mathrm{out,hx},j}$ are the exergy rate flowing in and out of the storage tank through the j-th heat exchanger [kW], respectively; $\dot{W}_{\mathrm{elec},k}$ is the rate of electricity supplied to the k-th electrical resistance [kW]; $\dot{X}_{\mathrm{L,tank}}$ is the rate of exergy leaked from the storage tank through its walls [kW]; $X_{\mathrm{s,tank}}$ is the exergy stored in the storage thermal tank [kWh].

Equation 6.65 varies depending on the kind of thermal storage tank being used. For instance, if a storage tank does not have any internal heat exchanger, the second term is removed. The different terms involved are calculated as follows:

$$
\dot{X}_{\mathrm{in,tank},i} = \dot{m}_{\mathrm{in,tank},i} \cdot c_{\mathrm{p,tank},i} \cdot \left[T_{\mathrm{in,tank},i} - T_0 - T_0 \cdot \ln \left(\frac{T_{\mathrm{in,tank},i}}{T_0} \right) \right] \tag{6.66}
$$

$$
\dot{X}_{\mathrm{out,tank},i} = \dot{m}_{\mathrm{out,tank},i} \cdot c_{\mathrm{p,tank},i} \cdot \left[T_{\mathrm{out,tank},i} - T_0 - T_0 \cdot \ln \left(\frac{T_{\mathrm{out,tank},i}}{T_0} \right) \right] \tag{6.67}
$$

$$
\dot{X}_{\mathrm{in,hx},j} = \dot{m}_{\mathrm{in,hx},j} \cdot c_{\mathrm{p,hx},j} \cdot \left[T_{\mathrm{in,hx},j} - T_0 - T_0 \cdot \ln \left(\frac{T_{\mathrm{in,hx},j}}{T_0} \right) \right] \tag{6.68}
$$

$$
\dot{X}_{\mathrm{out,hx},j} = \dot{m}_{\mathrm{out,hx},j} \cdot c_{\mathrm{p,hx},j} \cdot \left[T_{\mathrm{out,hx},j} - T_0 - T_0 \cdot \ln \left(\frac{T_{\mathrm{out,hx},j}}{T_0} \right) \right] \tag{6.69}
$$

$$
\dot{X}_{\mathrm{L,tank}} = U_{\mathrm{L,tank}} \cdot A_{\mathrm{tank}} \cdot (T_{\mathrm{avg,tank}} - T_{\mathrm{room}}) \cdot \left(1 - \frac{T_0}{T_{\mathrm{avg,tank}}} \right) \tag{6.70}
$$

$$
X_{\mathrm{s,tank}} = X_{\mathrm{tank}}(t) - X_{\mathrm{tank}}(t-1) \tag{6.71}
$$

in which $U_{\mathrm{L,tank}}$ is the overall tank heat loss coefficient per unit area [kW/(K$\cdot$ m^2)]; A_{tank} is the surface area of the storage tank [m^2]; $T_{\mathrm{avg,tank}}$ is the average temperature of the water inside the storage tank [K]; T_{room} is the air node temperature of the room where the storage tank is situated [K]; $X_{\mathrm{tank}}(t)$ and $X_{\mathrm{tank}}(t-1)$ are the amounts of exergy stored in the storage tank water at time t and $t-1$ [kWh], respectively, which are calculated as follows:

$$X_{\text{tank}} = \left(\frac{1 \text{ kWh}}{3,600 \text{ kJ}}\right) \cdot m_{\text{tank}} \cdot c_{\text{p,tank}} \cdot \left[T_{\text{avg,tank}} - T_0 - T_0 \cdot \ln\left(\frac{T_{\text{avg,tank}}}{T_0}\right)\right] \tag{6.72}$$

where $\left(\frac{1 \text{ kWh}}{3,600 \text{ kJ}}\right)$ is the unity conversion ratio, equal to one and unitless, to convert kJ in kWh.

Life cycle exergy destroyed objective functions

The life cycle exergy destroyed (LCX) by the generic solar combisystem corresponds to the exergy destroyed by each of its components. As a result, the LCX objective function for the generic solar thermal combisystem using the technical or physical boundary is calculated as follows:

$$\text{LCX}_{\text{tech}} = X_{\text{d,comb,tech}} = X_{\text{d,coll,tech}} + X_{\text{d,pump}} + X_{\text{d,hx}} + X_{\text{d,aux}} + X_{\text{d,tank}} \tag{6.73}$$

$$\text{LCX}_{\text{phys}} = X_{\text{d,comb,phys}} = X_{\text{d,coll,phys}} + X_{\text{d,pump}} + X_{\text{d,hx}} + X_{\text{d,aux}} + X_{\text{d,tank}} \tag{6.74}$$

6.4.4 Penalty function

Comfortable indoor air temperature can be ensured through one or more penalty functions instead of using another objective function. Penalty functions, penalizing unwanted or infeasible solutions, provide an easy way of handling constrained optimization problems. For instance, the optimization process presented (Djurica et al., 2007) made certain that thermal comfort was respected by using the percentage of people dissatisfied (PPD) index as a constraint. Thermal comfort can be assessed with the predicted mean vote (PMV) or PPD indexes, based on Fanger's model (Fanger, 1970). Penalty functions based on the supply space heating and domestic hot water temperatures were inserted in (Ghiaus & Jabbour, 2012) to ensure a thermal comfort threshold for a multi-source solar system. Thermal comfort was also set as a constraint in (Ng Cheng Hin & Zmeureanu, 2014), where a high amount was added to the value of each objective function as soon as the number of hours under the heating set point was above 550.

Since solar thermal combisystems provide both domestic hot water and space heating, two penalty functions, based on (Ng Cheng Hin & Zmeureanu, 2014), are added to each of the four aforementioned objective functions. To prevent Legionnaires disease, the lower DHW temperature is set at 55°C. If this condition is not met, the penalty function defined in Equation 6.75 is triggered. For space heating, the penalty function defined in Equation 6.76 is triggered when the number of hours under set point (HUSP) exceeds 550. As the house is divided into three zones, the limit of

550 corresponds to 183 hours per zone, which is 4.5% of the heating season time (from October 17th to May 1st). An arbitrary high penalty value is given to ensure that such solutions are not selected:

$$\mathrm{PEN}_{\mathrm{DHW}} = 500,000 \cdot lt\left(55, T_{\mathrm{DHW}}\right) \tag{6.75}$$

$$\mathrm{PEN}_{\mathrm{SH}} = 500,000 \cdot lt\left(550, \mathrm{HUSP}\right) \tag{6.76}$$

where $lt\left(\text{criterion}, \text{variable}\right)$ is equal to one if criterion is less than variable and equal to zero otherwise.

These two penalty functions are applied to Case study no. 1 only, which is presented in Chapter 8. Since Case study no. 2 is based on measurements, design solutions are considered only if the DHW and SH needs are satisfied.

Chapter 7

Micro multi-objective optimization algorithm[1]

Real-world optimization problems having only one objective function are rather the exception than the rule. Multi-objective optimization problems usually involve conflicting objectives, and therefore are more difficult to solve. Among the different MOO algorithms that have been developed, little emphasis has been placed on micro-MOO algorithms, which use a small population of solution candidates. Such algorithms are suitable for optimization problems where evaluating objective functions is time-consuming, which is the case of many engineering applications (Fuentes Cabrera & Coello Coello, 2010).

A micro-genetic algorithm for multi-objective optimization, named micro-GA, was proposed in (Coello Coello & Pulido, 2001), and then improved in (Pulido & Coello Coello, 2003). Both belong to the evolutionary algorithm family, which means that their optimization search consists in imitating natural selection. Another micro-MOO algorithm, called micro-MOPSO, was presented in (Fuentes Cabrera & Coello Coello, 2010), which was a micro version of the multi-objective particle swarm optimization (MOPSO) algorithm. To the best knowledge of the author, none of them have been used in building engineering and no further research has been conducted on micro-MOO algorithms. A micro-time variant multi-objective optimization (micro-TVMOPSO), which is a revised version of micro-MOPSO, is therefore proposed herein and will be used for the following two case studies.

[1]This chapter is mainly based on the paper "Rey, A., & Zmeureanu, R. (2017). Micro-Time Variant Multi-Objective Particle Swarm Optimization (micro-TVMOPSO) of a solar thermal combisystem [in press]. Swarm and Evolutionary Computation. doi: `https://doi.org/10.1016/j.swevo.2017.04.005`"

7.1 Micro-MOPSO algorithm

Proposed in (Fuentes Cabrera & Coello Coello, 2010), micro-MOPSO uses five candidate solutions and two external repositories. Non-dominated solutions found during the optimization search are stored in the first external repository, named auxiliary archive. A second repository, called final archive, is used to store the final non-dominated solutions that are given at the end of the optimization search. The non-dominated solutions within the final archive are sorted based on their crowding distance (Deb et al., 2002).

The final archive is also used to select the leader of the swarm. A subset of the final archive, composed of the non-dominated solutions having the highest crowding distance value, is selected and one solution is randomly chosen as the decision vector G^{best}. This mechanism favors the particles in the less populated areas in order to increase diversity. Once the leader is chosen, its closest neighbors, based on the Euclidean distance, are selected from the auxiliary archive to generate the swarm. Since the final archive contains only non-dominated solutions, it is pruned using the crowding distance mechanism when its maximum capacity is reached. If the maximum capacity of the auxiliary archive is exceeded, only the solutions that belong to the first five non-dominated fronts are kept. If there are still too many solutions belonging to the first five fronts, the crowding distance mechanism is used to filter out solutions. Due to its small number of particles, micro-MOPSO preserves diversity by using a re-initialization process (Fuentes Cabrera & Coello Coello, 2007) and a mutation operator (Michalewicz, 1996).

Micro-MOPSO outperformed NSGA-II in (Fuentes Cabrera & Coello Coello, 2010), but faced difficulties in approximating the true Pareto front of the ZDT4 benchmark problem (Zitzler et al., 2000). Besides, micro-MOPSO was compared to NSGA-II only. As reported in (Hu & Yen, 2015), the crowding distance operator used in micro-MOPSO tends to select the extreme non-dominated solutions forming the Pareto front which may lead to premature convergence.

7.2 Proposed micro-TVMOPSO algorithm

Three hypotheses are made in order to enhance micro-MOPSO's performance: (i) its lack of velocity constraint mechanism reduces its efficiency at searching for new non-dominated solutions, (ii) the

use of the crowding distance operator leads to premature convergence, and (iii) its main coefficients do not favor global exploration and local exploitation. Three modifications of micro-MOPSO are therefore proposed and presented in this section, which leads to the proposed micro-TVMOPSO algorithm.

As observed in (Durillo et al., 2009), MOPSO-based algorithms faced difficulties in approximating multi-frontal problems such as ZDT4 due to a lack of velocity limit. High velocities can position particles beyond the upper or lower bounds of the decision variables, known as "swarm explosion", which leads to undesired solutions. As a result, micro-TVMOPSO starts by incorporating the velocity constraint mechanism presented in (Nebro et al., 2009).

7.2.1 Velocity constraint mechanism

In order to prevent micro-TVMOPSO from the aforementioned problem, a constriction coefficient $\chi(t)$ multiplies Equation 2.6 (Clerc & Kennedy, 2002):

$$\chi(t) = \begin{cases} 1, & \text{if } \phi(t) \leq 4 \\ 2 \Big/ \left[2 - \phi(t) - \sqrt{\phi(t)^2 - 4 \cdot \phi(t)}\right], & \text{if } \phi(t) > 4 \end{cases} \tag{7.1}$$

where

$$\phi(t) = c_1(t) + c_2(t) \tag{7.2}$$

Instead of maintaining both c_1 and c_2 equal to 1.8, as in micro-MOPSO, each coefficient were varied randomly between 1.5 and 2.5 in (Nebro et al., 2009) to avoid $\chi(t)$ to be always equal to one. The constriction coefficient reduces, but it does not eliminate, the probability of the particles to go beyond the upper or lower bounds of the decision variables.

Before updating the position of each particle using Equation 2.7, the velocity associated with the j-th decision variable of the i-th particle is bounded by the following velocity constriction (Nebro et al., 2009):

$$v_i^j(t+1) = \begin{cases} \Delta j, & \text{if } v_i^j(t+1) > \Delta j \\ -\Delta j, & \text{if } v_i^j(t+1) \leq -\Delta j \\ v_i^j(t+1), & \text{otherwise} \end{cases} \tag{7.3}$$

where

$$\Delta j = \frac{u^j - l^j}{2} \tag{7.4}$$

in which u^j and l^j are the upper and lower boundaries of the j-th decision variable.

In addition to the constriction coefficient, this velocity constriction enables to reduce furthermore the probability of a particle to go beyond its bounds. After the velocity has been constrained and used in Equation 2.7, micro-TVMOPSO verifies whether or not the value of each decision variable is out of the search space. A decision variable exceeding its upper or lower bounds takes the value of that bound and its corresponding velocity is multiplied by 0.01 (Nebro et al., 2009) in order to reduce its momentum.

7.2.2 Leader and neighborhood selection

Proposed in (Hu & Yen, 2015) to overcome the issue associated with the crowding distance mechanism, the parallel cell coordinate system (PCCS) is used in micro-TVMOPSO as a leader selection and as an archive pruning mechanism.

Parallel cell coordinate system

The m-th objective of the k-th non-dominated solution in the archive, written $f_{k,m}$, is associated with an integer label number $L_{k,m}$ using Equation 7.5 (Hu & Yen, 2015). Thus, PCCS divides the archive into a 2-dimensional grid with $K \times M$ cells, where K and M are the archive size (i.e., number of non-dominated solutions changing over generations) and number of objectives, respectively.

$$L_{k,m} = \left\lceil K \cdot \frac{f_{k,m} - f_m^{\min}}{f_m^{\max} - f_m^{\min}} \right\rceil \tag{7.5}$$

where $\lceil x \rceil$ is the ceiling function, which returns the smallest integer greater than or equal to x; $f_m^{\min}$ and $f_m^{\max}$ are the minimum and maximum values of the m–th objective among all the K non-dominated solutions. The integer label number $L_{k,m} \in \{1, 2, \ldots, K\}$ is set to one if $f_{k,m}$ is equal to $f_m^{\min}$. Parallel cell coordinate system provides a way to compare non-dominated solutions. The integer label number $L_{k,m}$ provides a way of finding the non-dominated solutions in the 2-D grid created by the parallel cell coordinate system, which can then be compared using the concept of density.

Density

Instead of using the crowding distance operator, the concept of density is used in micro-TVMOPO to avoid premature convergence. The density of a particle x_k in the archive is calculated as follows (Hu & Yen, 2015):

$$Density\left(x_k\right) = \sum_{\substack{l=1 \\ k \neq l}}^{K} \frac{1}{PCD\left(x_k, x_l\right)} \tag{7.6}$$

where PCD is the parallel cell distance, calculated between x_k and the rest of the non-dominated solutions in the archive, is the sum of the differences of cell coordinates over all objectives M in the PCCS. The PCD of two non-dominated solutions x_k and x_l, $PCD\left(x_k, x_l\right)$, is computed as follows (Hu & Yen, 2015):

$$PCD\left(x_k, x_l\right) = \begin{cases} 0.5, & \text{if } \forall m, L_{k,m} = L_{l,m} \\ \sum\limits_{m=1}^{M} |L_{k,m} - L_{l,m}|, & \text{otherwise} \end{cases} \tag{7.7}$$

Thus, if the non-dominated solutions x_k and x_l share the same cells for all M objectives in the PCCS, the parallel cell distance is equal to 0.5 – value chosen in (Hu & Yen, 2015) to avoid division by zero. Since the density of a particle x_k is calculated using the PCD, its value is affected by all its neighbors. The solution with minimum density in the archive is located in the less crowded regions, and therefore might be worth exploring to maintain diversity.

Final archive mechanisms

The best position of each particle, that is P^{best}, is updated as in micro-MOPSO. The auxiliary archive mechanisms of micro-MOPSO remain also unchanged in micro-TVMOPSO; however, the proposed micro-TVMOPSO uses the density operator to prune the non-dominated solutions in the final repository. The leader of the swarm, that is G^{best}, is also selected using the density operator (instead of the crowding distance). The use of the density, which relies on PCCS, instead of the crowding distance should make micro-TVMOPSO more robust in maintaining diversity.

7.2.3 Time-variant parameters

Both micro-MOPSO and micro-TVMOPSO algorithms use the PSO updates given by Equations 2.6 and 2.7. However, instead of using a random inertia weight w, and two constant coefficients c_1 and c_2, whose values were originally set equal to 1.8, micro-TVMOPSO uses time-variant parameters. The velocity constraint mechanism presented in (Nebro et al., 2009), which includes the constriction coefficient χ, requires both c_1 and c_2 to vary randomly in the range [1.5, 2.5]. However, as observed in (Clerc & Kennedy, 2002), *global exploration* is emphasized using larger values for w and c_1, and smaller ones for c_2. On the contrary, *local exploitation* is emphasized using smaller values for w and c_1, and larger ones for c_2. As a result, micro-TVMOPSO is made adaptive by allowing the range of these two parameters as well as that of the inertia weight w to change over time as shown in Equations 7.8a to 7.9c. The range of w and c_1 decreases over generations while that of c_2 increases in order to enhance global exploration at the beginning of the optimization search and local exploitation at the end.

$$w(t) = \text{rand}(0, w_{\text{up}}(t)) \tag{7.8a}$$

$$c_1(t) = \text{rand}(c_{1,\text{up}}(t) - 1, c_{1,\text{up}}(t)) \tag{7.8b}$$

$$c_2(t) = \text{rand}(c_{2,\text{up}}(t) - 1, c_{2,\text{up}}(t)) \tag{7.8c}$$

in which

$$w_{\text{up}}(t) = w_{\text{ini}} - \Delta w \cdot \frac{t}{t_{\max}} \tag{7.9a}$$

$$c_{1,\text{up}}(t) = c_{1,\text{ini}} - \Delta c_1 \cdot \frac{t}{t_{\max}} \tag{7.9b}$$

$$c_{2,\text{up}}(t) = c_{2,\text{ini}} + \Delta c_2 \cdot \frac{t}{t_{\max}} \tag{7.9c}$$

where t and $t_{\max}$ are the generation index and maximum number of generations, respectively; Δw, Δc_1, and Δc_2 are constant increments of w, c_1, and c_2, respectively, whose values are calculated as the absolute difference between the initial ($w_{\text{ini}} = 1.0, c_{1,\text{ini}} = 2.5, c_{2,\text{ini}} = 2.5$) and final values ($w_{\text{fin}} = 0.6, c_{1,\text{fin}} = 1.5, c_{2,\text{fin}} = 3.5$) of w_{up}, $c_{1,\text{up}}$, and $c_{2,\text{up}}$.

The initial and final values of w_{up}, $c_{1,\text{up}}$, and $c_{2,\text{up}}$ are the parameter settings of micro-TVMOPSO which differ from micro-MOPSO. In micro-MOPSO, c_1 was a random number between [0, 1], and c_1 was equal to c_2, which were both set to 1.8. For the proposed micro-TVMOPSO, all the flight

control parameters are random numbers; however, their respective upper boundary varies as the optimization progresses (see Equations 7.9a to 7.9c) to enhance global exploration and local exploitation.

7.3 Experiments and results

The proposed micro-TVMOPSO is applied in this section along with eight other MOO algorithms, including micro-MOPSO, to 24 benchmark problems, and their performance is compared by using two performance metrics.

7.3.1 Algorithms for comparison

Eight MOO algorithms are used for comparison with the micro-TVMOPSO algorithm: (i) Non-dominated Sorting Genetic Algorithm-II (NSGA-II); (ii) Strength Pareto Evolutionary Algorithm 2 (SPEA-2), (iii) Pareto Archived Evolution Strategy (PAES), (iv) Archive-based Hybrid Scatter Search (AbYSS); (v) Multiobjective Evolutionary Algorithm based on Decomposition and Differential Evolution (MOEA/D-DE), (vi) Non-dominated Sorting Genetic Algorithm-III (NSGA-III), (vii) Multi-Objective Particle Swarm Optimization (MOPSO), and (viii) micro-Multi-Objective Particle Swarm Optimization (micro-MOPSO).

NSGA-II (Deb et al., 2002) is one of the most popular genetic algorithms, as mentioned in (Ben Yahia et al., 2015; Ghiasi et al., 2011). Using operators such as selection, crossover, and mutation to generate children from a parent population, NSGA-II sorts its children and parents based on their rank and crowding distance to always maintain its final population at a predefined number. SPEA-2 (Zitzler et al., 2001) is an archive-based multi-objective evolutionary algorithm, which maintains the size of its archive using a clustering technique. New candidate solutions are found by using binary tournament selection and polynomial mutation. PAES (Knowles & Corne, 2000) is also an archive-based multi-objective evolutionary algorithm, using an adaptive grid (i.e., the objective function space is divided into hypercubes) to maintain diversity. As mentioned in (Fuentes Cabrera & Coello Coello, 2010), PAES can be viewed as a form of micro-GA. AbYSS (Nebro et al., 2008) is an archive-based hybrid scatter search, which is based on scatter search templates. MOEA/D-DE (H. Li & Zhang, 2009) is an improved version of the MOEA/D algorithm (Q. Zhang & Li, 2007),

which decomposes MOO problems into a number of single objective optimization sub-problems; the objective of each problem is an aggregation of all the objectives. MOEA/D-DE uses differential evolution operator and polynomial mutation. As mentioned in (Zhou et al., 2011), MOEA/Ds are recent MOO algorithms which have proved to be effective in different application areas. MOPSO (Coello Coello et al., 2004) is the first multi-objective version of PSO. NSGA-III (Deb & Jain, 2014) is an extension of NSGA-II, which maintains diversity by supplying and updating a number of well-spread reference-points. Unlike the previous six optimization algorithms, MOPSO is based on swarm intelligence. Derived from MOPSO, micro-MOPSO (Fuentes Cabrera & Coello Coello, 2010) is a micro-algorithm using the PSO update pattern and two external repositories.

7.3.2 Benchmark problems

The performance of the selected MOO algorithms is assessed using the same seven benchmark problems used in (Fuentes Cabrera & Coello Coello, 2010): bi-objective benchmark problems from the ZDT test suites (Zitzler et al., 2000), KUR (Kursawe, 1996) and VNT3 test problems (Viennet et al., 1996). The analytical formulation of some benchmark problems is reported in Table 7.1. Ten benchmark problems from the Congress on Evolutionary Computation 2009 Competition (Q. Zhang et al., 2009) and seven benchmark problems from the DTLZ suites (Deb et al., 2001) were also used in (Rey & Zmeureanu, 2017). The number of variables used for each benchmark problem is equal to the number used in the reference papers, for instance 30 variables with the ZDT1 benchmark problem.

Table 7.1: Benchmark problems and analytical formulation of their Pareto front

Name	Variable and range	Objective functions
ZDT1	n = 30	$f_1(x) = x_1$
	$x_1, \ldots, x_n \in$ [0,1]	$f_2(x) = g(x) \cdot \left[1 - \sqrt{\frac{f_1(x)}{g(x)}}\right]$
ZDT2	n = 30	$f_1(x) = x_1$
	$x_1, \ldots, x_n \in$ [0,1]	$f_2(x) = g(x) \cdot \left[1 - \left(\frac{f_1(x)}{g(x)}\right)^2\right]$
ZDT3	n = 30	$f_1(x) = x_1$
	$x_1, \ldots, x_n \in$ [0,1]	$f_2(x) = g(x) \cdot \left[1 - \sqrt{\frac{f_1(x)}{g(x)}} - \frac{f_1(x)}{g(x)} \cdot \sin(10 \cdot \pi \cdot x_1)\right]$
ZDT4	n = 10	$f_1(x) = x_1$
	$x_1 \in$ [0,1]	$f_2(x) = g(x) \cdot \left[1 - \sqrt{\frac{x_1}{g(x)}}\right]$
	$x_2, \ldots, x_n \in$ [-5,5]	
ZDT6	n = 10	$f_1(x) = 1 - e^{-4 \cdot x_1} \cdot \sin^6(6 \cdot \pi \cdot x_1)$
	$x_1, \ldots, x_n \in$ [0,1]	$f_2(x) = 1 - \left(\frac{f_1(x)}{g(x)}\right)^2$

where

$$g(x) = \begin{cases} 1 + 9 \cdot \sum_{j=2}^{n} x_j/(n-1), & \text{for ZDT1, ZDT2, or ZDT3} \\ 1 + 10 \cdot (n-1) + \sum_{j=2}^{n} \left[{x_j}^2 - 10 \cdot \cos(4 \cdot \pi \cdot x_j)\right], & \text{for ZDT4} \\ 1 + 9 \left[\sum_{j=2}^{n} x_j/(n-1)\right]^{1/4}, & \text{for ZDT6} \end{cases}$$

7.3.3 Performance metrics

As mentioned in (Reyes-Sierra & Coello Coello, 2006), multi-objective optimization algorithms should provide: (i) convergence, (ii) spread, and (iii) uniformity. A MOO algorithm should minimize the distance between the non-dominated solutions and the true Pareto front (convergence), maximize the spread along the Pareto front (spread), and maximize the number of evenly spaced non-dominated solutions found (uniformity).

Two performance metrics are used to assess the three aforementioned criteria: (i) inverted generational distance (IGD) (Van Veldhuizen & Lamont, 1998) and (ii) hypervolume (HV) (Zitzler & Thiele, 1999). Both have been widely used in (Akay, 2013; Hu & Yen, 2015; Zhan et al., 2009). As reported in (M. Li et al., 2014), HV and IGD involve all the three aspects that performance metrics should cover. In addition, HV and IGD show high consistencies in evaluation compared to

other metrics (Jiang et al., 2014). A short description of those metrics is presented herein.

Inverted generational distance

IGD is a modification of the generational distance, which evaluates the Euclidean distance between each non-dominated solution in the objective space, found by the optimization algorithm, and all solutions from the true Pareto front, and uses the smallest distance found in the summation over all non-dominated solutions; whereas IGD calculates how far each solution of the true Pareto front is from the non-dominated solutions found:

$$\text{IGD} = \frac{\sqrt{\sum_{k=1}^{|P^*|} d(x_k^*, x_{\text{closest}})^2}}{|P^*|} \tag{7.10}$$

where $d(x_k^*, x_{\text{closest}})$ is the Euclidean distance, in the objective space, between the k-th solution of the true Pareto front and the closest non-dominated solution found by the MOO algorithm; $|P^*|$ is the cardinality of the true Pareto front, that is, the number of solutions from the true Pareto front. The smaller IGD, the closest the final non-dominated solutions are to the true Pareto front.

Hypervolume

HV assesses the volume covered by the non-dominated solutions in the objective space, which quantifies and encapsulates both convergence and diversity:

$$\text{HV} = \text{volume}\left(\bigcup_{k=1}^{K} V_k\right) \tag{7.11}$$

where V_k is the k-th hypercube constructed with the k-th solution in the objective space found by the algorithm and an arbitrary selected worst solution used as reference in the objective space (called sometimes the reference set); K is the number of non-dominated solutions found by the optimization algorithm. The closer are the non-dominated solutions found to the true Pareto front or the more evenly distributed, the larger is the value of HV. Unlike the IGD metric, a larger value of HV is desirable.

7.3.4 Results and discussion

For the sake of comparison with the micro-MOPSO algorithm proposed in (Fuentes Cabrera & Coello Coello, 2010), the total number of function evaluations is set equal to 3,000 for all the selected MOO algorithms. The maximum number of generations performed by each MOO algorithm is derived by considering the 3,000 function evaluations and their corresponding population size. The population size and other control parameter settings of each MOO algorithm are taken from their respective reference.

Since the selected MOO algorithms use stochastic methods, the performance of each algorithm is calculated from 120 independent optimization runs of each benchmark problem. All algorithms are launched using Java on an Intel Core i7-3770 CPU @ 3.40 GHz with 8 GB of RAM. The following six algorithms, NSGA-II, SPEA-2, PAES, AbySS, MOEA/D-DE, and NSGA-III are taken from jMetal 5.0 (Durillo & Nebro, 2011), which is an object-oriented Java-based framework for multi-objective optimization. The other three algorithms, MOPSO, micro-MOPSO, and the proposed micro-TVMOPSO, were implemented using the jMetal framework as a starting point. Both IGD and HV are taken directly from jMetal 5.0. Some results from (Rey & Zmeureanu, 2017) are presented in order to give confidence regarding the use of micro-TVMOPSO in the multi-objective optimization framework.

Many MOO algorithms face difficulties in approximating the true Pareto front of multi-frontal problems such that ZDT4, especially for small numbers of generations. Figure 7.1 shows the best results achieved for ZDT4 by NSGA-III, MOPSO, micro-MOPSO, and micro-TVMOPSO based on 120 independent optimization runs. The best approximation of the true Pareto front of ZDT4, that is, the optimization run leading to the smallest value of the IGD metric, is used for comparison. The proposed micro-TVMOPSO algorithm provides better results than the other MOO algorithms.

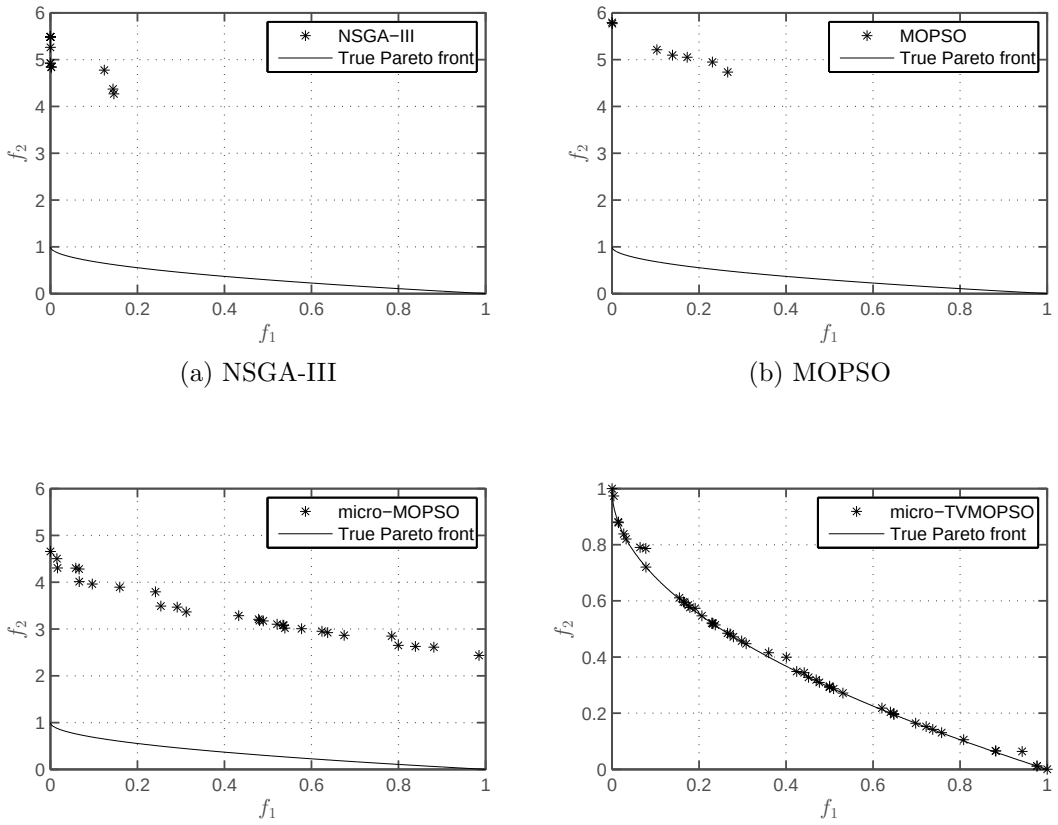

(a) NSGA-III (b) MOPSO

(c) micro-MOPSO (d) micro-TVMOPSO

Figure 7.1: Graphical comparison of the Pareto fronts found for ZDT4

As shown in Figure 7.2, micro-TVMOPSO was efficient at approximating the true Pareto front of other benchmark problems. All these benchmark problems have different properties such as: convex (ZDT1, ZDT4), concave (ZDT2, ZDT6, DTLZ2, DTLZ3, DTLZ4, DTLZ5, and DTLZ6), linear (DTLZ1), mixed (VNT3), discontinuous (ZDT2, DTLZ7), and complicated (UF1-UF10).

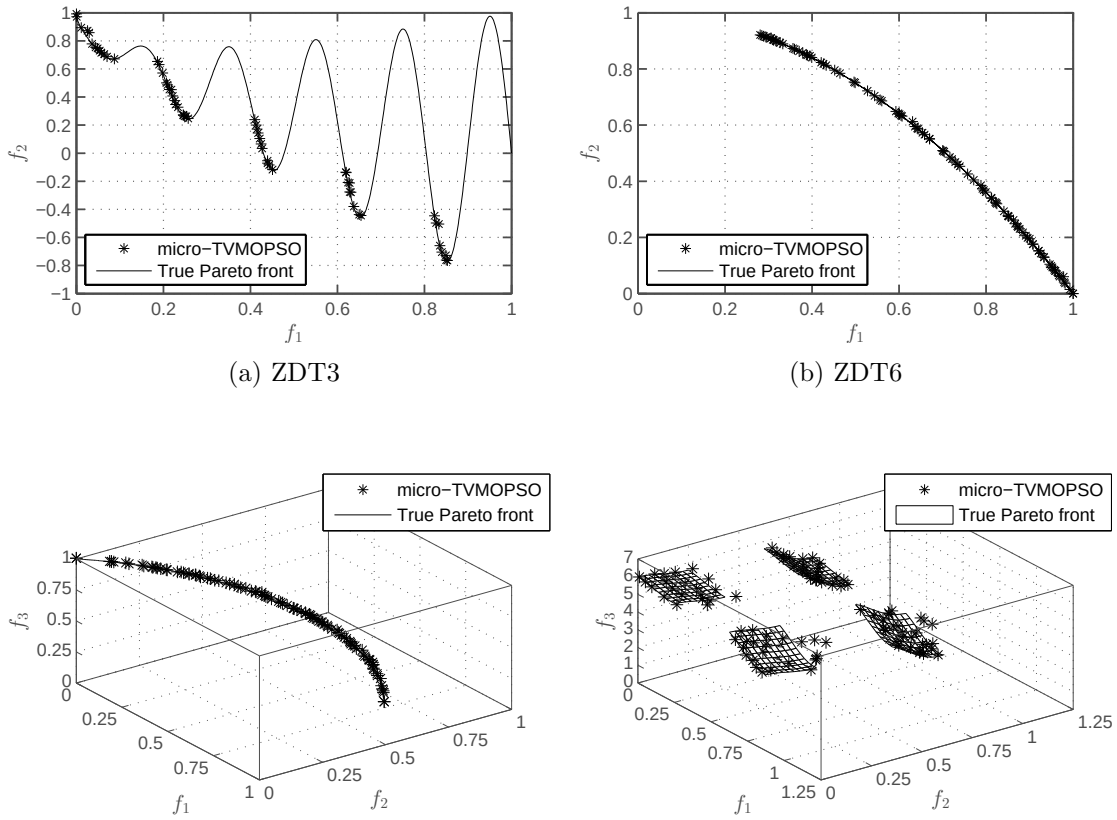

(a) ZDT3 (b) ZDT6

(c) DTLZ5 (d) DTLZ7

Figure 7.2: Micro-TVMOPSO results found on four benchmark problems

Tables 7.2 shows the HV metric of the each MOO algorithm applied to the selected benchmark problems, for which larger values indicate better convergence and spread. The median M(HV) and interquartile range (IQR) are used as an indication of central tendency and a measure of statistical dispersion. For each problem, the best results are highlighted in boldface, while a dash symbol "-" is used when the HV value is equal to zero.

Based on the results, micro-TVMOPSO is found to be efficient for a small number of function evaluations. The proposed micro-TVMOPSO algorithm is therefore used as an optimizer in the multi-objective optimization framework. Since micro-TVMOPSO aims at optimizing a generic solar thermal combisystem modeled in TRNSYS, it must be able to communicate with this external building performance simulation software.

Table 7.2: Comparison of the HV value of micro-TVMOPSO with the other MOO algorithms

Problem	HV	Multi-objective optimization algorithm								
		NSGA-II	SPEA-2	PAES	AbYSS	MOEA/D-DE	NSGA-III	MOPSO	micro-MOPSO	micro-TVMOPSO
ZDT1	M(HV)	0.227000	0.134000	0.492000	0.096800	0.258000	0.375000	0.375000	0.652000	**0.654000**
	IQR	0.060000	0.053000	0.120000	0.130000	0.090000	0.110000	0.150000	0.004500	**0.200000**
ZDT2	M(HV)	-	-	0.171000	-	-	-	0.224000	0.320000	**0.324000**
	IQR	-	-	0.150000	-	-	-	0.140000	0.003700	**0.002100**
ZDT3	M(HV)	0.247000	0.173000	0.347000	0.134000	0.266000	0.297000	0.205000	**0.484000**	0.366000
	IQR	0.036000	0.034000	0.110000	0.086000	0.067000	0.072000	0.120000	**0.020000**	0.160000
ZDT4	M(HV)	-	-	-	-	-	-	-	-	**0.579000**
	IQR	-	-	-	-	-	-	-	-	**0.063000**
ZDT6	M(HV)	-	-	0.451000	0.003440	0.255000	0.202000	0.530000	0.462000	**0.535000**
	IQR	-	-	0.300000	0.038000	0.077000	0.086000	0.038000	0.160000	**0.012000**
KUR	M(HV)	0.396000	0.395000	0.391000	**0.398000**	0.350000	0.321000	0.386000	0.377000	0.376000
	IQR	0.001800	0.002500	0.003000	**0.001700**	0.018000	0.051000	0.002800	0.008600	0.008800
VNT3	M(HV)	0.833000	0.829000	0.831000	0.832000	0.832000	0.828000	0.833000	**0.832000**	0.831000
	IQR	0.000780	0.134000	0.492000	0.096800	0.001800	0.375000	0.375000	**0.652000**	0.001300

7.4 Coupling of the generic model and optimization algorithm

Any multi-objective optimization problem involving implicit objective functions, which are evaluated by an external software through a procedure or subroutine, requires the selected multi-objective optimization algorithm to communicate with the external software. Communication involves an information source, which sends a message to a receiver. The goal of such a process is to exchange information, and therefore receivers must understand messages. In this case, micro-TVMOPSO and TRNSYS are both information source and receiver. As a result, micro-TVMPSO was coupled with TRNSYS as shown in Figure 7.3.

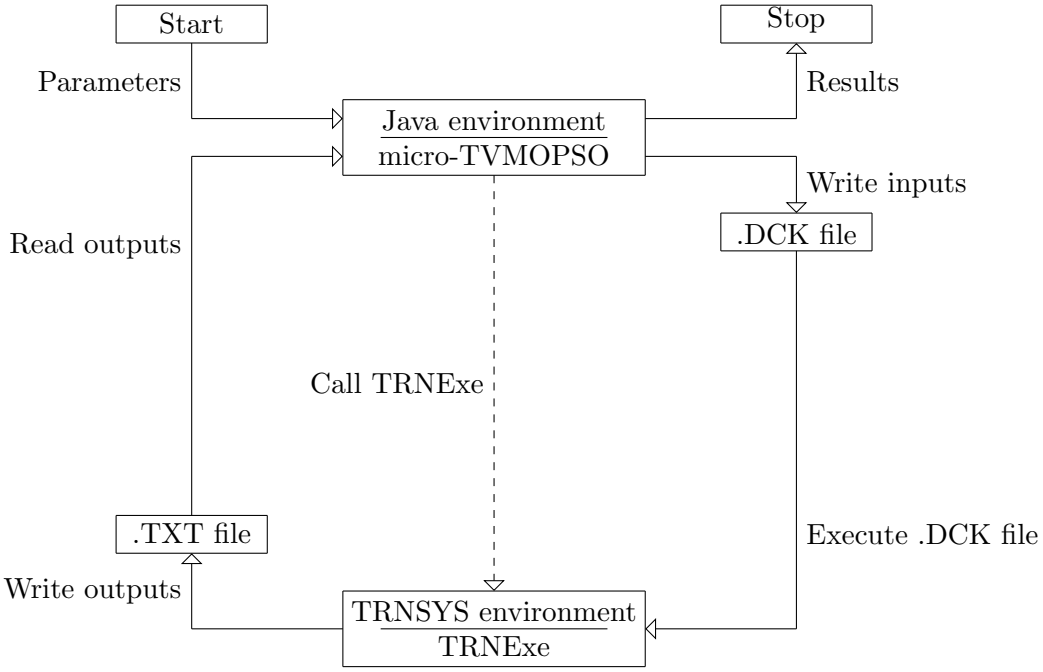

Figure 7.3: Flowchart of the intercommunication between micro-TVMOPSO and TRNSYS

The Java-based program – including the micro-TVMOPSO algorithm – starts by writing the values of the selected design variables in the TRNSYS deck file, which is a text file that contains all inputs for the TRNSYS simulation engine. Afterwards, micro-TVMOPSO calls TRNExe to launch TRNSYS simulations. In the TRNSYS environment, an output type writes the value of each objective function in a text file. After the TRNSYS simulation are completed, the micro-TVMOPSO extracts the value of each objective function. This process continues until the termination criterion is met, that is to say the maximum number of micro-TVMOPSO generations is reached. Since

the coupling process involves text files, micro-TVMOPSO could be coupled with other building performance simulation programs, such as EnergyPlus or Dymola. As long as the external software reads its inputs from text files and writes its outputs to text files, micro-TVMOPSO could be used. Since Java is an object-oriented programming, the capability of reading from and writing to text files is not specific to micro-TVMOPSO. In other words, any other multi-objective optimization algorithm developed in the same way as micro-TVMOPSO could communicate with an external software. Finally, Java is platform independent, so this process could work on any platform.

Chapter 8

Case study no. 1: Montreal, Quebec, Canada[1]

This chapter concentrates on the simulation-based residential solar thermal combisystem developed in (Leckner, 2008). This solar thermal combisystem was part of a net-zero energy house (NZEH), which was an energy efficient modified version of a typical 1994 Quebec house construction. Since the NZEH was achieved using photovoltaic panels, which are not considered in this doctoral thesis, the term is replaced by energy efficient house (EEH). The main details of the EEH and its solar thermal combisystem are first provided. An analysis of the solar thermal combisystem is then performed to provide some insights regarding its general behavior. Subsequently, a multi-objective optimization of the solar thermal combisystem is executed using the framework and micro-TVMOPSO algorithm developed in Chapters 6 and 7.

8.1 Overview of the EEH and its solar combisystem

This section presents the main physical properties of the energy efficient house and solar thermal combisystem developed in (Leckner, 2008). The objective is to present the base case before performing a multi-objective optimization to find what could be improved.

[1]This chapter is mainly based on the paper "Rey, A., & Zmeureanu, R. (2017). Multi-objective optimization framework for the selection of configuration and equipment sizing of solar thermal combisystems. Manuscript submitted for publication."

8.1.1 Energy efficient house model

The EEH is an energy efficient modified version of a typical 1994 Quebec house construction, developed in (Leckner, 2008). The EEH was originally equipped with photovoltaic panels to supply the additional energy demands for the house; however, photovoltaic panels are not considered in this thesis as they are beyond its scope. The EEH is a two story wood framed detached house with a total heated area of 208.4 m^2 and a natural infiltration of 1.22 air change per hour at 50 Pa. The house is divided into five zones in the TNRSYS environment: the unheated garage, three heated spaces, and unheated attic. The EEH's walls and windows comply with the minimum requirements of the R-2000 building standard in terms of thermal resistance (Leckner, 2008).

The EEH, whose artificial lighting is provided by compact fluorescent lamps, is modeled for a family of two parents and three children. The appliances used in the EEH are taken from EnerGuide and Energy Star listings, where 100% of the energy is converted into convected heat gains (Leckner, 2008). The hourly schedule for domestic hot water use is based on (Perlman & Mills, 1985), which corresponds to an overall consumption of 236 liters per day. As the EEH was assumed to be equipped with efficient low-flow mixtures and aerators, the hot water flow rate was reduced by 30% (Leckner, 2008). A thermostatic mixing valve was also installed on the DHW tank to enable the water within the tank to be at a temperature higher than 55°C, which corresponds to a lower limit to prevent Legionnaires' disease. The water going out of the thermal storage tank is therefore mixed with cold city water by the thermostatic mixing valve to ensure a constant temperature of 49°C. Finally, the EEH had a drain water heat recovery system to preheat the incoming cold city water using the wasted heat from the warm drain water (Leckner, 2008).

8.1.2 Solar combisystem model

Figure 8.1 shows the scheme of the solar thermal combisystem used in this first case study. This residential solar combisystem was developed in (Leckner, 2008) using TRNSYS. The solar combisystem configuration has two thermal storage tanks, one is dedicated to the DHW preparation, while the other is dedicated to the SH needs. Both the radiant floor and domestic hot water tanks are charged by solar energy through the flat-plate solar collectors array, and by electricity through their respective electrical heating elements.

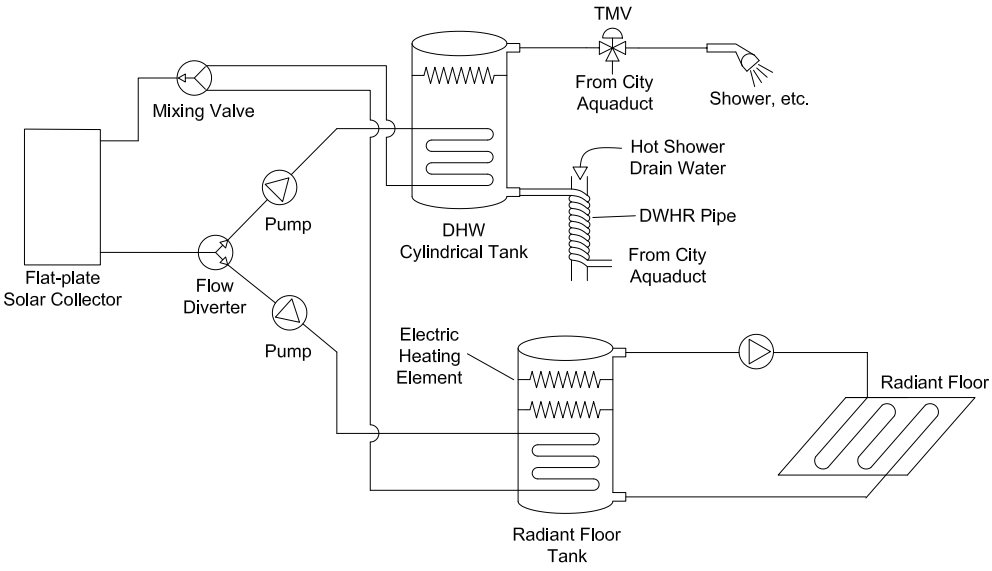

Figure 8.1: Scheme of the solar combisystem modeled in (Leckner, 2008)

Control strategies

As shown in figure 8.1, the 60% glycol-water mixture leaving the array of solar thermal collectors goes through a flow diverter (Type 11f), which is controlled by a differential controller (Type 2b) and a TRNSYS equation block to give priority to the RF tank. Solar energy harvested by the solar collectors as heat will be transferred to the RF tank if the following three conditions are met (Leckner, 2008): (i) it is the heating season (i.e., from October 17th to May 1st), (ii) the temperature of the glycol-water mixture is higher than that of the water in the tank surrounding the exiting section of the heat exchanger, and (iii) the temperature of the water in the top layer of the tank is less than to 55°C. If one of these conditions is violated, a second differential controller comes into play to determine whether the glycol-water mixture should be directed to the DHW tank. Two conditions must be met: (i) the temperature of the glycol-water mixture is higher than that of the water in the tank surrounding the exiting section of the heat exchanger, and (ii) the temperature of the water in the top layer of the tank is less than to 85°C. If none of these five conditions are met, no pump circulates the glycol-water mixture.

The immersed electrical heating elements are controlled using a 3-stage room thermostat and temperature deadband (Type 8b) as well as a TRNSYS equation block. To ensure thermal comfort,

the auxiliary heating elements in the upper and lower parts of the RF tank are turned on when the temperature on the top floor of the house drops below 21°C and 18°C, respectively, with a deadband of 0.5°C. These two temperature setpoints are set back by 3°C at night (i.e., from 11 pm to 7 am) to reduce energy use. The electrical heating element within the DHW tank is activated when the temperature of the water in the top layer drops below 55°C.

Simulation results from the EEH with base case solar combisystem

The initial solar combisystem shown in Figure 8.1 has two 300-L vertical thermal storage tanks. Both radiant floor (RF) and DHW tanks are charged by solar energy through four flat-plate solar collectors in parallel, each having an area of 2.51 m^2, and by electricity through their respective electric heating elements. The south-facing flat-plate collectors are roof-mounted with a tilt angle of 45°. The DHW tank has one heating element of 1 kW while the RF tank is equipped with two heating elements of 2 kW and 4 kW from top to bottom location. A one-year simulation of the energy efficiency house equipped with the base case thermal combisystem was performed in TRNSYS using a time step of 10 minutes and yielded a total electricity requirement for one year of 11,255 kWh, which corresponds to 54 kWh/m^2. With 15.8 kWh/m^2, that is 29.2%, space heating accounts for the most important energy end-use, whereas domestic hot water corresponds to only 2.7% with 310.8 kWh per year.

8.2 Optimization results and discussion

The multi-objective optimization aims at finding non-dominated design solutions for the solar combisystem configuration and equipment sizing based on the four objective functions (LCC, LCE, $LCX_{technical}$, and $LCX_{physical}$). The initial solar combisystem design was used as one of the candidate solutions of the first generation of micro-TVMOPSO. Due to the time-consuming nature of one single TRNSYS simulation (around 25 minutes), a maximum number of 100 generations was selected; the micro-TVMOPSO algorithm used five particles, which results in 500 TRNSYS simulations (five particles times 100 generations). For 500 TRNSYS simulations, micro-TVMOPSO lasted approximately 39 hours (i.e., one day and 14 hours). A total of 15 non-dominated solutions were found. For example, Figure 8.2 shows the nine non-dominated solutions out of the 15 solutions,

when only LCC and LCE objective functions are taken into consideration.

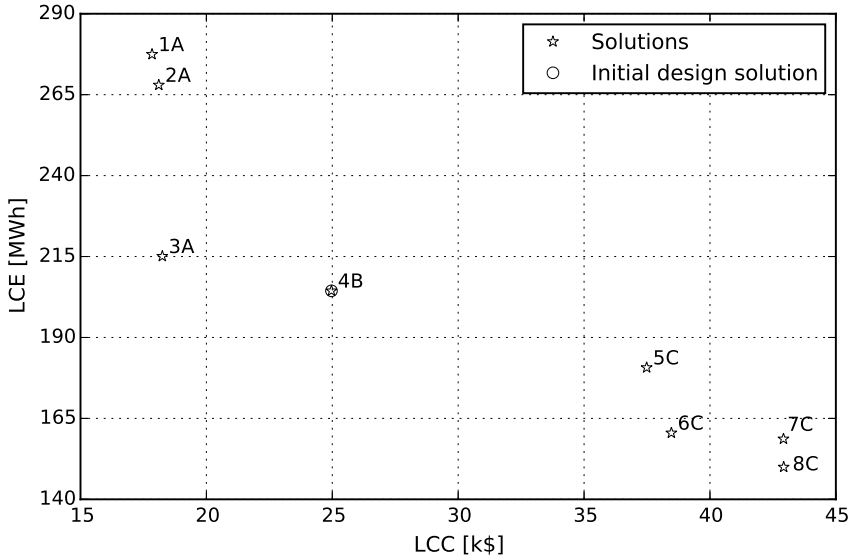

Figure 8.2: LCE vs. LCC approximation of the Pareto front using micro-TVMOPSO for Case study no. 1

As shown in Figure 8.3, three different solar combisystem configurations were found, each one with different equipment sizing. As shown in Table 8.1, configuration A, with solutions 1A, 2A, and 3A, corresponds to the non-dominated solutions having the lowest LCC values. This configuration uses flat-plate collectors ($B_1^1 = 1$) and one relatively small thermal storage tank without stratifying devices ($B_4^1 = 1$).

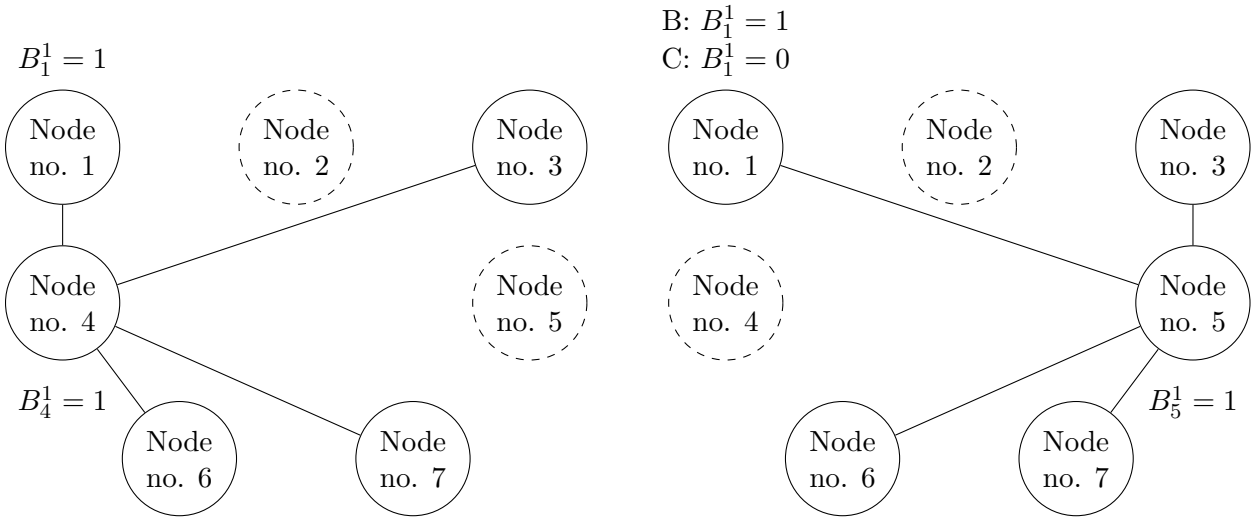

(a) Configuration A (b) Configurations B and C

Figure 8.3: Configurations of the Pareto solutions found by micro-TVMOPSO for LCE vs. LCC for Case study no. 1

Both configurations B and C have two thermal storage tanks without stratifying devices; the configuration B is equipped with flat-plate collectors ($B_1^1 = 1$) whereas configuration C is equipped with evacuated tube collectors ($B_1^2 = 1$). Two thermal storage tanks enable a better thermal stratification, which reduces the LCE value. Non-dominated solutions having the configuration C, with solutions 6C, 7C, and 8C, are represented at the lower right corner since they lead to the lowest LCE values, but also higher LCC ones. Low LCE values can be achieved by increasing the number of solar collectors; however, a trade-off exists between the energy savings and embodied energy. ETCs are more energetically efficient, but more expensive than FPCs. The former is preferred to reduce the LCE objective function, while the latter is more suitable for decreasing the LCC objective function. An increase of the concrete heating floor slab thickness enables storing more thermal energy, which saves energy and reduces temperature swings inside the house, but increases the initial cost.

The characteristics of five out of the eight non-dominated solutions are listed in Table 8.1. Micro-TVMOPSO found a non-dominated solution (no. 1) that reduced the LCC value by 29% compared with the initial design solution (no. 4), but increased the LCE value by 72%. To the other extreme, solution no. 8 reduced the LCE value by 27%, and increased the LCC value by 36%. Compared to the initial design solution (solution no. 4), higher solar collector inclinations were

found for both LCC and LCE objective functions, which generate higher water temperatures during the heating season. An increase of the number of solar collectors and thickness of the concrete floor slab from 0.06 m (solution no. 1) to 0.20 m (solution no. 8) resulted in a significant increase of LCC from $17,840 to $42,930, while the LCE decreased from 277.46 MWh to 149.96 MWh. Storage tank volumes can remain unchanged with an increase of slab thickness (e.g., solutions no. 4 and no. 6). All the non-dominated solutions used internal electrical resistances ($B_3^1 = 1$) rather than external water heaters. External water heaters might therefore not be suitable under such financial and environment conditions.

Table 8.1: Decision variable values of some non-dominated solutions found by micro-TVMOPSO for LCE vs. LCC for Case study no. 1

Decision variable	Solution				
	No. 1	No. 3	No. 4	No. 6	No. 8
Configuration	A	A	B	C	C
$B_{1,4}$	1	1	0	0	0
$B_{1,5}$	0	0	1	1	1
$B_{2,4}$	0	0	0	0	0
$B_{2,5}$	0	0	0	0	0
$B_{3,4}$	1	1	0	0	0
$B_{3,5}$	0	0	1	1	1
$B_{4,6}$	1	1	0	0	0
$B_{4,7}$	1	1	0	0	0
$B_{5,6}$	0	0	1	1	1
$B_{5,7}$	0	0	1	1	1
B_1^1	1	1	1	0	0
B_1^2	0	0	0	1	1
B_2^1	0	0	0	0	0
B_2^2	0	0	0	0	0
B_3^1	1	1	1	1	1
B_3^2	0	0	0	0	0
B_3^3	0	0	0	0	0
B_4^1	1	1	0	0	0
B_4^2	0	0	0	0	0
B_5^1	0	0	1	1	1
B_5^2	0	0	0	0	0
Number of flat-plate collectors [-]	1	3	4	–	–
Number of evacuated-tube collectors [-]	–	–	–	7	7
Tilt angle of array A1 [°]	60	65	45	75	70
Tilt angle of array A2 [°]	–	–	–	–	–
Flow rate per collector area [kg/(h·m$^2_{\text{coll}}$)]	115.0	80.0	45.0	39.6	9.9
Volume of tank no. 1 (DHW or both) [L]	500	500	300	300	300
Volume of tank no. 2 (SH) [L]	–	–	300	300	1,100
Tank no. 1 auxiliary power at high location [kW]	8.5	3	1	7.5	5.5
Tank no. 1 auxiliary power at low location [kW]	6.5	14	0	5.5	5.5
Tank no. 2 auxiliary power at high location [kW]	–	–	2	1	1
Tank no. 2 auxiliary power at low location [kW]	–	–	4	14.5	14.5
DHW heater auxiliary power [kW]	–	–	–	–	–
SH heater auxiliary power [kW]	–	–	–	–	–
Floor slab thickness [m]	0.06	0.06	0.06	0.20	0.20
Objective function					
Life cycle cost [k$]	17.84	18.25	24.97	38.47	42.93
Life cycle energy use [MWh]	277.46	215.08	204.42	160.51	149.96
Life cycle exergy destroyed (technical boundary) [MWh]	361.49	481.62	547.07	770.59	778.20
Life cycle exergy destroyed (physical boundary) [MWh]	262.09	204.71	164.41	124.67	120.35

Figure 8.4 shows six non-dominated solutions when only the $LCX_{technical}$ and $LCX_{physical}$ objective functions are taken into consideration, while Table 8.2 shows some of their characteristics.

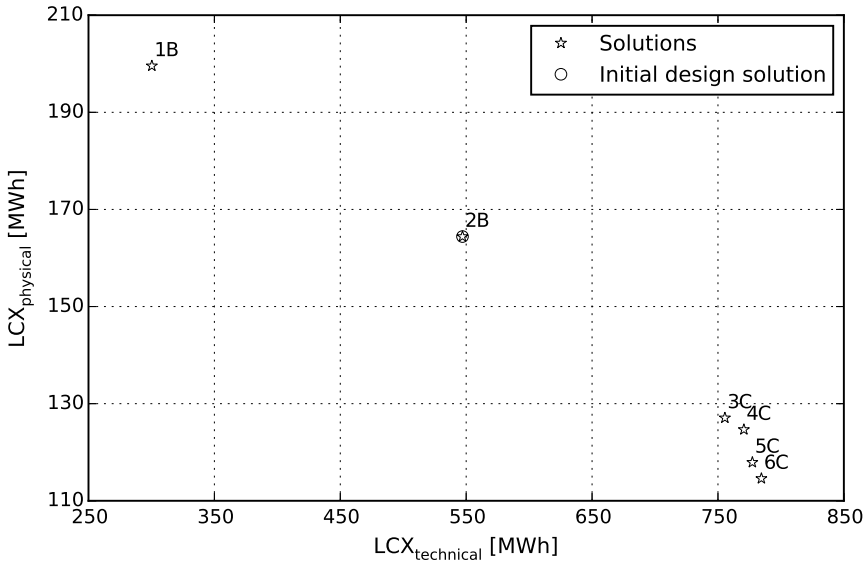

Figure 8.4: $LCX_{physical}$ vs. $LCX_{technical}$ approximation of the Pareto front using micro-TVMOPSO for Case study no. 1

Compared to the initial design solution (solution no. 2), micro-TVMOPSO was able to find more exergy-effective solutions using both boundaries. Only configurations B and C were found to minimize the exergy destruction. While the minimum $LCX_{technical}$ was obtained by using one single FPC, the minimum $LCX_{physical}$ was achieved with seven ETCs. As already observed in (Ng Cheng Hin & Zmeureanu, 2014), the LCC and $LCX_{technical}$ objective functions present similarities, so do the LCE and $LCX_{physical}$. Compared to the initial design solution, the micro-TVMOPSO algorithm was able to reduce the $LCX_{technical}$ and $LCX_{physical}$ by 45.1% and 28.3%, respectively.

Table 8.2: Decision variable values of some non-dominated solutions found by micro-TVMOPSO for $LCX_{physical}$ vs. $LCX_{technical}$ for Case study no. 1

Decision variable	Solution			
	No. 1	No. 2	No. 3	No. 6
Configuration	B	B	C	C
Number of flat-plate collectors [-]	1	4	–	–
Number of evacuated-tube collectors [-]	–	-	7	7
Tilt angle of array A1 [°]	60	45	80	65
Tilt angle of array A2 [°]	–	–	–	–
Flow rate per collector area [kg/(h·m$^2_{coll}$)]	20.0	45.0	40.1	39.6
Volume of tank no. 1 (DHW or both) [L]	300	300	300	300
Volume of tank no. 2 (SH) [L]	100	300	300	1,100
Tank no. 1 auxiliary power at high location [kW]	0.5	1	5.5	7.5
Tank no. 1 auxiliary power at low location [kW]	0.5	0	5.5	5.5
Tank no. 2 auxiliary power at high location [kW]	3	2	1	1
Tank no. 2 auxiliary power at low location [kW]	0.5	4	14.5	14.5
DHW heater auxiliary power [kW]	–	–	–	–
SH heater auxiliary power [kW]	–	–	–	–
Floor slab thickness [m]	0.06	0.06	0.26	0.20
Objective function				
Life cycle cost [k$]	19.32	24.97	43.11	42.98
Life cycle energy use [MWh]	238.33	204.42	146.18	150.50
Life cycle exergy destroyed (technical boundary) [MWh]	300.34	547.07	755.50	784.49
Life cycle exergy destroyed (physical boundary) [MWh]	199.67	164.41	127.07	114.59

The multi-objective optimization framework was able to reduce, compared to the initial design solution, the life cycle cost by 28.6%, the life cycle energy use by 26.6%, the life cycle exergy destroyed by 45.1% for technical boundary and by 28.3% for the physical boundary, respectively. The solar fraction, which is part of all the needs covered by solar energy, is also included in Table 7.3 for comparison purposes. The LCC and $LCX_{technical}$ optimal combisystem designs, which tend to reduce the number of solar collectors, have smaller solar fraction values of 0.21 and 0.26, compared to the LCE and $LCX_{physical}$ optimal combisystem designs whose solar fraction values are equal to 0.72 and 0.74, respectively.

The different configurations and equipment sizing found by the multi-objective optimization framework are not necessarily the best feasible designs, since there is no guarantee of finding the Pareto front for such a search space (without testing all the decision vectors). Nevertheless, the multi-objective optimization framework was able to find a reduction of each objective compared to the initial design solution (i.e., base case solar combisystem). One storage tank with a small

number of flat-plate collectors was found to be the best way of reducing the LCC value. Using two thermal storage tanks enhances thermal stratification and reduces the LCE, $LCX_{technical}$ and $LCX_{physical}$. No configuration used external auxiliary heaters, since their initial cost is not offset by future energy savings. Natural gas is not a viable option for such an energy efficient house located in a province where the cost of electricity is low. Different designs could be however found for different climatic and financial conditions. For countries where the price of electricity is more expensive, a larger number of solar thermal collectors could be found as well as larger thermal storage tanks to store more solar energy. Evacuated-tube collectors could even be a viable alternative to flat-plate collectors.

Chapter 9

Case study no. 2: Massachusetts, USA

This chapter focuses on a solar thermal combisystem installed in Massachusetts, USA. One of the leading international manufacturers of solar water heating technologies has given accessed to data collection from this solar combisystem, which has been monitored since January 2014. Measurements are used to validate the solar combisystem model. Afterwards, a multi-objective optimization is performed using the framework developed in Chapter 6.

9.1 Overview of the residential solar combisystem

As shown in Figure 9.1, the solar thermal combisystem is composed of two distinct arrays of three solar thermal collectors each, giving a total of six solar thermal collectors. Both arrays of solar thermal collectors (i.e., arrays A1 and A2) are south-facing, but have two distinct tilt angles equal to 90° and 65° above the horizontal, respectively. Solar energy is harvested by a heat-transfer fluid, which is a 40% glycol-water mixture, going through the solar thermal collectors.

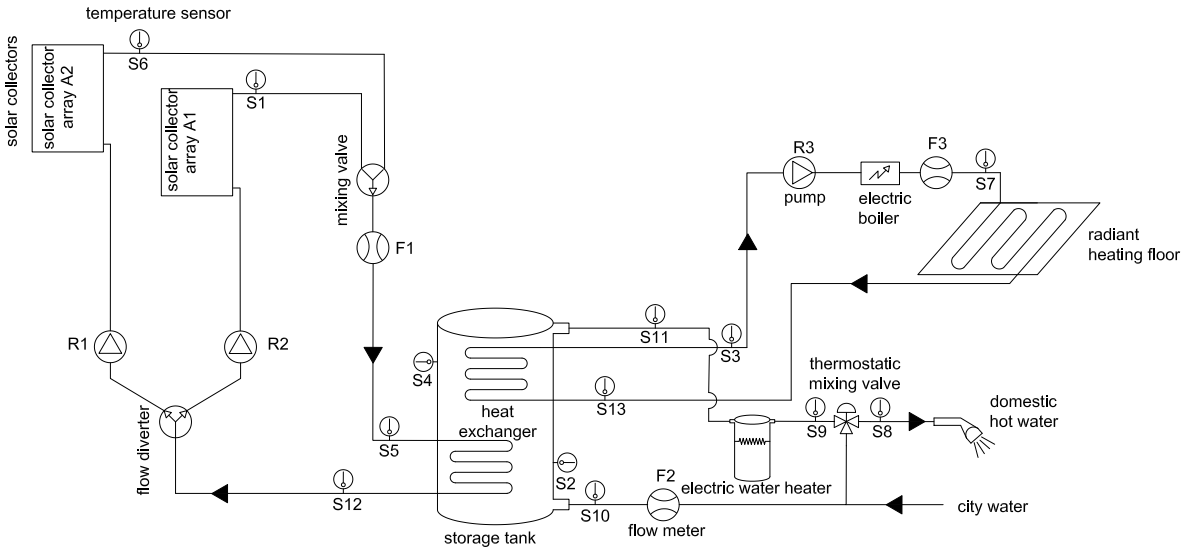

Figure 9.1: Scheme of the monitored solar combisystem installed in Massachusetts, USA

One storage tank, which allows solar energy to be stored, is used for the domestic hot water and space heating needs. Additional energy is provided, when required, by an electric boiler for the radiant floor and by an electric water heater for the domestic hot water. Temperature sensors and flow meters have been installed at the location indicated in Figure 9.1 and record measurements every minute. Average values are calculated to provide other data resolutions: five-minute interval, hourly, and daily. Hourly values are used, unless otherwise stated. Table 9.1 lists all the available sensors. All the mass flow rates are provided in L/min but were converted to kg/s, unless otherwise stated.

Table 9.1: List of the sensors monitoring the solar thermal combisystem

Sensor	Measured physical quantity	Unit
S0	Outdoor air temperature (available only since March 2015)	°C
S1	Outlet temperature of A2 array	°C
S2	Temperature of the lower part of the storage tank	°C
S3	Temperature of the water leaving the tank and going to the radiant floor	°C
S4	Temperature of the upper part of the storage tank	°C
S5	Average temperature from both arrays of solar collectors	°C
S6	Outlet temperature of A1 array	°C
S7	Supply temperature for the radiant floor	°C
S8	Supply domestic hot water temperature	°C
S9	Temperature leaving the electrical water heater	°C
S10	Temperature of the city water	°C
S11	Temperature of the hot water leaving the thermal storage tank	°C
S12	Return temperature to the solar thermal collectors	°C
S13	Return temperature from the radiant floor	°C
F1	Mass flow rate of the heat-transfer fluid of the solar collector loop	L/min
F2	Mass flow rate of the cold city water	L/min
F3	Mass flow rate of the water going through the radiant floor	L/min

The solar thermal combisystem is installed in a house of approximately 110 m^2, inhabited by a family; however, no detailed information about the house nor about the energy-related people's behavior is available. As the outside air temperature and solar radiation were not measured on site during the validating period, they were obtained for the year 2014 from (Weather Analytics, 2016) and for the year 2016 from (IES, 2017).

9.2 Energy performance indices

Two energy performance indices were selected to assess the energy performance of the solar thermal combisystem:

1. Thermal efficiency of the solar collectors;

2. Thermal energy stored in the storage tank.

As shown in Figure 9.1, the residential solar thermal combisystem has two different flat-plate collector arrays in parallel, A1 and A2, which have two distinct tilt angles equal to 90° and 65°, respectively. Therefore, the thermal efficiency given in Equation 5.3 is estimated as:

$$\eta_{\text{coll}} = 100 \cdot \frac{\dot{m}_{\text{coll,F1}} \cdot c_{\text{p,coll}} \cdot (T_{\text{S5}} - T_{\text{S12}})}{A_{\text{A1}} \cdot G_{\text{tot,A1}} + A_{\text{A2}} \cdot G_{\text{tot,A2}}} \tag{9.1}$$

where $\dot{m}_{\text{coll,F1}}$ is the total heat-transfer fluid mass flow rate [kg/s]; T_{S5} and T_{S12} are the outlet and inlet temperatures of the flat-plate collector arrays [°C], respectively; A_{A1} and A_{A2} are the gross areas of the solar collector arrays A1 and A2 [m^2], respectively; $G_{\text{tot,A1}}$ and $G_{\text{tot,A2}}$ are the total solar irradiances incident on the solar collector arrays A1 and A2 [W/m^2], respectively.

Since the thermal storage tank is not equipped with any electric heater, its thermal energy stored, denoted by Q_{stored}, can be calculated as:

$$Q_{\text{stored}} = Q_{\text{supply}} - (Q_{\text{DHW,tank}} + Q_{\text{SH,tank}}) \tag{9.2}$$

in which each component can be calculated as follows:

$$Q_{\text{supply}} = \Delta t \cdot \dot{m}_{\text{coll,F1}} \cdot c_{\text{p,coll}} \cdot (T_{\text{S5}} - T_{\text{S12}}) \tag{9.3}$$

$$Q_{\text{DHW,tank}} = \Delta t \cdot \dot{m}_{\text{DHW,F2}} \cdot c_{\text{p,water}} \cdot (T_{\text{S11}} - T_{\text{S10}}) \tag{9.4}$$

$$Q_{\text{SH,tank}} = \Delta t \cdot \dot{m}_{\text{SH,F3}} \cdot c_{\text{p,water}} \cdot (T_{\text{S3}} - T_{\text{S13}}) \tag{9.5}$$

where Q_{supply} is the solar energy supplied as heat to the thermal storage tank [J]; $Q_{\text{DHW,tank}}$ and $Q_{\text{SH,tank}}$ are the amounts of energy supplied by the storage tank for domestic hot water and space heating purposes [J], respectively; Δt is the time step between two measurements [s]; $\dot{m}_{\text{DHW,F2}}$ and $\dot{m}_{\text{SH,F3}}$ are the water mass flow rate for DHW and SH needs [kg/s], respectively; $c_{\text{p,water}}$ is the specific heat capacity of water at constant pressure [J/(kg·°C)]; T_{S11} and T_{S10} are the temperatures of the water leaving and entering the thermal storage tank [°C], respectively; T_{S3} and T_{S13} are the temperatures of the water leaving and entering the internal heat exchanger within the thermal storage tank for spacing heating [°C], respectively.

The domestic hot water and space heating energy needs $Q_{\text{DHW,aux}}$ and $Q_{\text{SH,aux}}$, which take into account additional auxiliary energy use, are expressed as:

$$Q_{\text{DHW,aux}} = \Delta t \cdot \dot{m}_{\text{DHW,F2}} \cdot c_{\text{p,water}} \cdot (T_{\text{S9}} - T_{\text{S10}}) \tag{9.6}$$

$$Q_{\text{SH,aux}} = \Delta t \cdot \dot{m}_{\text{SH,F3}} \cdot c_{\text{p,water}} \cdot (T_{\text{S7}} - T_{\text{S13}}) \tag{9.7}$$

where T_{S9} and T_{S7} are the temperatures of the water leaving the electric water heater and electric boiler [°C], respectively.

9.3 Data analysis of the monitored solar combisystem

Data collection gives the opportunity of gathering information that can provide valuable insights; however, the misuse of data can lead to false conclusions. Anything being measured has an inherent noise or randomness which introduces uncertainty. As mentioned in (Reddy, 2011), measurements made in the field are more subject to errors than the ones made under the controlled conditions of a laboratory setting. Uncertainty arises from any measurement, so the uncertainty analysis is necessary. Data analysis including outlier detection is therefore conducted to extract useful information from the monitored solar thermal combisystem, followed by the uncertainty analysis.

9.3.1 Outlier detection and missing data

As defined in (Hawkins, 1980), "an outlier is an observation which deviates so much from the other observations as to arouse suspicious that is was generated by a different mechanism". Outlier detection consists in identifying data points which differ significantly from the remaining data. One of the most common methods to cope with outliers disregards data points lying outside the mean of the data set plus or minus its standard deviation times a coefficient, which is usually equal to two or three.

Nevertheless, as mentioned in (Leys et al., 2013), three problems come up from using such a method: (i) the distribution is assumed to be normal (including outliers), (ii) both the mean and standard deviation are strongly influenced by outliers, and (iii) it is highly unlikely to detect outliers in small sample (Cousineau & Chartier, 2010). As a result, the median absolute deviation (MAD) was proposed as an alternative in (Leys et al., 2013). The median of a set of values, denoted by M, gives an indication of central tendency while being less sensitive to outliers. The MAD is defined as follows (Huber, 1981):

$$\mathrm{MAD}\,(x) = b \cdot \mathrm{M}\,(|x_i - \mathrm{M}\,(x)\,|) \tag{9.8}$$

where x_i is the i-th occurrence of a batch of observations denoted by x; $\mathrm{M}(\cdot)$ is the median operator; b is a constant, whose value has as an impact on the outlier detection. The higher it is, the more conservative the outlier detection becomes.

A value of 2.5 was suggested in (Leys et al., 2013). Following this recommendation, the median

absolute deviation of the thermal efficiency of the flat-plate collectors, as shown in Equation 9.9, is used to detect outliers from the data gathered between January 1st and December 31st, 2014.

Prior to screening the measurements for outliers, missing data should be handled. As mentioned in (Reddy, 2011), several approaches can be applied to deal with missing data. The simplest and most obvious is to use observations with complete data only. Such an approach does not cause the analysis to become biased if the missing data fraction is not substantial. As shown in Figure 9.2, three periods of missing data for the year 2014 (pointed out by the missing data labels) are determined using the average temperature leaving the two distinct arrays of flat-plate collectors, which is monitored by the sensor S5: (i) March 8th to March 11th, (ii) September 15th from 1:00 am to 2:00 am, and (iii) November 27th from 3:00 pm to 5:00 pm.

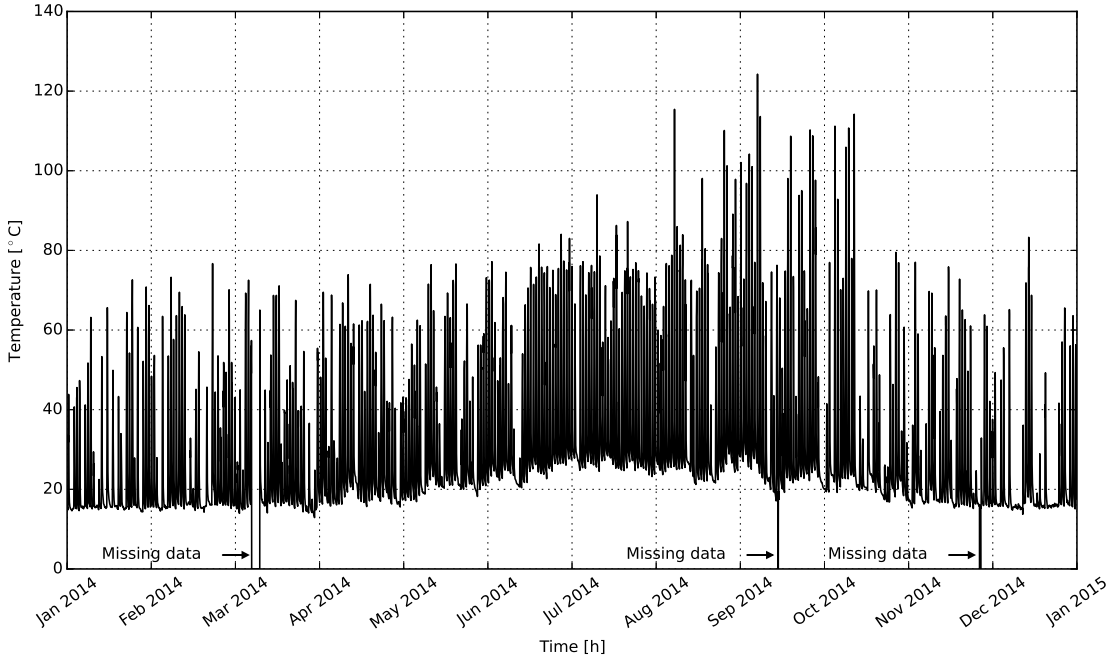

Figure 9.2: Heat-transfer fluid temperature measured by the sensor S5 from January 1st to December 31st, 2014

These three periods are not taken into consideration in the data analysis. After handling missing data, data points associated with a thermal efficiency value greater than 100%, which is physically impossible, were discarded as obvious outliers. An outlier detection using the MAD of the thermal efficiency of the flat-plate collectors is then performed as:

$$\eta_{\text{coll},i} \text{ is } \begin{cases} \text{an outlier,} & \text{if } \eta_{\text{coll},i} > MAD\left(\eta_{\text{coll},i}\right) = 2.5 \cdot \text{M}\left(\left|\eta_{\text{coll},i} - \text{M}\left(\eta_{\text{coll}}\right)\right|\right) \\ \text{not an outlier,} & \text{otherwise} \end{cases} \tag{9.9}$$

where $\eta_{\text{coll},i}$ is the i-th occurrence of the batch of thermal efficiency values, which is calculated with Equation 9.1.

The hourly measurements required to calculate η_{coll} are first divided into two categories: the heating season (i.e., from October 15th to May 10th) and non-heating season (i.e., from May 11th to October 14th). This separation allows taking into account that the solar thermal combisystem does not operate similarly during each of the two seasons. Each category is then subdivided into 24 bins to group the measurements per hour. For example, all the measurements between 3:00 pm and 4:00 pm during the heating season are stored in the same bin. Breaking the data based on the hour of the day better represents the daily pattern of solar availability and energy use in the house. Figure 9.4b presents the measurements from Figure 9.4a, where the outliers detected by the MAD of the thermal efficiency on a scale of 0% to 100% were removed.

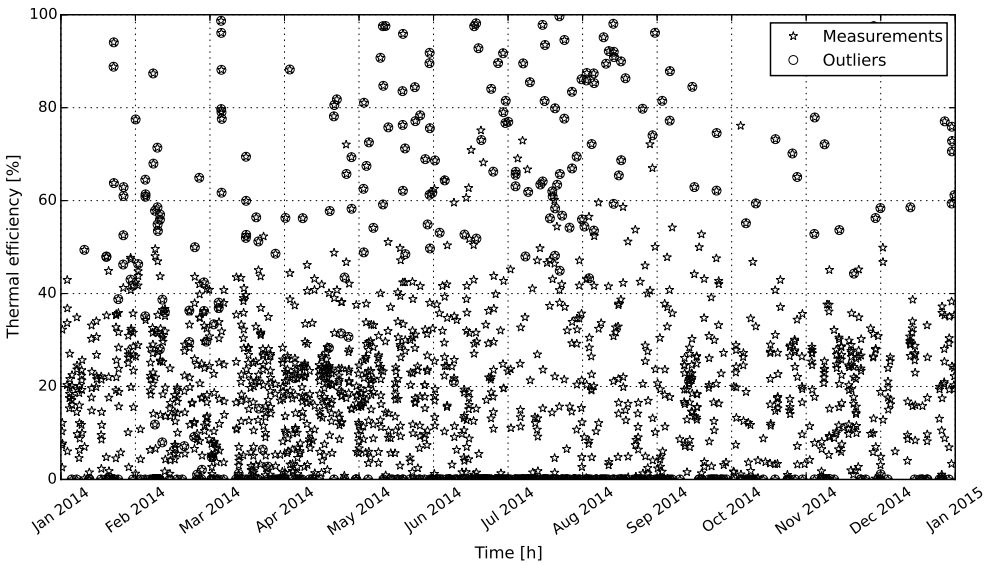

(a) Thermal efficiency of the flat-plate collectors including outliers

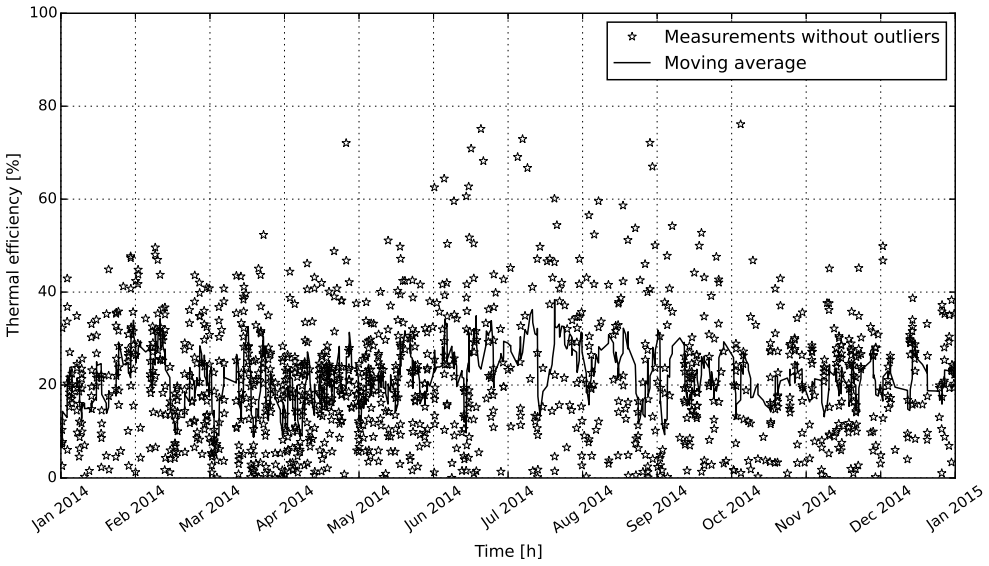

(b) Thermal efficiency of the flat-plate collectors without outliers

Figure 9.3: Effect of the outliers removal using the MAD of the thermal efficiency of the flat-plate collectors from January 1st to December 31st, 2014

Solar radiation and outside air temperature were obtained for the year 2014 from (Weather Analytics, 2016), as they were not measured on site during the studying period. Weather Analytics uses the Climate Forecast System Reanalysis (CFSR) data set, which estimates the outside air temperature and solar radiation based on a full atmospheric model using observational data and past model verifications. This might be one of the reasons for the presence of outliers.

Figure 9.4 depicts the relative frequency of the thermal efficiency of the flat-plate collectors from October 15th to May 10th (i.e., heating season), and from May 11th to October 14th (i.e., non-heating season). In the heating season, the thermal efficiency varies from 0% to 52%, with the median and average at around 21%. In the non-heating season, the thermal efficiency varies from 0% to 76%, with the median and average around 20% and 22%, respectively.

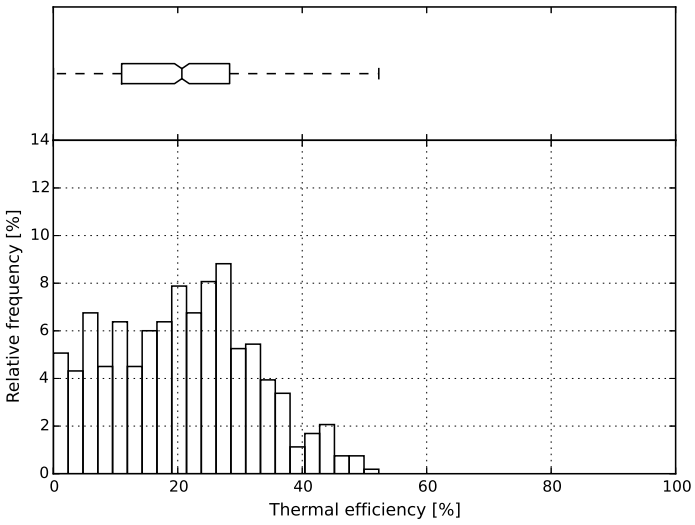

(a) Relative frequency of the thermal efficiency of the flat-plate collectors for the heating season

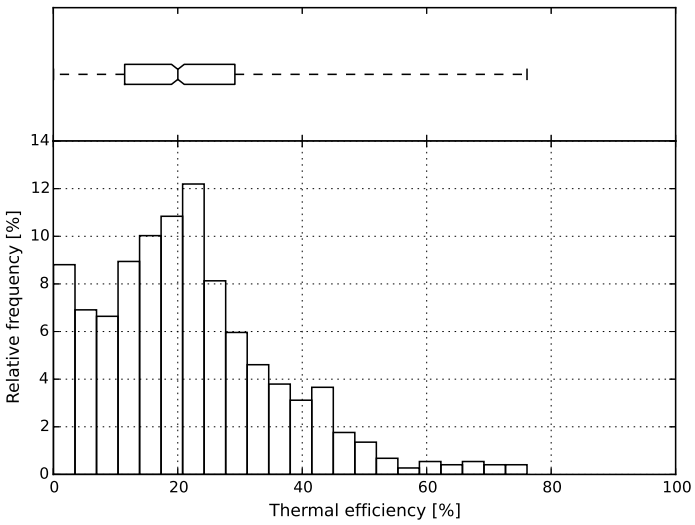

(b) Relative frequency of the thermal efficiency of the flat-plate collectors for the non-heating season

Figure 9.4: Relative frequency of the thermal efficiency of the flat-plate collectors from January 1st to December 31st, 2014

Based on Figure 9.2, the sensor S5 monitoring the average heat-transfer fluid temperature leaving the flat-plate collectors is assumed to be close to the thermal storage tank, inside the house,

since no negative temperature values are observed in winter. As a result, the thermal efficiency of the flat-plate collectors, calculated using Equation 9.1, includes the pipe thermal losses. For instance, in (Ayompe & Duffy, 2013), a solar water heating system was installed in Dublin, Ireland, using solar thermal collectors on a flat roof. The solar thermal collector and system efficiencies were equal to 45.6% and 37.8%, respectively. Significant pipe heat losses were found whereas the solar heating system was installed in Dublin, whose climate was referred to as temperate. Flat-plate collectors were investigated in (Thundil et al., 2012), where thermal efficiencies close to 25% were found. An average thermal efficiency of 22%, as calculated in this thesis, is therefore not out of the normal range for such a residential solar thermal combisystem.

9.3.2 Uncertainty analysis

Uncertainty arises from any measurement, so the uncertainty analysis is necessary to clarify the range of expected energy performance indices. Errors in measurements can be separated into two parts: (i) bias errors, and (ii) random errors.

Overall uncertainty

Bias errors, also called systematic errors, are fixed values. They are provided by manufacturers at a specified confidence level. Random errors are non-repeatable inaccuracies, which can be estimated by repeating a measurement. Any measurement of a variable x can be defined as follows:

$$x = x_{\text{best}} \pm U_x \tag{9.10}$$

where x_{best} is the best estimate of the variable x (i.e., the measured value); U_x is the overall uncertainty in the measurement.

The overall uncertainty in a measured variable x at a specified confidence level, denoted by U_x, combines the random and bias uncertainty estimates, and can be expressed as (Reddy, 2011):

$$U_x = \sqrt{{B_x}^2 + \left(\frac{t \cdot s_x}{\sqrt{n}}\right)^2} \tag{9.11}$$

where B_x is the uncertainty in the bias or fixed component at the specified confidence level; s_x is the standard deviation estimates for the random component; n is the sample size; t is the t-value at the specified confidence level for the appropriate degrees of freedom.

Propagation of errors

Assuming a variable y depending on n measured variables such that:

$$y = f\left(x_1, \ldots, x_n\right) \tag{9.12}$$

The uncertainty in y is calculated using the general formula for error propagation as follows (Reddy, 2011):

$$U_y = \sqrt{\left(\frac{\partial y}{\partial x_1} \cdot U_{x_1}\right)^2 + \ldots + \left(\frac{\partial y}{\partial x_n} \cdot U_{x_n}\right)^2} \tag{9.13}$$

where U_{x_i} is the overall uncertainty in the i-th measured variable x, calculated using Equation 9.11.

Equation 9.13 is applied to the energy performance indices so as to estimate their respective overall uncertainty. The overall uncertainty in η_{coll} is determined as follows:

$$\begin{aligned} U_{\eta_{coll}} = \Bigg[& \left(\frac{\partial \eta_{\text{coll}}}{\partial \dot{m}_{\text{coll,F1}}} \cdot U_{\dot{m}_{\text{coll,F1}}}\right)^2 + \left(\frac{\partial \eta_{\text{coll}}}{\partial c_{\text{p,coll}}} \cdot U_{c_{\text{p,coll}}}\right)^2 + \left(\frac{\partial \eta_{\text{coll}}}{\partial T_{\text{S5}}} \cdot U_{T_{\text{S5}}}\right)^2 \\ & + \left(\frac{\partial \eta_{\text{coll}}}{\partial T_{\text{S12}}} \cdot U_{T_{\text{S12}}}\right)^2 + \left(\frac{\partial \eta_{\text{coll}}}{\partial A_{\text{A1}} \cdot U_{A_{\text{A1}}}}\right)^2 + \left(\frac{\partial \eta_{\text{coll}}}{\partial A_{\text{A2}} \cdot U_{A_{\text{A2}}}}\right)^2 \\ & + \left(\frac{\partial \eta_{\text{coll}}}{\partial G_{\text{tot,A1}}} \cdot U_{G_{\text{tot,A1}}}\right)^2 + \left(\frac{\partial \eta_{\text{coll}}}{\partial G_{\text{tot,A2}}} \cdot U_{G_{\text{tot,A2}}}\right)^2 \Bigg]^{1/2} \end{aligned} \tag{9.14}$$

As mentioned in Section 9.1, the weather conditions under which the residential solar combisystem operates are not measured on site, so the uncertainties related to the measurements of $G_{\text{tot,A1}}$ and $G_{\text{tot,A2}}$ are unknown. The uncertainty in the specific heat of the 40% glycol-water heat-transfer fluid is neglected. Assuming that the uncertainty in the areas of the solar collector arrays can be neglected, the overall uncertainty in the thermal efficiency of the flat-plate collectors is calculated as follows:

$$U_{\eta_{\text{coll}}} = \left[\left(\frac{\partial \eta_{\text{coll}}}{\partial \dot{m}_{\text{coll,F1}}} \cdot U_{\dot{m}_{\text{coll,F1}}}\right)^2 + \left(\frac{\partial \eta_{\text{coll}}}{\partial T_{\text{S5}}} \cdot U_{T_{\text{S5}}}\right)^2 + \left(\frac{\partial \eta_{\text{coll}}}{\partial T_{\text{S12}}} \cdot U_{T_{\text{S12}}}\right)^2\right]^{1/2} \tag{9.15}$$

The overall uncertainty in the calculation of the thermal energy stored in the storage tank is given as follows:

$$U_{Q_{\text{stored}}} = \sqrt{U^2_{Q_{\text{supply}}} + U^2_{Q_{\text{DHW,tank}}} + U^2_{Q_{\text{SH,tank}}}} \tag{9.16}$$

where:

$$U_{Q_{\text{supply}}} = \left[\left(\frac{\partial Q_{\text{supply}}}{\partial \dot{m}_{\text{coll,F1}}} \cdot U_{\dot{m}_{\text{coll,F1}}} \right)^2 + \left(\frac{\partial Q_{\text{supply}}}{\partial c_{\text{p,coll}}} \cdot U_{c_{\text{p,coll}}} \right)^2 + \left(\frac{\partial Q_{\text{supply}}}{\partial T_{\text{S5}}} \cdot U_{T_{\text{S5}}} \right)^2 + \left(\frac{\partial Q_{\text{supply}}}{\partial T_{\text{S12}}} \cdot U_{T_{\text{S12}}} \right)^2 \right]^{1/2} \tag{9.17}$$

$$U_{Q_{\text{DHW,tank}}} = \left[\left(\frac{\partial Q_{DHW,tank}}{\partial \dot{m}_{\text{DHW,F2}}} \cdot U_{\dot{m}_{\text{DHW,F2}}} \right)^2 + \left(\frac{\partial Q_{\text{supply}}}{\partial c_{\text{p,water}}} \cdot U_{c_{\text{p,water}}} \right)^2 + \left(\frac{\partial Q_{DHW,tank}}{\partial T_{\text{S11}}} \cdot U_{T_{\text{S11}}} \right)^2 + \left(\frac{\partial Q_{DHW,tank}}{\partial T_{\text{S10}}} \cdot U_{T_{\text{S10}}} \right)^2 \right]^{1/2} \tag{9.18}$$

$$U_{Q_{\text{SH,tank}}} = \left[\left(\frac{\partial Q_{SH,tank}}{\partial \dot{m}_{\text{SH,F3}}} \cdot U_{\dot{m}_{\text{SH,F3}}} \right)^2 + \left(\frac{\partial Q_{\text{supply}}}{\partial c_{\text{p,water}}} \cdot U_{c_{\text{p,water}}} \right)^2 + \left(\frac{\partial Q_{SH,tank}}{\partial T_{\text{S13}}} \cdot U_{T_{\text{S13}}} \right)^2 + \left(\frac{\partial Q_{SH,tank}}{\partial T_{\text{S3}}} \cdot U_{T_{\text{S3}}} \right)^2 \right]^{1/2} \tag{9.19}$$

More details about the calculations are given in Appendix A.

Uncertainty calculations

Table 9.2 lists the features of each sensor used to monitor the residential solar thermal combisystem, where the bias error is given at a specified confidence level of 95%.

Table 9.2: Features of the sensors used to monitor the solar thermal combisystem

Sensor	Value	Unit
RESOL PT1000 Temperature sensor (RESOL, 2015b)		
Measurement precision	$\pm$ 0.3 + 0.005 $\cdot\lvert T\rvert$	°C
Range of measurement	[-30.0, +150.0]	°C
RESOL V40-15 flowmeter (RESOL, 2015a)		
Measurement precision	$\pm$ 5%	kg/s
Range of measurement	[0.008, 0.83]	kg/s
MINOL Minomess 130 flowmeter (Minol, 2015)		
Measurement precision	$\pm$ 5%	kg/s
Range of measurement	[0.017, 1.39]	kg/s

Random errors are unpredictable differences from one measurement to the next one due to unknown effects. They can be estimated through statistical analysis by repeating the same measurement as many times as possible. The monitoring data of the solar thermal combisystem depend

on external conditions that are difficult to control, such as the outside temperature. Accordingly, small samples of 31 measurements with the shortest time interval available (i.e., one minute between two measurements) are selected. It is assumed that environmental conditions do not significantly vary during each selected time period. The standard deviation of each sample s_x is calculated as follows:

$$s_x = \frac{1}{n-1} \cdot \sum_{i=1}^{n} (x_i - \overline{x})^2 \tag{9.20}$$

where n is the sample size; x_i is the i-th measurement; $\overline{x}$ is the arithmetic mean.

The average random error of each physical variable is estimated from November 17th to November 22nd, 2014, that is, 278 samples of 31 measurements. This time frame is chosen because both the domestic hot water and radiant floor were used by the people living in the house. Table 9.3 reports the average random error in the measurements over the 278 samples.

Table 9.3: Random errors in the measurements from November 17th to November 22nd, 2014

Sensor	Random error	Unit
RESOL PT1000 temperature sensor		
S1	± 0.3	°C
S2	± 0.1	°C
S3	± 0.2	°C
S4	± 0.2	°C
S5	± 0.2	°C
S6	± 0.3	°C
S7	± 0.3	°C
S8	± 0.2	°C
S9	± 0.3	°C
S10	± 0.6	°C
S11	± 0.2	°C
S12	± 0.1	°C
S13	± 0.3	°C
RESOL V40-15 flowmeter		
F1 (Solar loop)	± 0.0004	kg/s
MINOL Minomesss 130 flowmeter		
F2 (DHW loop)	± 0.0004	kg/s
F3 (SH loop)	± 0.0004	kg/s

Since the measurements can be either higher or lower than the arithmetic mean, the t-value is the critical value for a two-tailed confidence level. For a degree of freedom equal to 30 and a specified confidence level of 95% (i.e., α equal to 0.05), the t-value is equal to 2.042 (Reddy, 2011).

The overall uncertainty in the thermal efficiency of the flat-plate collectors and that in the thermal energy stored in the storage tank, which are calculated using Equations 9.15 to 9.19, can now be determined. Both overall uncertainties as well as the overall uncertainty in each physical variable are used in the next section to clarify the range of expected values in order to gain confidence in the model validation.

9.4 Model validation

The model of the residential solar thermal combisystem is developed in the TRNSYS 16 simulation environment using some of the components presented in Chapter 5. TRNSYS allows linking system components together to simulate the thermal performance of complex energy systems. As mentioned in (Coakley et al., 2014), one of the primary advantage of forward models over inverse ones is their ability to predict system behavior given previously unobserved conditions. Nevertheless, significant differences can occur between the thermal performance of a system and its BPS model. Validation procedures aim at assessing the discrepancies between model outputs and measured data to determine whether or not models provide accurate and reliable results. A model can be considered validated when one or several acceptance criteria are fulfilled. There is however a lack of validation standard for solar thermal combisystems.

9.4.1 Lack of explicit standards

Acceptance criteria for calibration of buildings, and by extension for validation, are given in (ASHRAE, 2002) and (EVO, 2012). Both use the normalized mean bias error (NMBE) and coefficient of variation of the root mean square error (CVRMSE) defined by Equations 9.21 and 9.22. However, as reported in Table 9.4, (ASHRAE, 2002) and (EVO, 2012) do not recommend the same values. Although acceptance criteria for the calibration of the whole building energy use exist, there are no standards for the calibration (or validation) of solar thermal combisystems.

Table 9.4: Acceptance criteria for the calibration of the whole building energy use

Standard/Guideline	Maximum monthly values		Maximum hourly values	
	NMBE	CVRMSE	NMBE	CVRMSE
ASHRAE Guideline (ASHRAE, 2002)	5	15	10	30
IPMVP (EVO, 2012)	20	–	5	20

For instance, due to a lack of standards, variations between predicted and measured values for a solar water heating system were quantified in (Ayompe et al., 2011) using percentage mean absolute error (PMAE) and percentage mean error (PME). Another solar water heating system model was validated in (Abdalla, 2013) using the PMAE for solar fraction, where a value of 10% was found.

9.4.2 Validation procedure

In order to validate the BPS model of this residential solar thermal combisystem, four metrics are used: (i) normalized mean bias error (NMBE), (ii) coefficient of variation of the root mean squared error (CVRMSE), (iii) percentage mean error (PME), and (iv) percentage mean absolute error (PMAE).

The normalized mean bias error (NMBE) is defined as (ASHRAE, 2002):

$$\text{NMBE} = \frac{\sum_{i=1}^{n} (y_i - \hat{y}_i)}{(n-p) \cdot \overline{y}} \tag{9.21}$$

where y_i is the i-th variable observation; $\hat{y}_i$ is the i-th simulation-predicted value of the observed variable; n is the number of variable observations; p is the degree of freedom; $\overline{y}_i$ is the arithmetic mean of the variable observations.

The coefficient of variation of the root mean square error (CVRMSE) is a normalized measure of dispersion, which is defined as follows (ASHRAE, 2002):

$$\text{CVRMSE} = 100 \cdot \frac{\text{RMSE}}{\overline{y}} \tag{9.22}$$

where RMSE is the root-mean-square error calculated as (ASHRAE, 2002):

$$\text{RMSE} = \sqrt{\frac{\sum_{i=1}^{n} (y_i - \hat{y}_i)^2}{(n-p)}} \tag{9.23}$$

The percentage mean absolute error (PMAE) and percentage mean error (PME) are defined as follows (Ayompe et al., 2011):

$$\text{PMAE} = \frac{100}{n} \cdot \sum_{i=1}^{n} \frac{|\hat{y}_i - y_i|}{y_i} \tag{9.24}$$

$$\text{PME} = \frac{100}{n} \cdot \sum_{i=1}^{n} \frac{\hat{y}_i - y_i}{y_i} \tag{9.25}$$

Although there are no standards for the validation of solar thermal combisystem models, the order of magnitude given for the first two metrics (i.e., Equations 9.21 and 9.22) in (ASHRAE, 2002) and (EVO, 2012) are taken as relative references for the validation. Each metric is applied to the two energy performance indicators as well as some of the monitored temperatures, as shown in Table 9.5.

Table 9.5: Statistical indices of the difference between predictions and measurements of the solar combisystem for the year 2014

Sensor/indicators	NMBE [%]	CVRMSE [%]	PMAE [%]	PME [%]
Sensor				
S1	-0.7	11.4	5.4	2.7
S2	8.7	24.3	20.7	-1.6
S3	0.3	2.4	0.3	-0.2
S4	9.1	25.1	21.7	-2.4
S5	-0.8	13.5	5.0	1.5
S6	2.4	12.6	8.4	2.4
S7	-0.7	4.2	0.8	0.8
S9	6.2	25.0	23.7	1.7
S11	-4.0	20.5	18.2	9.0
S12	-2.1	14.3	6.0	3.8
Performance indicator				
η_{coll}	7.3	29.3	25.0	18.7
Q_{stored}	7.6	35.5	21.4	5.5

Figures 9.5a and 9.5b display the measured and simulated temperatures of the heat-transfer fluid leaving the two solar thermal collector arrays A1 and A2 from November 17 to November 23, 2014. The uncertainty in the temperatures measured by the sensors S1 and S6 (i.e., the outlet temperatures of the arrays A2 and A1, respectively) are reported to show the level of confidence in the measurements. The values obtained using the BPS model follow the same trend as the measurements (i.e., the simulated temperatures fit well the measurements), which gives confidence regarding the model validation.

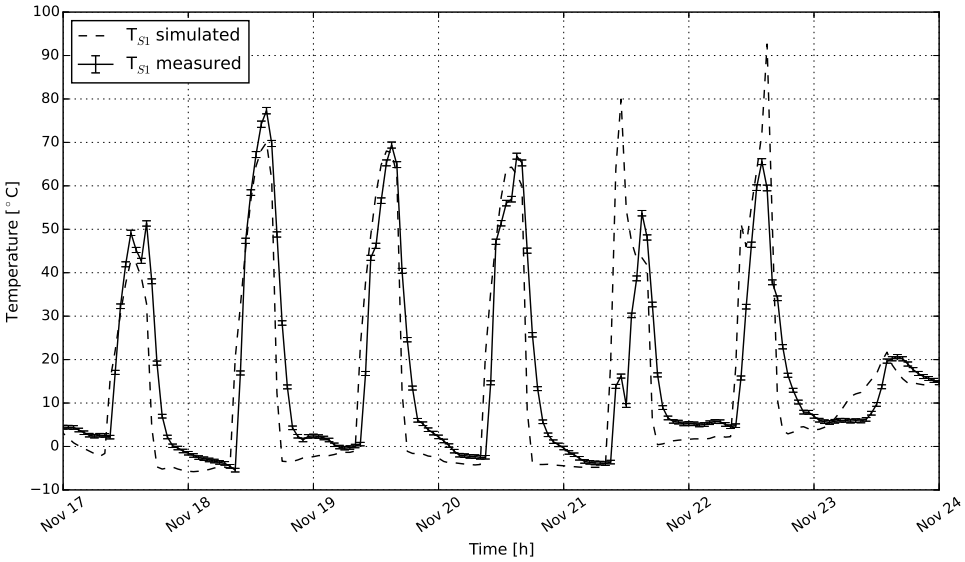

(a) Heat-transfer fluid temperature T_{S1} of the array A2

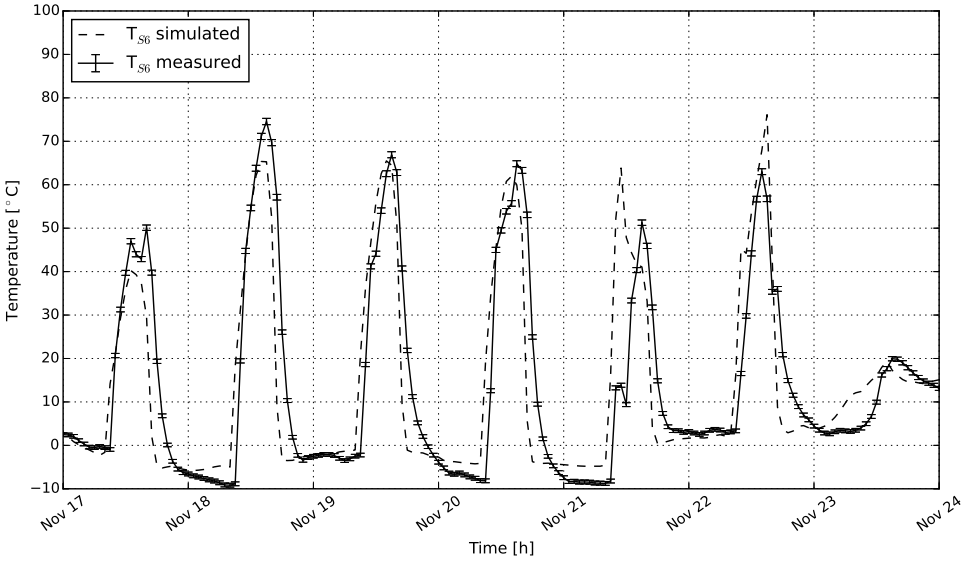

(b) Heat-transfer fluid temperature T_{S6} of the array A1

Figure 9.5: Comparison of the measured and simulated temperatures leaving both A1 and A2 from November 17th to November 23rd, 2014

The temperatures of the heat-transfer fluid entering and leaving both arrays (i.e., S12 and S5) are shown in Figure 9.6. The simulated temperatures fit relatively well the measurements; however, Figure 9.6b shows some discrepancies from November 17 to November 23 due to an overestimation of the temperatures leaving both the array A1 and A2.

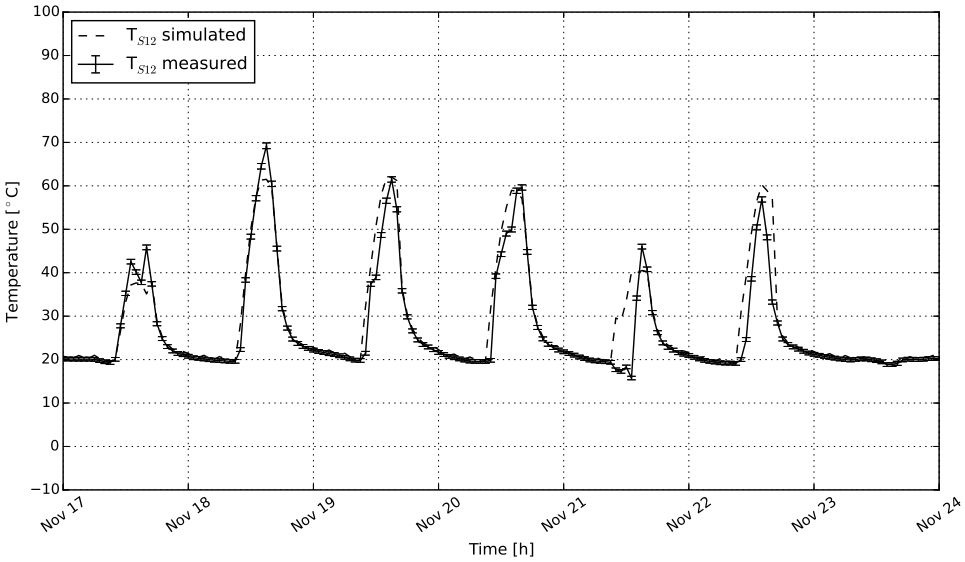

(a) Heat-transfer fluid temperature T_{S12} of the array A2

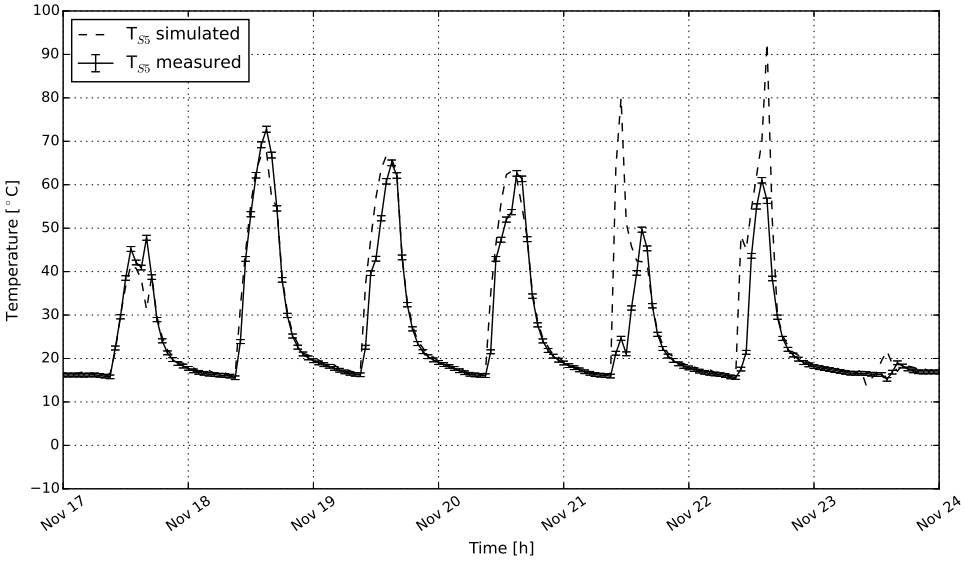

(b) Heat-transfer fluid temperature T_{S5} leaving the arrays A1 and A2

Figure 9.6: Comparison of the measured and simulated temperatures leaving both A1 and A2 from November 17th to November 23rd, 2014

Figure 9.7 presents the temperatures associated with the thermal storage tank. Even though a slight delay can be observed between the simulated and measured temperatures, the simulated temperature of the sensors S2 and S4 follow relatively well the measurements.

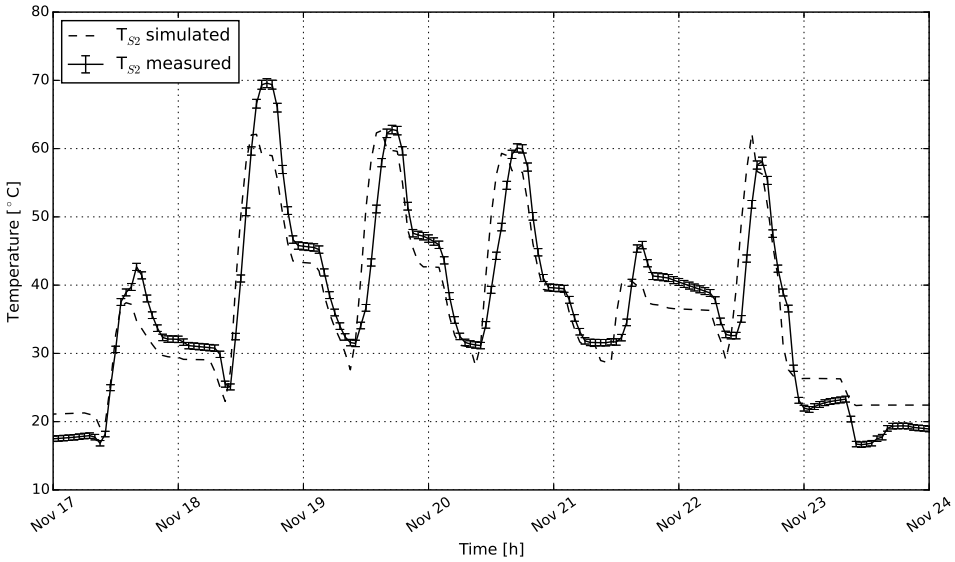

(a) Water temperature T_{S2} of the lower part of the thermal storage tank

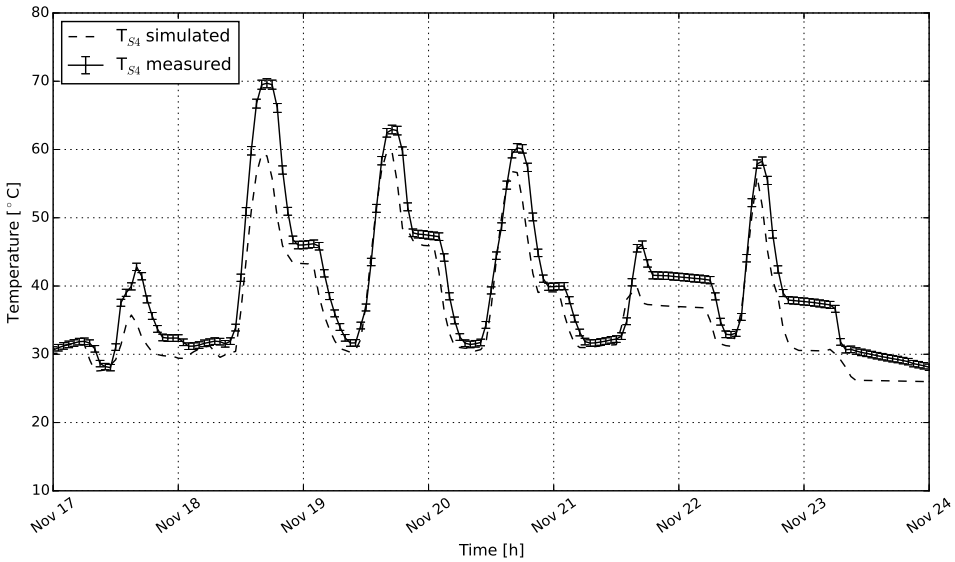

(b) Water temperature T_{S4} of the upper part of the thermal storage tank

Figure 9.7: Comparison of the measured and simulated water temperatures associated with the thermal storage tank from November 17th to November 23rd, 2014

Figure 9.8 displays the water temperatures from the thermal storage tank for DHW and SH purposes which are recorded using sensors S11 and S3, respectively. The simulated temperatures fit the measurements well.

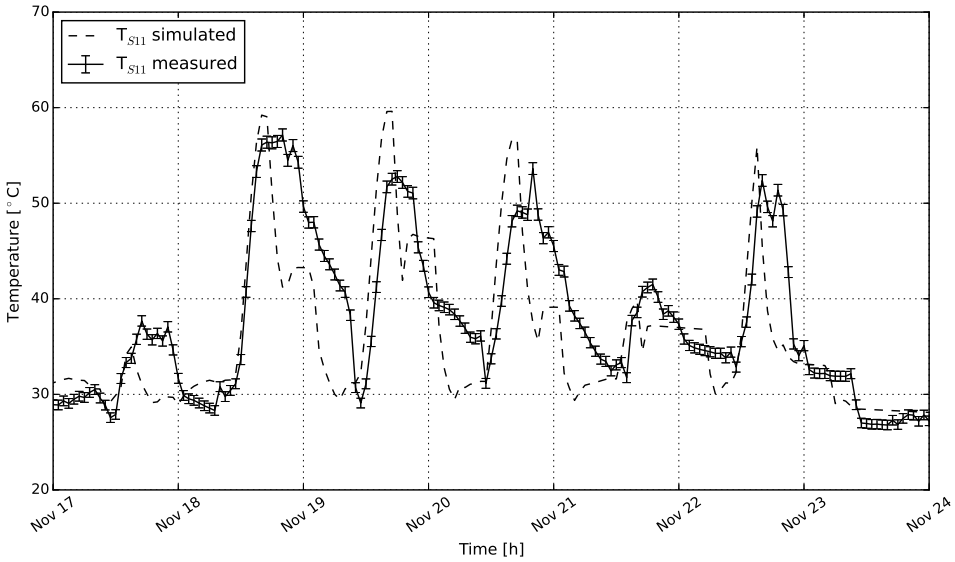

(a) DHW temperature T_{S11} leaving the thermal storage tank

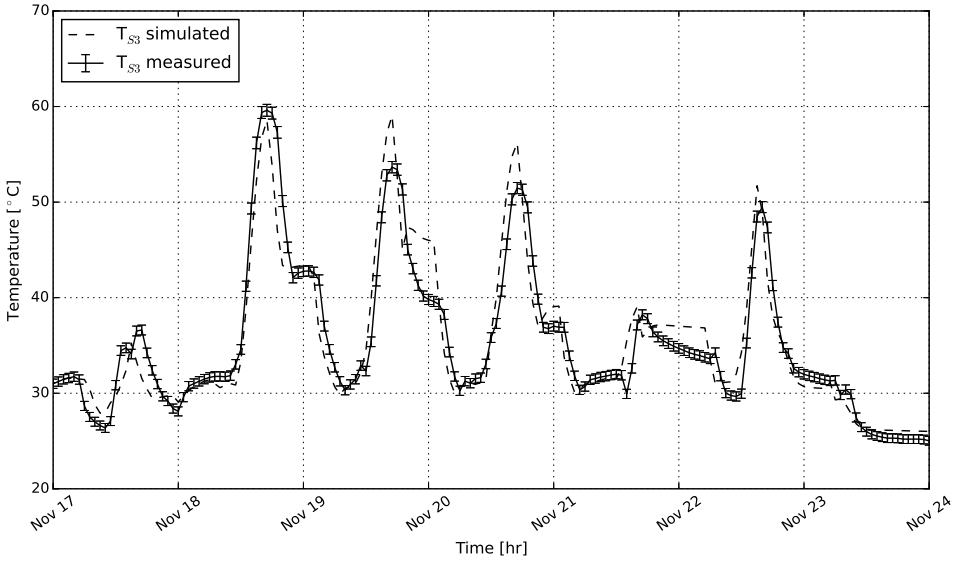

(b) Water temperature T_{S3} leaving the thermal storage tank for space heating purposes

Figure 9.8: Comparison of the measured and simulated water temperatures from the thermal storage tank for DHW and SH purposes from November 17th to November 23rd, 2014

Figure 9.9 shows the thermal energy stored calculated with the measured and simulated data using Equation 9.2. Compared to Figures 9.5 to 9.8, larger discrepancies occur between the measured and simulated values. While the overall uncertainty in the calculated thermal energy harvested by the solar collectors is relatively small, the overall uncertainty in the calculated thermal energy

stored in the storage tank is larger due to the propagation of errors.

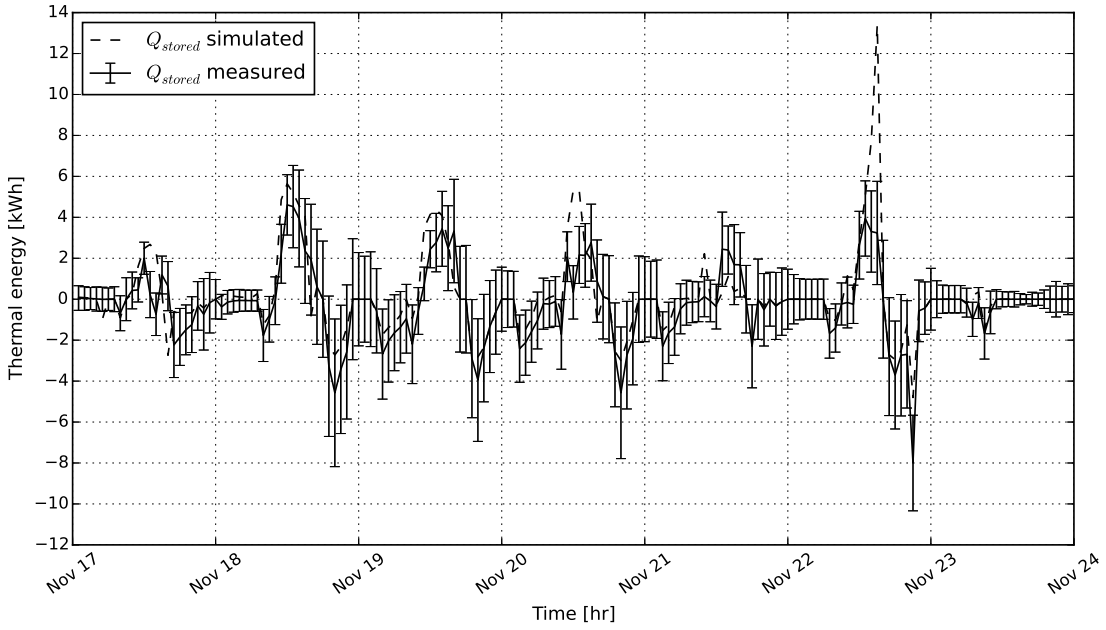

Figure 9.9: Comparison of the measured and simulated thermal energy stored in the thermal storage tank from November 17th to November 23rd, 2014

As shown in Table 9.5 or in Figures 9.5 to 9.8, the simulated temperatures and thermal energy stored fit relatively well the measurements, which gives confidence about the model validation.

Before optimizing this residential solar thermal combisystem using the multi-objective optimization framework developed, a tend data analysis is performed to better understand the thermal behavior of the solar combisystem.

9.5 Trend data analysis

A summary of the main characteristics of the data is provided in this section to gain additional insights. Some descriptive statistics are given to better understand the solar thermal combisystems behavior. The minimum, maximum, average, standard deviation (s_x), median, and median absolute deviation (MAD) of the temperatures and flow rates recorded during the year 2016 are reported in Table 9.6. The year 2016 is preferred over the year 2014 for three reasons: (i) more recent data, (ii) outdoor air temperature measured on site, (iii) no missing data for calculating the domestic hot water and space heating energy needs $Q_{\text{DHW,aux}}$ and $Q_{\text{SH,aux}}$ using Equations 9.6 and 9.7. The

last reason is of paramount importance for the multi-objective optimization of the residential solar combisystem.

Table 9.6 provides some insights about the solar thermal combisystems behavior. For example, the water temperature of the upper part of the thermal storage tank, recorded by sensor S4, is higher than that of the lower part, measured by sensor S2, on average (52.1°C vs. 50.0°C, respectively). A thermal stratification due to a change in water's density with temperature can therefore be observed. The DHW temperature after the electric water heater, measured with sensor S9, is on average 45.0°C. The temperature T_{S6}, which corresponds to the array A2 having a tilt angle of 65°, reaches higher values than the temperature T_{S1}, which corresponds to the array A1 having a tilt angle of 90°.

Table 9.6: Random errors and overall uncertainties in the measurements from November 17th to November 22nd, 2014

Sensor	Min	Max	Average $\pm s_x$	Median ± MAD
Temperature [°C]				
S1	16.6	83.8	55.2 ± 12.2	55.0 ± 08.1
S2	10.6	75.5	50.0 ± 19.5	49.1 ± 18.6
S3	22.5	53.6	29.4 ± 05.2	27.6 ± 01.6
S4	20.4	76.6	52.1 ± 18.7	56.0 ± 17.4
S5	13.6	80.7	53.5 ± 15.6	55.1 ± 10.8
S6	23.9	96.8	61.0 ± 13.7	62.6 ± 08.8
S7	22.8	42.5	29.3 ± 03.1	28.2 ± 00.8
S8	19.5	34.1	26.6 ± 02.9	26.4 ± 02.2
S9	38.9	50.0	45.0 ± 01.7	45.0 ± 01.3
S10	07.4	23.6	15.0 ± 04.3	13.9 ± 03.6
S11	23.0	71.0	49.6 ± 14.3	54.0 ± 10.2
S12	14.2	74.4	38.2 ± 13.3	34.8 ± 07.8
S13	21.6	36.8	26.6 ± 02.1	26.0 ± 01.0
Mass flow rate [kg/s]				
F1 (Solar loop)	0.0015	0.3019	0.0938 ± 0.0799	0.0697 ± 0.0503
F2 (DHW loop)	0.0003	0.0335	0.0094 ± 0.0065	0.0076 ± 0.0038
F3 (SH loop)	0.0199	0.1113	0.0612 ± 0.0072	0.0612 ± 0.0029

As shown in Figures 9.10a and 9.10b, the water temperature of the upper and lower parts of the thermal storage tank experienced large variations through the year 2016. However, the interquartile range shows that the thermal storage tank was mainly discharged during the heating season, due to space heating in winter.

Some temperatures such as the ones recorded by the sensors S7 or S8 do not significantly change during the year (independently of the season considered), because both are controlled by an auxiliary heating device upstream.

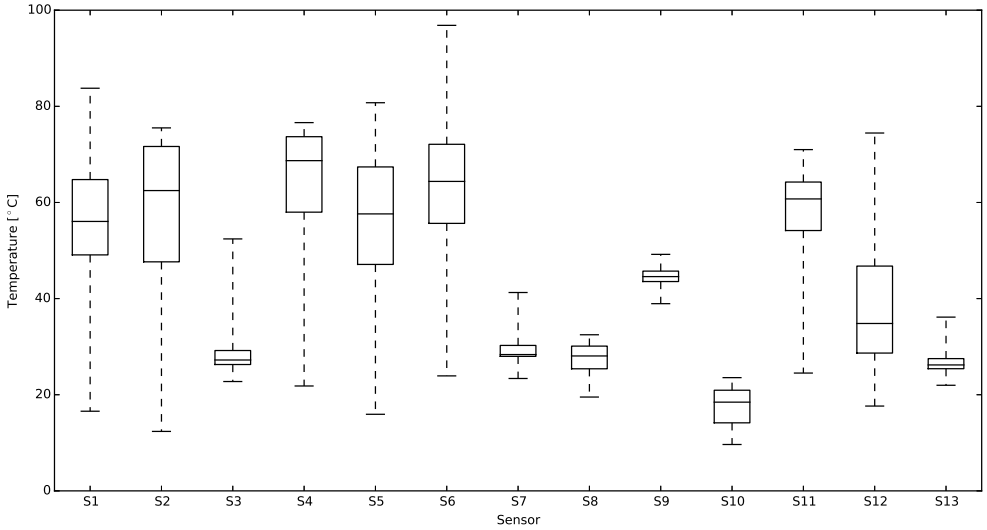

(a) Box-plots representing the measured temperatures during the heating season

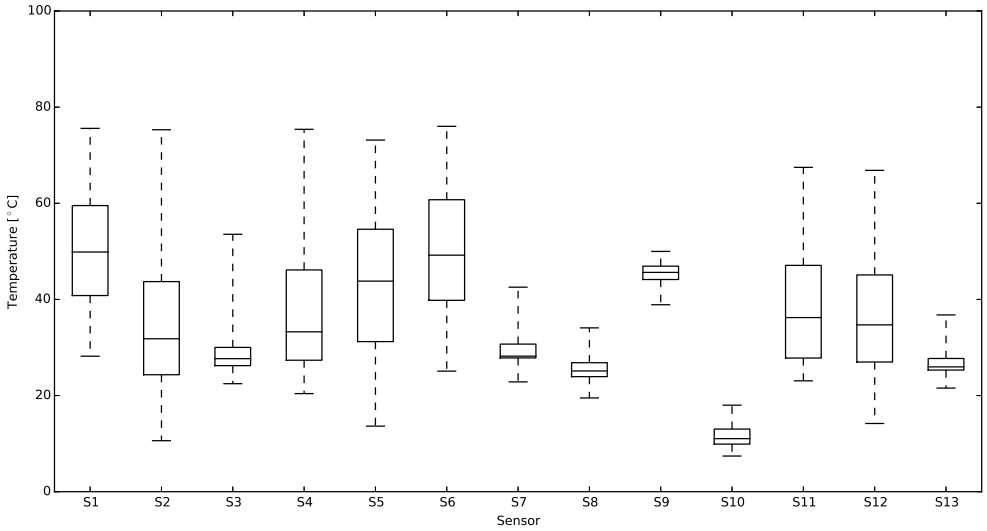

(b) Box-plots representing the measured temperatures during the non-heating season

Figure 9.10: Box-plots representing the temperatures measured by each available sensor for the year 2016

Figures 9.11 to 9.13 display the daily average evolution of some recorded temperatures for two periods of one week (one during the heating season and another during the non-heating season). The first period is from July 17th to July 23rd, 2016, while the second is from February 17th to

February 23rd, 2016.

Figure 9.11a shows that T_{S5}, the temperature of the heat-transfer fluid entering the storage tanks heat exchanger on the solar loop side, is significantly higher than T_{S1} and T_{S6} (i.e., the temperatures of the heat-transfer fluid leaving the arrays A1 and A2, respectively) at night. This supports the fact that the temperature sensor S5 is inside the house, close to the storage tank. When the solar thermal combisystem operates, T_{S5} is often lower than T_{S1} or T_{S6}, which is due to pipe thermal losses. On average, during the heating season, T_{S1} is higher than T_{S6}. A tilt angle of 90° enables harvesting more solar energy than one of 65°. The opposite can be observed during the non-heating season, as shown in Figure 9.11b, where significantly higher temperatures are reached on average by T_{S6} compared to T_{S1}.

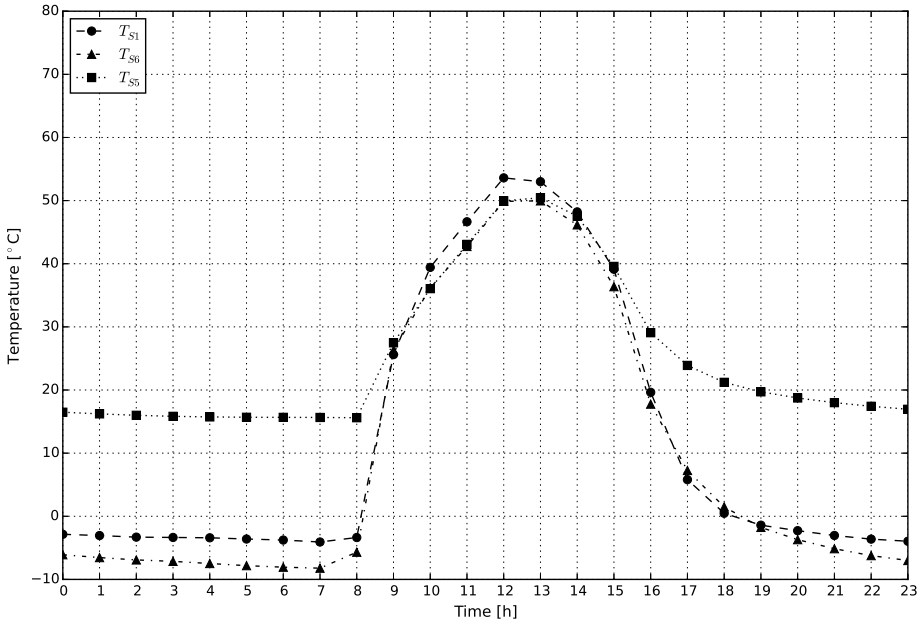

(a) Daily average solar loop temperatures from February 17th to February 23rd, 2016

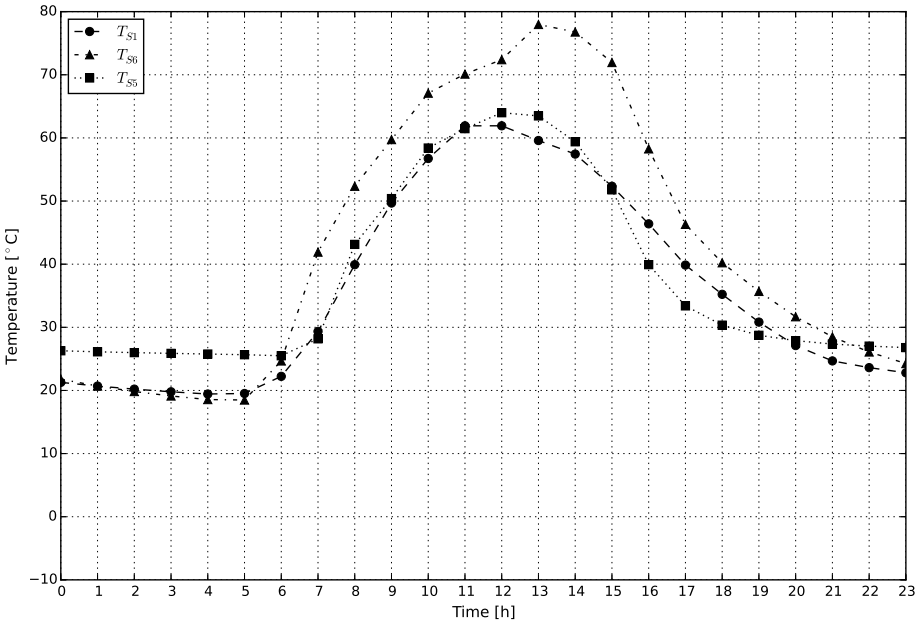

(b) Daily average solar loop temperatures from July 17th to July 23rd, 2016

Figure 9.11: Daily average solar loop temperatures based on the year 2016

As shown in Figure 9.12, T_{S2} and T_{S4} (i.e., the water temperatures of the lower and upper parts of the thermal storage tank, respectively) follow on average the evolution of the solar loop temperatures with a small delay (e.g., T_{S2} and T_{S4} reach a peak one hour after the one reached by T_{S5}). The DHW temperature after the electric water heater, measured with sensor S9, is relatively constant (independently of the season considered). The largest temperature difference between T_{S2} and T_{S4} occurs in the morning around 08:00 am, which is due to a consumption of DHW. Lower temperature variations are observed in Figure 9.12b where the thermal storage tank is almost fully charged.

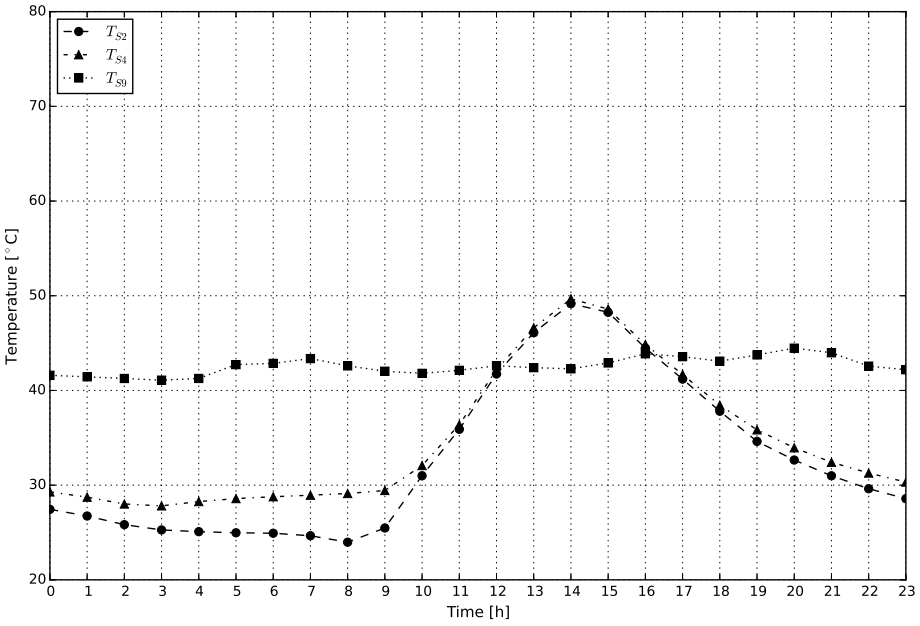

(a) Daily average DHW loop temperatures from February 17th to February 23rd, 2016

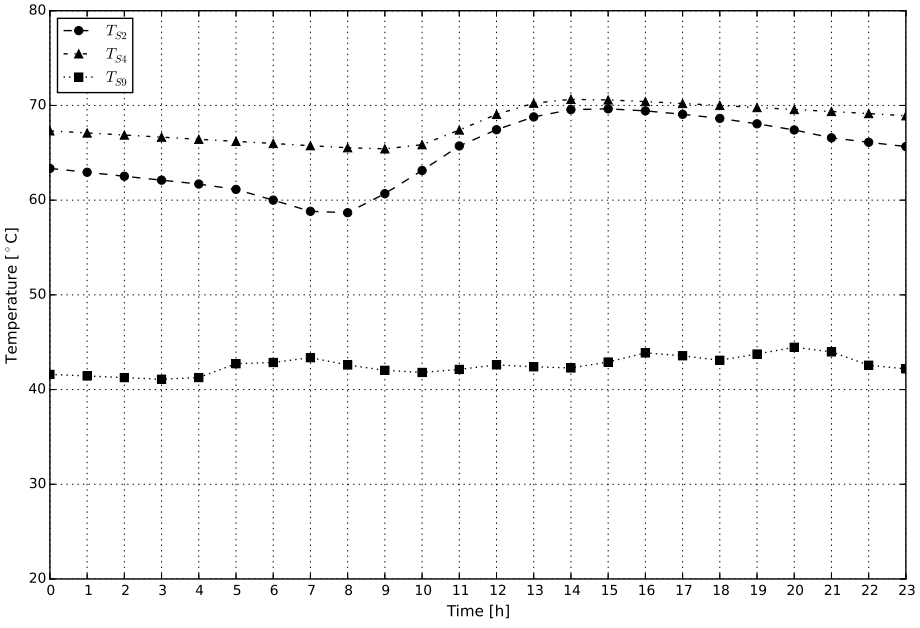

(b) Daily average DHW loop temperatures from July 17th to July 23rd, 2016

Figure 9.12: Daily average DHW temperatures based on the year 2016

Figures 9.13b and 9.13b depict the SH temperatures during the heating and non-heating seasons. During the heating season, all the SH temperatures T_{S7}, T_{S3}, and T_{S13} are close to one another. The supply temperature for the radiant floor T_{S7}, which is measured after the auxiliary water heater,

is slightly higher than the others in the morning. Additional auxiliary energy is therefore required during this period. As shown in Figure 9.13b, during the non-heating season, T_{S3} and T_{S13} reach high temperatures compared to T_{S7}. Sensors S3 and S13 are probably next to the thermal storage tank, whereas S7 is closer to the radiant heating floor.

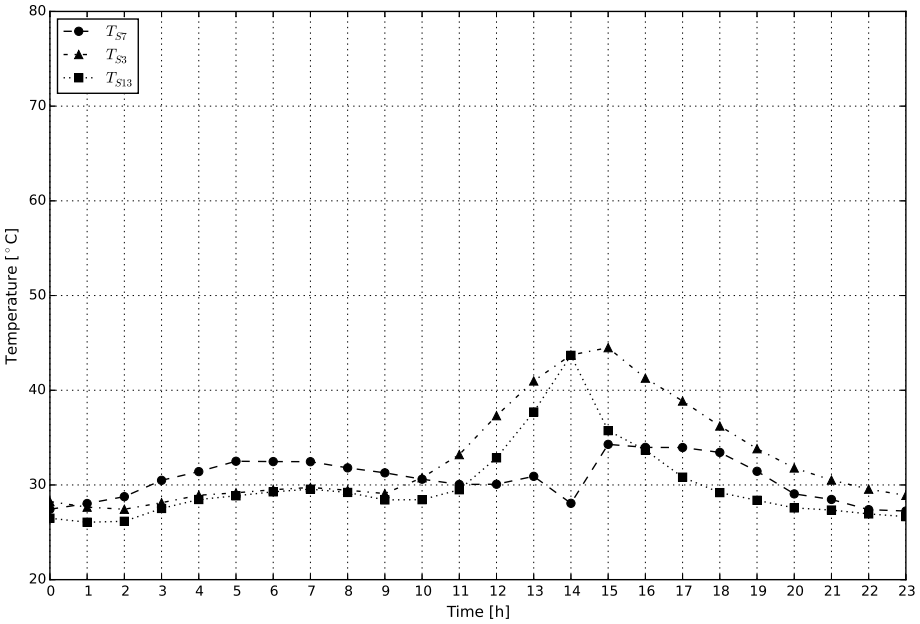

(a) Daily average SH loop temperatures from February 17th to February 23rd, 2016

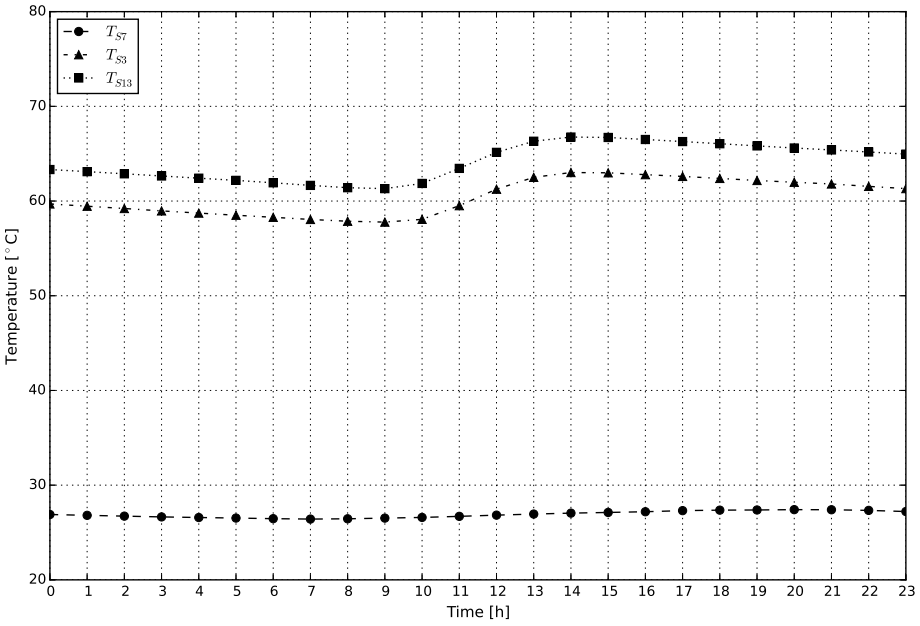

(b) Daily average SH loop temperatures from July 17th to July 23rd, 2016

Figure 9.13: Daily average SH temperatures based on the year 2016

Figure 9.14 shows the monthly production of thermal energy by the six flat-plate collectors as well as the monthly energy used for DHW and SH purposes for the year 2016, calculated using Equations 9.3 as well as Equations 9.6 and 9.7.

Different trends can be seen: (i) the production of heat increases in summer with a peak during June and July, (ii) the DHW energy used oscillates around a value of 200 kWh with a decrease in summer due to higher cold city water temperatures, and (iii) the SH energy used decreases from winter to summer (where no thermal energy is used). From September 25th to the end of the year 2016, the flow meter installed on the solar collector loop was not working for unknown reasons. As a result, no data was available on the production of thermal energy.

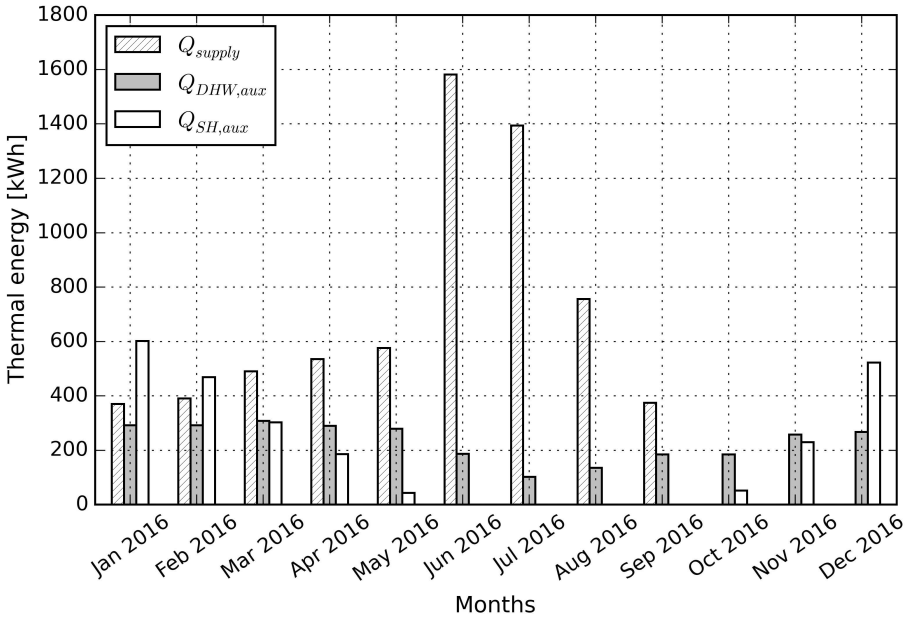

Figure 9.14: Monthly thermal energy production as well as DHW and SH energy used for the year 2016

The monthly amounts of additional auxiliary energy provided for DHW and SH purposes are shown in Figure 9.15. Over the entire year, 555.7 kWh and 1,287.5 kWh are consumed for DHW and SH needs. Nevertheless, no additional auxiliary energy is required from June to September.

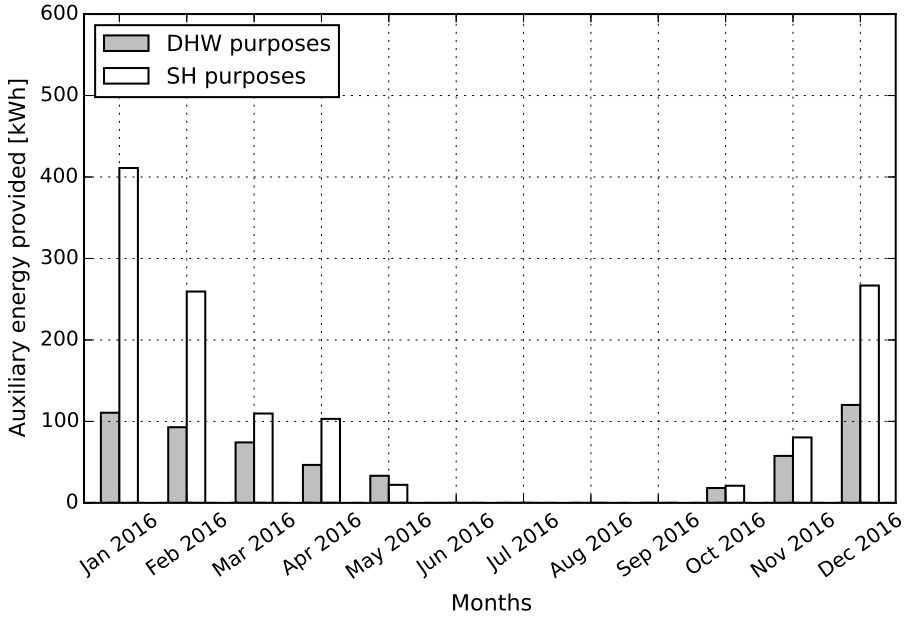

Figure 9.15: Monthly auxiliary energy provided for DHW and SH purposes during the year 2016

Since March 2015, the outdoor air temperature is measured on site; however, solar radiation is not. Both the outdoor air temperature and solar radiation were therefore obtained for the year 2016 from (IES, 2017). A comparison between both the outdoor air temperature measured on site and from the weather file is presented in Figures 9.16 and 9.17.

Figure 9.16 presents a graphical comparison, which shows that both data sources have the same trend. Freezing-temperatures (below zero degree) are prevalent in winter, which makes the use of an anti-freeze heat-transfer fluid necessary.

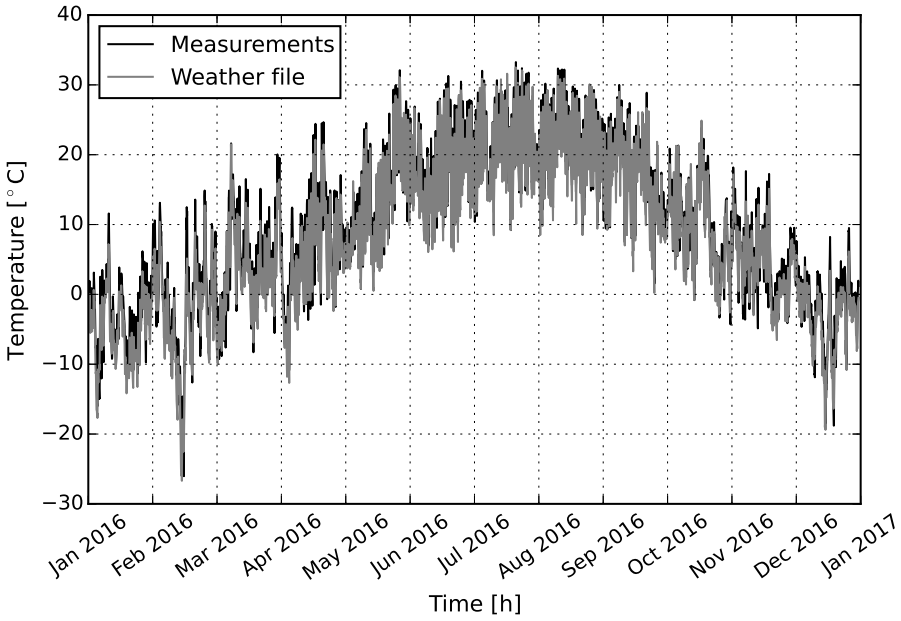

Figure 9.16: Evolution of the outdoor air temperature measured on site and that from the weather file for the year 2016

A more quantitative comparison is provided in Figure 9.17, where the use of the root mean square error, defined in Equation 9.23, between the outdoor air temperature measured on-site and that from the weather file results in values from 2.0°C to 3.1°C .

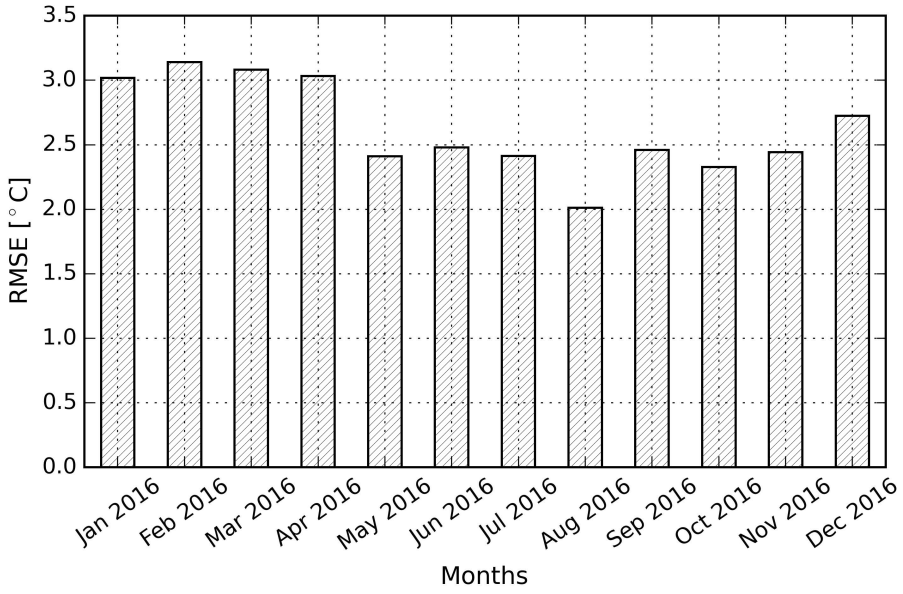

Figure 9.17: RMSE between the outdoor air temperature measured on site and that from the weather for the year 2016

Figure 9.18 represents the relative frequency of the DHW temperature after the electric water heater for the year 2016, that is, sensor S9. The distribution follows a normal distribution with an average temperature of 45.0°C and a standard deviation of 1.7°C, which is illustrated with the dashed line. The set point temperature can therefore be considered to be 45.0°C.

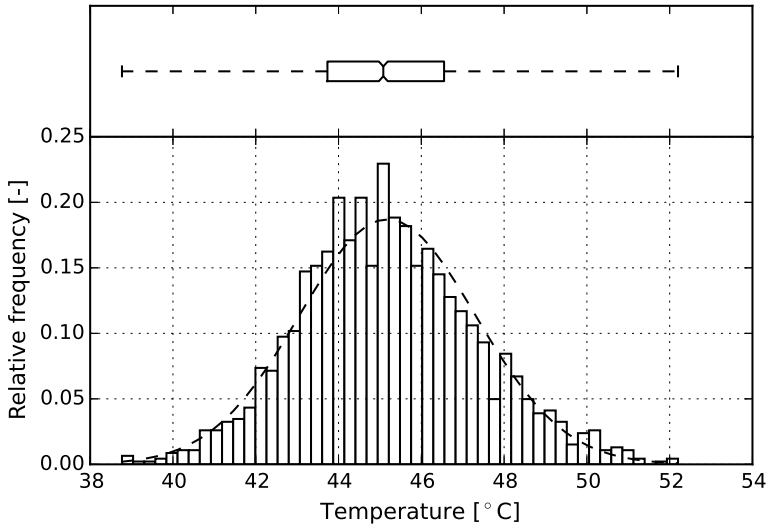

Figure 9.18: Relative frequency of the DHW temperature for the year 2016

The water temperature measured by sensor S7 follows also a normal distribution with an average temperature of 29.3°C and a standard deviation of 3.1°C. The set point temperature for space heating is set to 29.3°C. The DHW and SH energy used for the year 2016, calculated using Equations 9.6 and 9.7, is computed with the measured and aforementioned set point temperature values. Each set point temperature model well the control strategy of the solar thermal combisystem, which can be illustrated in Figure 9.19.

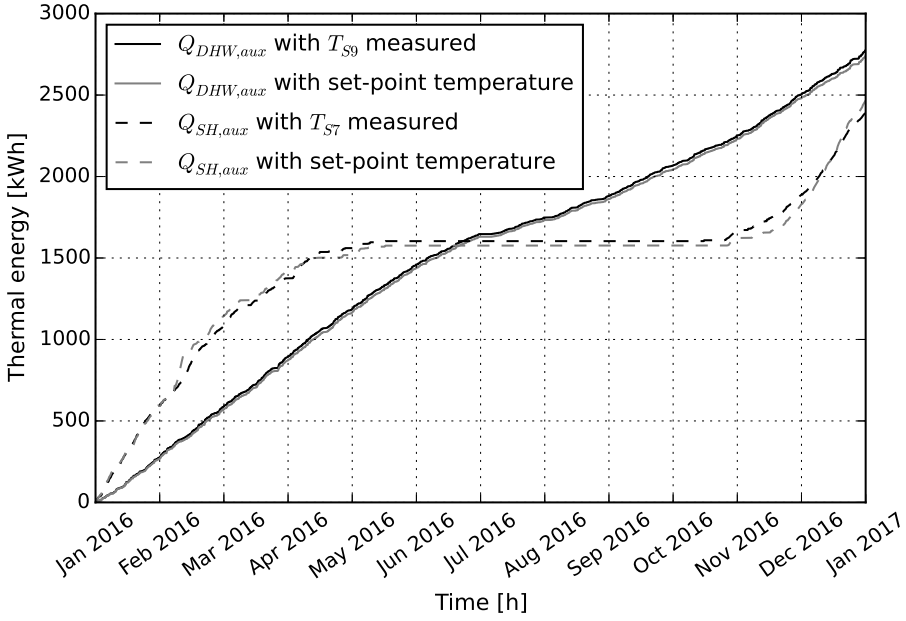

Figure 9.19: Comparison of the DHW and SH needs computed with the measured and set point temperature values

9.6 Optimization results and discussion

The optimization framework presented in Chapter 6 is now applied to this solar thermal combisystem. The generic solar combisystem model, developed in TRNSYS, was slightly modified compared to Case study no. 1. Since this case study is based on measurements, a data reader (Type 9c) reads from a text file the measurements of the existing solar thermal combisystem, which are then used as inputs by several TRNSYS types. Physical variables read by the data reader are listed in Table 9.7. The multi-zone building (Type 56a) is no longer required because the calculation of the DHW and SH needs (normally performed by TRNSYS with Type 56a) is replaced by an equation block computing the DHW and SH loads based on the measurements. As a result, the decision variable

associated with the floor slab thickness is removed from the optimization model. Case study no. 2 also uses different financial criteria than Case study no. 1, which were summarized in Section 6.4.1.

Table 9.7: List of the physical variables provided by the data reader (Type 9c)

Physical variable	Unit
Temperature of the city water	°C
Temperature leaving the electrical water heater for DHW purposes	°C
Temperature of the water leaving the tank and going to the radiant floor	°C
Return temperature from the radiant floor	°C
Supply temperature for the radiant floor	°C
Mass flow rate of the city water	kg/s
Mass flow rate of the water going through the radiant floor	kg/s
Mass flow rate of the water going through the radiant floor	kg/s

The micro-TVMOPSO algorithm presented in Chapter 7 is used along with the multi-objective optimization framework from Chapter 6 to find the best feasible solar combisystem designs through a multi-objective optimization. The initial solar combisystem design was used as one of the candidate solutions of the first generation of micro-TVMOPSO. Due to the time-consuming nature of one single TRNSYS simulation (around 40 minutes), a maximum number of 100 generation was selected; the micro-TVMOPSO algorithm used five particles, which results in 500 TRNSYS simulations (five particles times 100 generations). For 500 TRNSYS simulations, micro-TVMOPSO lasted approximately 79 hours (i.e., three days and seven hours). A total of 32 non-dominated solutions were found.

For instance, Figure 9.22 shows the four non-dominated solutions out of the 32 solutions, when only two objective functions are taken into consideration: LCC and LCE. Micro-TVMOPSO found non-dominated solutions that are more cost-effective and energy-effective than the initial design solution (solution no. 3). Compared to the initial design solution, micro-TVMOPSO found non-dominated solutions whose LCC and LCE values were decreased by to 8.3% and 25.8%, respectively.

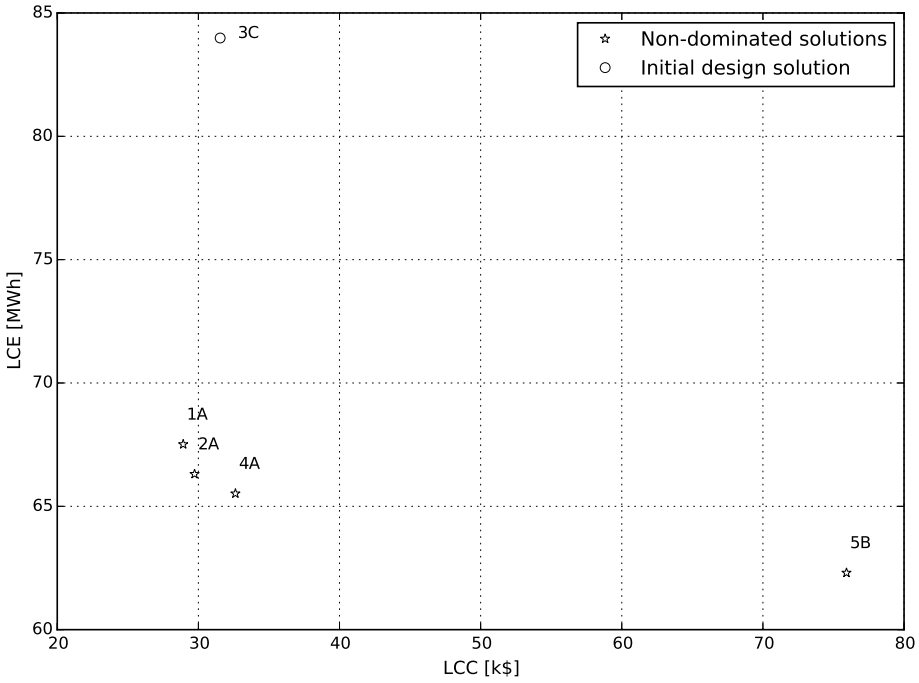

Figure 9.20: LCE vs. LCC approximation of the true Pareto front using micro-TVMOPSO for Case study no. 2

Two configurations were found, each one with different equipment sizing, as illustrated in Figure 9.21. The main difference between the initial design solution is the number of arrays of solar collectors. Each configuration found by micro-TVMOPSO is equipped with only one array. As reported in Table 9.8, configuration A, with solutions 1A, 2A, and 4A, use flat-plate collectors ($B_1^1 = 1$) and one thermal storage tank without stratifying devices ($B_4^1 = 1$). The solutions mainly differ by the number of flat-plate-collectors and auxiliary power units. Solutions 1A and 4A have higher numbers of flat-plate collectors and a lager thermal storage tank, compared to solution 2A, which enable them to harvest more solar energy as heat and therefore reduce additional auxiliary energy needs. Solution 2A has an lower initial cost (fewer flat-plate collectors and a smaller thermal storage tank), but relies more on auxiliary electric energy.

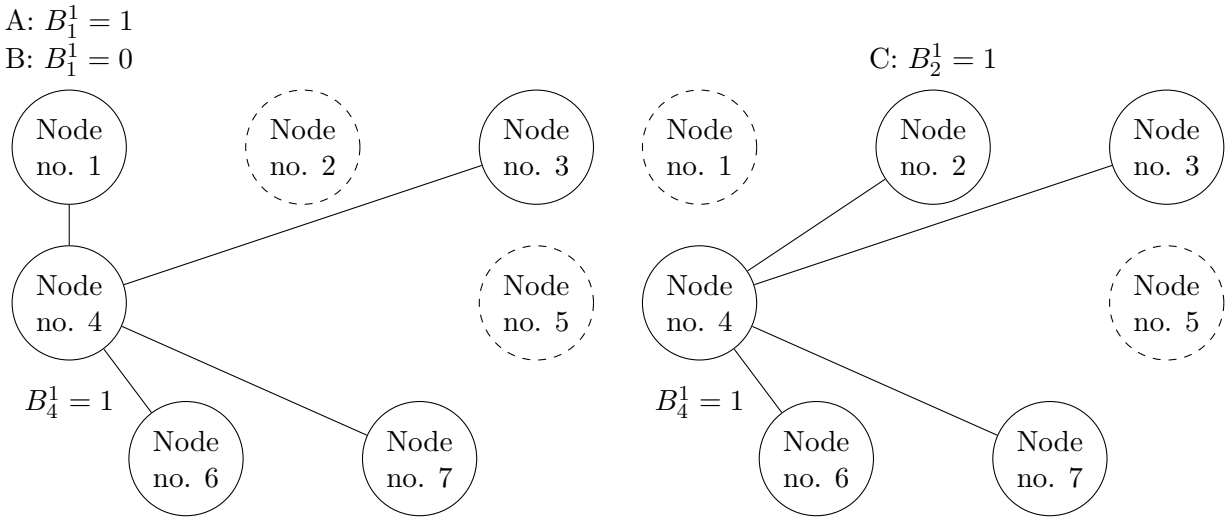

(a) Configurations A and B

(b) Configurations B and C

Figure 9.21: Configurations of the Pareto solutions found by micro-TVMOPSO for LCE vs. LCC and initial configuration for Case study no. 2

Both configurations A and B have one thermal storage tank without stratifying devices; the configuration A is equipped with flat-plate collectors ($B_1^1 = 1$) whereas configuration B is equipped with evacuated tube collectors ($B_1^1 = 0$). No non-dominated solution equipped with two thermal storage tanks were found. As shown with solution no. 5, evacuated tube collectors can harvest more solar energy, but come with a significant extra cost (an increase in LCC of 132.7% between solutions no. 4 and No. 5 for a decrease in LCE of only 4.9%).

The characteristics of the four non-dominated solutions, out of the 32 non-dominated solutions found, are reported in Table 9.8. Compared to the initial design solution, one array of flat-plate collectors with a tilt angle of 65° and one of evacuated tube collectors with a tilt angle of 75° were found to be more suitable for each objective function than two arrays of flat-plate collectors with different tilt angles (65° and 90°).

Table 9.8: Decision variable values of the non-dominated solutions found by micro-TVMOPSO for LCE vs. LCC for Case study no. 2

Decision variable	Solution			
	No. 1	No. 2	No. 4	No. 5
Configuration	A	A	A	B
$B_{1,4}$	1	1	1	1
$B_{1,5}$	0	0	0	0
$B_{2,4}$	0	0	0	0
$B_{2,5}$	0	0	0	0
$B_{3,4}$	1	1	1	1
$B_{3,5}$	0	0	0	0
$B_{4,6}$	1	1	1	1
$B_{4,7}$	1	1	1	1
$B_{5,6}$	0	0	0	0
$B_{5,7}$	0	0	0	0
B_1^1	1	1	1	0
B_1^2	0	0	0	1
B_2^1	0	0	0	0
B_2^2	0	0	0	0
B_3^1	0	0	0	0
B_3^2	1	1	1	1
B_3^3	0	0	0	0
B_4^1	1	1	1	1
B_4^2	0	0	0	0
B_5^1	0	0	0	0
B_5^2	0	0	0	0
Number of flat-plate collectors [-]	11	4	8	–
Number of evacuated-tube collectors [-]	–	–	–	13
Tilt angle of array A1 [°]	75	75	75	65
Tilt angle of array A2 [°]	–	–	–	–
Flow rate per collector area [kg/(h·m$^2_{\text{coll}}$)]	16.4	10.0	12.7	10.0
Volume of tank no. 1 (DHW or both) [L]	1,200	300	1,100	1,000
Volume of tank no. 2 (SH) [L]	–	–	–	–
Tank no. 1 auxiliary power at high location [kW]	–	–	–	–
Tank no. 1 auxiliary power at low location [kW]	–	–	–	–
Tank no. 2 auxiliary power at high location [kW]	–	–	–	–
Tank no. 2 auxiliary power at low location [kW]	–	–	–	–
DHW heater auxiliary power [kW]	8	1.5	2	1.5
SH heater auxiliary power [kW]	0.5	7.5	7.5	6.5
Objective function				
Life cycle cost [k$]	28.92	29.73	32.62	75.92
Life cycle energy use [MWh]	67.51	66.31	65.52	62.30
Life cycle exergy destroyed (technical boundary) [MWh]	338.95	449.31	636.23	762.97
Life cycle exergy destroyed (physical boundary) [MWh]	181.27	227.53	336.40	323.22

An increase of the number of solar collectors does not necessarily lead to a large decrease of the LCE value since the total energy used throughout the year is relatively small. Solutions no. 1 and no. 2 are close to each other in the objective space (in terms of LCC and LCE), but do not have similar sizing. Solution no. 1 has 11 flat-plate collectors and a large thermal storage tank of 1,200 L, whereas solution no. 2 has 4 flat-plate collectors and a small storage tank of 300 L. Solution no. 2 has a smaller investment cost and a smaller amount of embodied energy than solution no. 1; however, solution no. 2 relies more on auxiliary energy. All the non-dominated solutions used external electric heaters ($B_3^2 = 1$), as the initial design solution.

Figure 9.22 shows 16 non-dominated solutions found by micro-TVMOPSO for another combination of two objective functions: LCE and $\text{LCX}_{\text{technical}}$. Micro-TVMOPSO found non-dominated solutions that are more energy-effective and exergy-effective than the initial design solution (solution no. 15). Compared to the initial design solution, micro-TVMOPSO was able to find non-dominated solutions whose LCE and $\text{LCX}_{\text{technical}}$ values were decreased by to 64.3% and 25.8%, respectively. Since the LCC and $\text{LCX}_{\text{technical}}$ objective functions present similarities, decreasing the LCE objective function increases the $\text{LCX}_{\text{technical}}$.

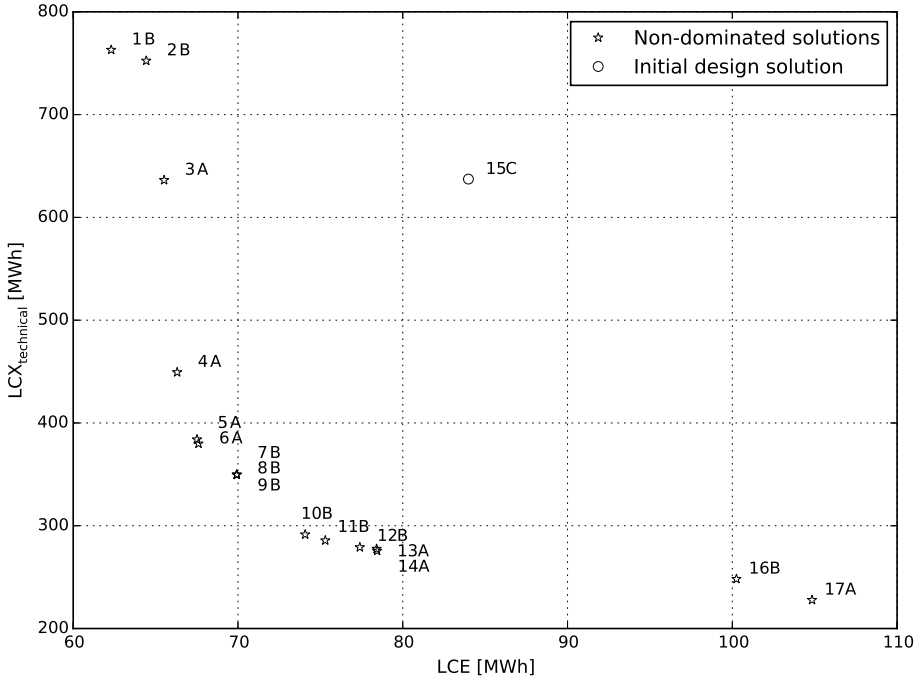

Figure 9.22: $\text{LCX}_{\text{technical}}$ vs. LCE approximation of the true Pareto front using micro-TVMOPSO for Case study no. 2

Compared to the initial design solution, the micro-TVMOPSO algorithm was able to reduce the LCC and LCE by 8.3% and 25.8%, respectively, as well as $LCX_{technical}$ and $LCX_{physical}$ by 64.3% and 40.1%, respectively. The multi-objective optimization framework was able to find a reduction of each objective compared to the initial design solution (i.e., base case solar combisystem). Different designs could be however found for different climatic and economic conditions.

Chapter 10

Conclusion

A summary of the main conclusions and contributions of this research is presented in this chapter, followed by a list of potential opportunities for future work.

10.1 Summary

This thesis explored the following research areas: (i) design of solar thermal combisystems; (ii) use of multi-objective optimization methods; (ii) micro multi-objective optimization algorithms; and (v) validation of solar combisystem models.

A preliminary study was fist conducted on multi-objective optimization method. Non-classical methods were found more suitable for optimizing solar thermal combisystems. A generic model for solar combisystems was constructed, which enables the selection of one solar combisystem configuration among several options as well as its sizing. A multi-objective optimization framework was developed for optimizing solar combisystems, based on mixed integer nonlinear programming models. A micro objective optimization algorithm, named micro-TVMOPSO, was created to overcome time constraint associated with building performance simulations. An application of the multi-objective optimization framework to two case studies led to decreasing objective functions up to 45.1% for Case study no. 1 and up to 64.3% for Case study no. 2. A lack of validation standards for solar thermal combisystems was detected and a methodology from data collection to optimization was presented in Case study no. 2.

Solar combisystem designs depend highly on specific climatic and economic conditions. Two arrays of solar thermal collectors with different tilt angles instead of one array did not come out as a valuable option. Evacuated-tube collectors were found in both cases more efficient at harvesting

solar energy, but not cost-effective enough for be an alternative solution to the initial design. The number of solar thermal collectors plays a key role in the overall performance of solar thermal combisystems. The maximum number of solar collectors, which was set equal to 22, was never attained. Larger numbers of solar collectors do not necessarily lead to better solutions because a trade-off exist between investment and savings (in terms of cost or energy). Compared to solar water heating systems, where angles of inclination should be equal to the latitude, higher inclinations are preferable for solar thermal combisystems because more heat is required in winter for space heating. The mass flow rate of the heat-transfer fluid does not have a significant impact on the overall performance.

One or two thermal storage tanks are viable options. Two thermal storage tanks increase energy savings due to a better stratification, but come with a higher investment which must be pay off over the life cycle to be worthwhile. No solutions used thermal stratifying devices, which can be unsuitable for such climatic and economic conditions or were not found during the optimization search. Electric resistances were used in Case study no. 1 whereas electric water heaters were preferred in Case study no. 2.

Multi-objective optimizations of solar thermal combisystems offer the advantage, over single-objective ones, of providing information for better compromised decisions. Optimizing both the selection of a configuration and its sizing provides a flexibility which can lead to alternative solutions increasing the overall performance of the solar combisystem being studied. The multi-objective optimization framework developed in this thesis, with the micro-TVMOPSO algorithm, can be applied to other engineering systems to enhance their performance.

10.2 Contributions

Solar thermal combisystems present a promising alternative to the use of fossil fuels in buildings, which can reduce greenhouse gas emissions and provide a more sustainable means of handling a growing energy management problem. Their apparent benefits should not prevent research studies from being conducted in order to enhance their overall performance. This research concentrated on developing a generic way of getting the most out of solar thermal combisystems through optimization. The main contributions of this thesis are:

1. A multi-objective optimization framework for optimizing solar thermal combisystems. Designing a solar combisystem requires selecting an appropriate configuration, and then sizing its components. A flexible generic model, whose concept could be extended to other building research areas, was first developed. A mixed integer nonlinear programming model was then created in co-operation with the generic model for optimizing both the selection of configuration and equipment sizing of solar combisystems.

2. A micro multi-objective optimization algorithm for time-consuming optimization problems. Many engineering problems suffer from time constraint for various reasons. One of them is the substantial computing time of building performance simulation programs. The challenge of making optimization accessible for as many engineering problems as possible was addressed with micro-TVMOPSO.

3. Application of the multi-objective optimization framework with micro-TVMOPSO to two case studies. Solar combisystem designs depend on financial and environmental conditions, so an application can result in design guidelines for a specific region.

4. A methodology for optimizing solar combisystems: from data collection to optimization. Outlier detection, uncertainty analysis, and model validation are different steps that should be considered before optimizing solar thermal combisystems.

10.3 Future work

During this research on the multi-objective optimization of solar combisystems, different topics where potential opportunities for future work could be valuable were identified and are listed herein:

1. A limited number of solar combisystem configurations were considered for the sake of simplicity; however, as shown in the literature review, recent research studies paid attention to solar combisystems equipped with a heat pump or more efficient storage (using phase change materials or thermochemical reactions), solar combi-plus systems for cooling needs, or solar combisystems using PV/T hybrid solar collectors to produce electricity. New technologies or configurations could be studied by slightly modifying the multi-objective optimization framework. Other renewable energy sources, such as geothermal energy, could also be considered.

2. Special attention has been paid to decomposition-based multi-objective evolutionary algorithms to tackle many-objective optimization problems. A set of reference points is supplied during the optimization search. Each point can be viewed as a position vector starting from the origin. These reference points or vectors are then used for decomposing the optimization problem into subproblems, which are optimized simultaneously. Such an approach enables maintaining a high diversity since non-dominated solutions are compared based on well-spread reference points. Micro multi-objective optimization algorithms, due to their small population size, face difficulties in preserving diversity. Using a decomposition-based approach for micro multi-objective optimization algorithms could make them more robust.

3. Stopping an optimization process is not an easy task. Most optimization algorithms use a fixed number of generations. Defining a stopping criterion for multi-objective optimization algorithms has become an important research area. An adaptive version of entropy (from information theory) was proposed in (Hu & Yen, 2015) as a measure of the optimization status. This entropy function could be coupled with a steady-state detection mechanism to at least detect when there is no sense in proceeding with the optimization search. A steady-state detection mechanism assesses whether or not a criterion, here entropy, varies compared to previous data points. A steady-state means that entropy, which is a measure of the optimization status, does not change. A trigger function can then be used to stop the optimization search and save time – when a maximum value of the entropy function is found.

4. The generic solar combisystem model involves different configurations inside the same TRNSYS file. Model complexity results in time-consuming simulations. Simulation and optimization parts were kept as separate as possible in this thesis to maintain flexibility. For a small number of configurations, which would be preselected, the generic solar combisystem model could be divided into different TRNSYS files, one for each configuration. One decision variable will then be allocated to the choice of the TRNSYS file. This approach, which does not allow as much flexibility, could save some computing time and make the multi-objective optimization more affordable.

References

Abdalla, N. (2013). Validated trnsys model for solar assisted space heating system. In *1st international conference & exhibition on the applications of information technology to renewable energy processes and systems.* Amman, Jordan.

Agudelo, A., & Cortés, C. (2010). Thermal radiation and the second law. *Energy*, *35*, 679-691.

Akay, B. (2013). Synchronous and asynchronous Pareto-based multi-objective Artificial Bee Colony algorithms. *Journal of Global Optimization*, *57*, 415-445.

Andersen, E., & Furbo, S. (2007). Theoretical Comparison of Solar Water/Space-Heating Combi Systems and Stratification Design Options. *Solar Energy*, *129*, 438-448.

Ardente, F., Beccali, G., Cellura, M., & Lo Brano, V. (2005). Life cycle assessment of a solar thermal collector: sensitivity analysis, energy and environmental balances. *Renewable Energy*, *30*(2), 109-130.

Asaee, S. R., Urgusal, V. I., & Beausoleil-Morrison, I. (2014). Preliminary study for solar combisystem potential in Canadian houses. *Applied Energy*, *130*, 510-518.

Asaee, S. R., Urgusal, V. I., & Beausoleil-Morrison, I. (2016). Techno-economic study of solar combisystem retrofit in the Canadian housing stock. *Solar Energy*, *125*, 426-443.

ASHRAE. (2002). *Guideline 14-2002: Measurement of Energy and Demand Savings.* Atlanta, Georgia: American Society of Heating, Refrigerating and Air-Conditioning Engineers (ASHRAE).

Ataei, A., Assadia, M. K., Parand, R., Sharee, N., Raoufinia, M., & Kani, A. H. (2009). Solar Combi-Systems a New Solution for Space Heating in Buildings. *Journal of Applied Sciences*, *9*(8), 1458-1465.

Ayompe, L. M., & Duffy, A. (2013). Analysis of the thermal performance of a solar water heating system with flat plate collectors in a temperate climate. *Applied Thermal Engineering*, *58*(1), 447-454.

Ayompe, L. M., Duffy, A., McCormack, S. J., & Conlon, M. (2011). Validated TRNSYS model for forced circulation solar water heating systems with flat plate and heat pipe evacuated tube collectors. *Applied Thermal Engineering*, *31*(8), 1536-1542.

Bahria, S., Amirat, M., Hamidat, A., Ganaoui, M. E., & Slimani, M. E. A. (2016). Parametric study of solar heating and cooling systems in different climates of Algeria – A comparison between conventional and high-energy-performance buildings. *Energy*, *113*, 521-535.

Bank of Canada. (2016). *Renewing Canadas Inflation-Control Agreement – Bank of Canada.* Retrieved on May 11, 2016, from `http://www.bankofcanada.ca/core-functions/monetary-policy/renewing-canadas-inflation-control-agreement/#optimal-inflation-target`

Beckman, W. A., Broman, L., Fiksel, A., Klein, S. A., & Lindberg, E. (1994). Trnsys, the most complete solar energy system modeling and simulation software. *Renewable Energy*, *5*, 486-488.

Ben Yahia, W., Ayadi, O., & Masmoudi, F. (2015). A Sensitivity Analysis of Multi-objective Cooperative Planning Optimization Using NSGA-II. In *Multiphysics Modelling and Simulation for Systems Design and Monitoring, Proceedings of the Multiphysics Modelling and Simulation for Systems Design Conference* (p. 327-337). Sousse, Tunisia.

Bornatico, R., Pfeiffer, M., Witzig, A., & Guzzella, L. (2012). Optimal sizing of a solar thermal building installation using particle swarm optimization. *Energy*, *41*(1), 31-37.

Bravo, R. H., & Flocker, F. W. (2012). Designing HVAC systems using particle swarm optimization. *HVAC & Research*, *18*(5), 845-857.

Brideau, S. A., Beausoleil-Morrison, I., Kummert, M., & Wills, A. (2016). Inter-model comparison of embedded-tube radiant floor models in BPS tools. *Journal of Building Performance Simulation*, *9*(2), 190-209.

Britto, A., & Pozzo, A. (2014). Using reference points to update the archive of MOPSO algorithms in Many-Objective Optimization. *Neurocomputing*, *127*, 78-87.

Cabeza, L. F., Rinción, L., Vilariño, V., Pérez, G., & Castell, A. (2014). Life cycle assessment (LCA) and life cycle energy analysis (LCEA) of buildings and the building sector: A review. *Renewable and Sustainable Energy Reviews*, *29*, 394-416.

Cao, F., Zhao, L., Zhang, F., & Guo, L. (2014). Redesign of a Water Heating System Using Evacuated Tube Solar Collectors: TRNSYS simulation and Techno-Economic Evaluation. *Heat Transfer Engineering*, *35*, 556-566.

Çengel, Y. A., & Boles, M. A. (2006). *Thermodynamics An Engineering Approach.* New York City, NY, USA: McGraw-Hill Higher Education.

Chantrelle, F. P., Lahmidi, H., Keilholz, W., Mankibi, M. E., & Michel, P. (2011). Development of a multicriteria tool for optimizing the renovation of buildings. *Applied Energy*, *88*(4), 1386-1394.

Chow, T. T., Pei, G., Fong, K. F., Lin, Z., Chan, A. L. S., & Li, J. (2009). Energy and exergy analysis of photovoltaicthermal collector with and without glass cover. *Applied Energy*, *86*, 310-316.

Clarke, J., Colclough, S., Griffiths, P., & McLeskey, J. T. (2014). A passive house with seasonal solar energy store: in situ data and numerical modelling. *International Journal of Ambient Energy*, *35*(1), 37-50.

Clerc, M., & Kennedy, J. (2002). The particle swarm – explosion, stability, and convergence in multidimensional complex space. *IEEE Transactions on Evolutionary Computation*, *6*(1), 58-73.

Coakley, D., Raftery, P., & Keane, M. (2014). A review of methods to match building energy simulation models to measured data. *Renewable and Sustainable Energy Reviews*, *37*, 123-141.

Coelho, J. P., de Moure Oliveira, P. B., & Cunha, J. B. (2005). Greenhouse air temperature predictive control using the particle swarm optimisation algorithm. *Computers and electronics in agriculture*, *49*(3), 330-344.

Coello Coello, C. A. (2006). Evolutionary Multi-Objective Optimization: A Historical View of the Field. *IEEE Computational Intelligence Magazine*, *1*(1), 28-36.

Coello Coello, C. A., & Lechuga, M. S. (2002). MOPSO: A proposal for multiple objective particle swarm optimization. In *Proceedings of the 2002 Congress on Evolutionary Computation (CEC '02).* Honolulu, HI.

Coello Coello, C. A., & Pulido, G. T. (2001). Multiobjective Optimization using a Micro-Genetic Algorithm. In *Proceedings of the Genetic and Evolutionary Computation Conference* (p. 274-282). Morgan Kaufmann Publishers Inc.

Coello Coello, C. A., Pulido, G. T., & Lechuga, M. S. (2004). Handling Multiple Objectives With Particle Swarm Optimization. *IEEE Transactions on evolutionary computation*, *8*(3), 256-279.

Colclough, S., & McGrath, T. (2015). Net energy analysis of a solar combisystem with Seasonal Thermal Energy Store. *Applied Energy*, *147*, 611-616.

Cousineau, D., & Chartier, S. (2010). Outliers detection and treatment: A review. *International journal of Psychological Research*, *3*(1), 58-67.

Deb, K. (2001). *Multi-Objective Optimization Using Evolutionary Algorithms.* New York, NY, USA: John Wiley & Sons.

Deb, K., & Jain, H. (2014). An Evolutionary Many-Objective Optimization Algorithm Using Reference-Point-Based Nondominated Sorting Approach, Part I: Solving Problems With Box Constraints. *IEEE Transactions on Evolutionary Computation*, *18*(6), 577-601.

Deb, K., Pratap, A., Agarwal, S., & Meyarivan, T. (2002). A Fast and Elitist Multiobjective Genetic Algorithm NSGA-II. *IEEE transactions on evolutionary computation*, *6*(2), 182-197.

Deb, K., Thiele, L., Laumanns, M., & Zitzler, E. (2001). *Scalable test problems for evolutionary multi-objective optimization.* Dept. Comput. Eng. Netw. Lab., ETH Zurich, Zurich, Switzerlnd, TIK-Tech, Rep. 112. Retrieved on July 06, 2017, from `http://e-collection.library.ethz.ch/eserv/eth:24696/eth-24696-01.pdf`

Deng, S., Dai, Y. J., & Wang, R. Z. (2013). Performance optimization and analysis of solar combi-system with carbon dioxide heat pump. *Solar Energy*, *98*, 212-225.

Department of Revenue. (2016). *A Guide to Sales and Use Tax.* Retrieved on April 13, 2016, from `http://www.mass.gov/dor/individuals/taxpayer-help-and-resources/tax-guides/salesuse-tax-guide.html`

Dincer, I. (2002). The role of exergy in energy policy making. *Energy Policy*, *30*, 137-149.

Dincer, I., & Rosen, M. A. (2006). *EXERGY: Energy, Environment and Sustainable Development.* New York, USA: Elsevier Science.

Djurica, N., Novakovic, V., Holst, J., & Mitrovic, Z. (2007). Optimization of energy consumption in buildings with hydronic heating systems considering thermal comfort by use of computer-based tools. *Energy and Buildings*, *39*, 471-477.

Duffie, J. A., & Beckman, W. A. (2006). *Solar Engineering of Thermal Processes.* Hoboken, NJ, USA: John Wiley & Sons, Inc.

Durillo, J. J., García-Nieto, J., Nebro, A. J., Coello Coello, C. A., Luna, F., & Alba, E. (2009). Multi-objective particle swarm optimizers: An experimental comparison. In *International Conference on Evolutionary Multi Criterion Optimization* (p. 495-509). Berlin Heidelberg: Springer.

Durillo, J. J., & Nebro, A. J. (2011). jMetal: A java framework for multi-objective optimization. *Advances in Engineering Software*, *42*(10), 760-771.

Evins, R. (2013). A review of computational optimisation methods applied to sustainable building design. *Renewable and Sustainable Energy Reviews*, *22*, 230-245.

EVO. (2012). *International Performance Measurement & Verification Protocol Concepts and Options for Determining Energy and Water Savings Volume I.* Efficiency Valuation Organisation (EVO). Golden, CO, US. Retrieved on July 11, 2017, from `http://www.nrel.gov/docs/fy02osti/31505.pdf`

Fanger, P. O. (1970). *Thermal comfort: Analysis and applications in environmental engineering.* Copenhagen, Denmark: Danish Technical Press.

Fesanghary, M., Asadi, S., & Geem, Z. W. (2012). Design of low-emission and energy-efcient residential buildings using a multi-objective optimization algorithm. *Building and Environment*, *49*, 245-252.

Fiedler, F., Nordlander, S., Persson, T., & Bales, C. (2006). Thermal performance of combined solar and pellet heating systems. *Renewable Energy*, *31*, 73-88.

Fister, J. I., Yang, X., Fister, I., Brest, J., & Fister, D. (2013). A Brief Review of Nature-Inspired Algorithms for Optimization. *Elektrotehniški vestnik*, *3*, 1-7. Retrieved on July 11, 2017, from `http://dblp.uni-trier.de/db/journals/corr/corr1307.html#FisterYFBF13`

Fuentes Cabrera, J. C., & Coello Coello, C. A. (2007). Handling Constraints in Particle Swarm Optimization using a Small Population Size. In *Mexican International Conference on Artificial Intelligence* (p. 41-51). Berlin Heidelberg: Springer.

Fuentes Cabrera, J. C., & Coello Coello, C. A. (2010). Micro-MOPSO: A Multi-Objective Particle Swarm Optimizer That Uses a Very Small Population Size. In *Multi-objective swarm intelligent systems* (p. 83-104). Berlin Heidelberg: Springer.

Fuller, S. K., & Petersen, S. R. (1996). *LIFE-CYCLE COSTING MANUAL for the Federal Energy Management Program.* National Institue of Standards and Technology. Retrieved on July 11, 2017, from `http://fire.nist.gov/bfrlpubs/build96/PDF/b96121.pdf`

Fuller, S. K., Petersen, S. R., & Dellísola, A. (1995). *Life Cycle Costing for Design Professionals.* McGraw-Hill Companies.

Gaz Métro. (2016). *Rates and conditions.* Retrieved on May 11, 2016, from `http://www.grandeentreprise.gazmetro.com/tarifsconditions/default.aspx?culture=en-ca`

Ghiasi, H., Pasini, D., & Lessard, L. (2011). A non-dominated sorting hybrid algorithm for multi-objective optimization of engineering problems. *Engineering Optimization*, *43*(1), 39-59.

Ghiaus, C., & Jabbour, N. (2012). Optimization of multifunction multi-source solar systems by design of experiments. *Solar Energy*, *86*, 593-607.

Glembin, J., Haselhorst, T., Steinweg, J., Föste, S., & Rockendorf, G. (2016). Direct integration of solar heat into the space heating circuit. *Solar Energy*, *131*, 1-20.

Glembin, J., & Rockendorf, G. (2012). Simulation and evaluation of stratified discharging and charging devices in combined solar thermal systems. *Solar Energy*, *86*, 407-420.

Goldberg, D. E. (1989). *Genetic Algorithms in Search, Optimization, and Machine Learning.*

Government of Canada. (2016). *Cost-Benefit Analysis of the Canada Small Business Financing Program.* Retrieved on May 11, 2016, from `https://www.ic.gc.ca/eic/site/061.nsf/eng/h_02912.html`

Gürzenich, D., & Mathur, J. (1998). *Material and Energy Demand for selected renewable energy technologies.* International Bureau of the BMBF.

Hadorn, J.-C., Weiss, W., Suter, J.-M., & Letz, T. (2002). SYSTEM DESIGNS AND PERFORMANCE OF SOLAR COMBISYSTEMS. In *Proc. EuroSun 02.* Bologna, Italy.

Haimes, Y. Y., Lasdon, L. S., & Wismer, D. A. (1971). On a bicriterion formulation of the problems of integrated system identification and system optimization. *IEEE Transactions on Systems*, *1*, 296-297.

Hang, Y., Qu, M., & Zhao, F. (2012). Economic and environmental life cycle analysis of solar hot water systems in the United States. *Energy and Buildings*, *45*, 181-188.

Harvey, L. D. D. (2006). *A Handbook on Low-Energy Buildings and District-Energy Systems: Fundamentals Techniques and Examples.* London, Sterling, VA, USA: Earthscan.

Hasan, A., Vuolle, M., & Sirén, K. (2008). Minimisation of life cycle cost of a detached house using combined simulation and optimisation. *Building and Environment*, *43*, 2022-2034.

Hasni, A., Taibi, R., Draoui, B., & Boulard, T. (2011). Optimization of Greenhouse Climate Model Parameters Using Particle Swarm Optimization and Genetic Algorithms. *Energy Procedia*, *6*, 371-380.

Hawkins, D. M. (1980). *Identification of Outliers.* London, England: Chapman & Hall.

Hazami, M., Mehdaoui, F., Naili, N., Noro, M., Lazzarin, R., & Guizani, A. (2017). Energetic, exergetic and economic analysis of an innovative Solar CombiSystem (SCS) producing thermal and electric energies: Application in residential and tertiary households. *Energy Conservation and Management*, *140*, 36-50.

Heimrath, R., & Haller, M. (2007). *The Reference Heating System, the Template Solar System.* Report A2 of Subtask A of IEA-SHC Task 32 Advanced storage concepts for solar and low energy buildings.

Hepbasli, A. (2012). Low exergy (LowEx) heating and cooling systems for sustainable buildings and societies. *Renewable and Sustainable Energy Reviews*, *16*, 73-104.

Home Performance Coalition. (2012). *Past Events.* Retrieved on July 06, 2017, from `https://www.yumpu.com/en/document/view/36270727/solar-thermal-combisystems-for-space-heating-amp-domestic-hot-water`

Hooke, R., & Jeeves, T. A. (1961). "Direct Search" Solution of Numerical and Statistical Problems. *Journal of the Association for Computing Machinery (ACM)*, *8*(2), 212-229.

Hu, W., & Yen, G. G. (2015). Adaptive Multiobjective Partice Swarm Optimization Based on Parallel Cell Coordinate System. *IEEE Transactions on Evolutionary Computation*, *19*(1), 1-18.

Huber, P. J. (1981). *Robust statistics.* New York, USA: John Wiley & Sons.

Hugo, A., Zmeureanu, R., & Rivard, H. (2010). Solar combisystem with seasonal thermal storage. *Journal of Building Performance Simulation*, *3*(4), 255-268.

Hydro Québec. (2016). *Comparison of Electricity Prices.* Retrieved on May 11, 2016, from `http://www.hydroquebec.com/business/rates-and-billing/rates/comparison-of-electricity-prices/`

IES. (2017). *Integrated Environmental Solutions (IES).* Retrieved on July 10, 2017, from `http://www.iesve.com/`

IRENA. (2016). *IRENA – The International Renewable Energy Agency.* Retrieved on July 06, 2017, from http://www.irena.org/home/index.aspx?PriMenuID=12&mnu=PriPriMenuID=12&mnu=Pri

Islam, H., Jollands, M., & Setunge, S. (2015). Life cycle assessment and life cycle cost implication of residential buildings - A review. *Renewable and Sustainabl eEnergy Reviews*, *42*, 129-140.

Jetler, S. M. (1981). Maximum conversion efficiency for the utilization of direct solar radiation. *Solar Energy*, *26*, 231-236.

Jiang, S., Ong, Y.-S., Zhang, J., & Feng, L. (2014). Consistencies and contradictions of performance metrics in Multiobjective Optimization. *IEEE Transactions on Cybernetics*, *44*(12), 2391-2404.

Jordan, U., & Vajen, K. (2000). Influence of the DHW Load Profile on the Fractional Energy Savings: A Case Study of a Solar Combi-System with TRNSYS Simulations. *Solar Energy*, *69*, 197-208.

Kaçan, E. (2015). Exergetic optimization of basic system components for maximizing exergetic efficiency of solar combisystems by using response surface methodology. *Energy and Buildings*, *91*, 65-82.

Kaçan, E., & Ulgen, K. (2012). Energy analysis of Solar Combisystems in Turkey. *Energy Conversion and Management*, *64*, 378-386.

Kaçan, E., & Ulgen, K. (2014). Energy and exergy analysis of solar combisystems. *International Journal of Exergy*, *14*(3), 364-387.

Kalogirou, S. A. (2004a). Environmental benefits of domestic solar energy systems. *Energy Conservation & Management*, *45*(1), 3075-3092.

Kalogirou, S. A. (2004b). Solar thermal collectors and applications. *Progress in Energy and Combustion Science*, *30*(13), 231-295.

Kalogirou, S. A. (2009). Thermal performance, economic and environmental life cycle analysis of thermosiphon solar water heaters. *Solar Energy*, *83*, 39-48.

Kennedy, J., & Eberhart, R. (1995). Particle Swarm Optimization. In *Proc. IEEE Int. Conf. Neural Networks* (p. 1942-1948).

Kim, I. Y., & de Weck, O. L. (2006). Adaptive weighted sum method for multiobjective optimization: a new method for Pareto front generation. *Structural and Multidisciplinary Optimization*, *31*(2), 105-116.

Klein, S. A., Duffie, J. A., Mitchell, J. C., Kummer, J. P., Thornton, J. W., Bradley, D. E., ... Kummert, M. (2017). *TRNSYS 17: A Transient System Simulation Program.* Solar Energy Laboratory, University of Wisconsin, Madison, USA. Retrieved on July 06, 2017, from `http://sel.me.wisc.edu/trnsys/index.html`

Knowles, J. D., & Corne, D. W. (2000). Approximating the nondominated front using the Pareto Archived Evolution Strategy. *Evolutionary Computation*, *8*(2), 149 - 172.

Kursawe, F. (1996). *A variant of evolution strategies for vector optimization.* Berlin, Germany: Springer-Verlag.

Kusyy, O., & Vajen, K. (2012). Simulation-based Estimation of the Optimization Potential of Dynamic Controller Settings for Solar Thermal Combisystems. *Strojarstvo: časopis za teoriju i praksu u strojarstvu*, *54*(6), 471-475.

Landry, M., & Gagnon, Y. (2015). Energy Storage: Technology Applications and Policy Options. *Energy Procedia*, *79*, 315-320.

Lavappa, P. D., & Kneifel, J. D. (2015). *Energy Price Indices and Discount Factors for Life-Cycle Cost Analysis 2015.* National Institue of Standards and Technology. Retrieved on July 06, 2017, from `http://nvlpubs.nist.gov/nistpubs/ir/2015/NIST.IR.85-3273-30.pdf`

Leckner, M. (2008). *Life Cycle Energy and Cost Analysis of a Net Zero Energy House (NZEH) Using a Solar Combisystem* (M.S. thesis). Dept. Build. Eng., Concordia Univ., Montreal, QC

Leckner, M., & Zmeureanu, R. (2011). Life cycle cost and energy analysis of a Net Zero Energy House with solar combisystem. *Applied Energy*, *88*, 232-241.

Letz, T., Bales, C., & Perers, B. (2009). A new concept for combisystems characterization: The FSC method. *Solar Energy*, *83*, 1540-1549.

Leys, C., Ley, C., Klein, O., Bernard, P., & Licata, L. (2013). Detecting outliers: Do not use standard deviation around the mean, use absolute deviation around the mean. *Journal of Experimental Social Psychology*, *49*(4), 764-766.

Li, H., & Zhang, Q. (2009). Multiobjective Optimization Problems With Complicated Pareto Sets, MOEA/D and NSGA-II. *IEEE Transactions on Evolutionary Computation*, *13*(2), 284-302.

Li, M., Yang, S., & Liu, X. (2014). Diversity Comparison of Pareto Front Approximations in Many-Objective Optimization. *IEEE Transactions on Cybernetics*, *44*(12), 2568-2584.

Lin, Z., Lee, C. K., Fong, K. F., & Chow, T. T. (1997). Comparison of annual energy performances with different ventilation methods for temperature and humidity control. *Energy and Buildings*, *43*(12), 3599-3608.

Luke, S. (2015). *Essentials of Metaheuristics* (second ed.). Lulu. (Available for free at http://cs.gmu.edu/∼sean/book/metaheuristics/)

Lund, P. (2005). Sizing and applicability considerations of solar combisystems. *Solar Energy*, *78*, 59-71.

Lundh, M., Zass, K., Wilhelms, C., Vajen, K., & Jordan, U. (2010). Influence of store dimensions and auxiliary volume configuration on the performance of medium-sized solar combisystems. *Solar Energy*, *84*, 1095-1102.

Machairas, V., Tsangrassoulis, A., & Axarli, K. (2014). Algorithms for optimization of building design: A review. *Renewable and Sustainable Energy Reviews*, *31*, 101-112.

Magnier, L., & Haghighat, F. (2010). Multiobjective optimization of building design using TRNSYS simulations, genetic algorithm, and Artificial Neural Network. *Building and Environment*, *45*(3), 739-746.

Mahdavi, S., Shiri, M. E., & Rahnamayan, S. (2015). Metaheuristics in large-scale global continues optimization: A survey. *Information Sciences*, *295*, 407-428.

Maria, A. (1997). INTRODUCTION TO MODELING AND SIMULATION. In *Proceedings of the 1997 winter simulation conference.* Atlanta, USA.

Marler, R. T., & Arora, J. S. (2010). The weighted sum method for multi-objective optimization: new insights. *Structural and Multidisciplinary Optimization*, *41*, 853-862.

Martinopoulos, G., & Tsalikis, G. (2014). Active solar heating systems for energy efficient buildings in Greece: A technical economic and environmental evaluation. *Energy and Buildings*, *68*, 130-137.

MATLAB. (2017). *MATLAB – MathWorks The Language of Technical Computing.* Retrieved on May 03, 2017, from `https://www.mathworks.com/products/matlab.html`

Mauthner, F., & Weiss, W. (2013). *Solar Heat Worldwide Markets and Contribution to the Energy Supply 2011.* AEE – Institute for Sustainable Technologies. Hamburg, Germany. Retrieved on July 06, 2017, from `https://www.iea-shc.org/data/sites/1/publications/Solar-Heat-Worldwide-2013.pdf`

Mette, B., Kerskes, H., Drück, H., & Müller-Steinhagen, H. (2013). New highly efficient regeneration process for thermochemical energy. *Applied Energy*, *109*, 353-359.

Michalewicz, Z. (1996). *Genetic Algorithms + Data Structures = Evolution Programs.* Berlin, Germany: Springer-Verlag.

Minol. (2015). *Minol USA - Submetering.* Retrieved on September 24, 2015, from `http://www.minolusa.com/pdf/Minomess-Meter-Information.pdf`

Moore, J., & Chapman, R. (1999). *Application Of Particle Swarm To Multiobjective Optimization.*

Moran, M. J., & Shapiro, H. N. (2004). *Fundamentals of Engineering Thermodynamics.* Hoboken, NJ, USA: John Wiley & Sons.

Moslemi, H., & Zandieh, M. (2011). Comparisons of some improving strategies on MOPSO for multi-objective (r, Q) inventory system. *Expert Systems with Applications*, *38*(10), 12051-12057.

Nebro, A. J., Durillo, J. J., García-Nieto, J., Coello Coello, C. A., Luna, F., & Alba, E. (2009). SMPSO: A New PSO-based Metaheuristic for Multi-objective Optimization. In *2009 IEEE*

Symposium on Computational Intelligence in Multi-Criteria Decision-Making (MCDM'09) (p. 66-73). Nashville, TN, USA: IEEE.

Nebro, A. J., Luna, F., Alba, E., Dorronsoro, B., Durillo, J. J., & Behamb, A. (2008). AbYSS: Adapting Scatter Search to Multiobjective Optimization. *IEEE Transactions on Evolutionary Computation*, *12*(4), 439-453.

Ng Chen Hin, J. (2013). *Life Cycle Optimization of a Residential Solar Combisystem for Minimum Cost, Energy Use and Exergy Destroyed* (M.S. thesis). Dept. Build. Eng., Concordia Univ., Montreal, QC

Ng Cheng Hin, J., & Zmeureanu, R. (2014). Optimization of a residential solar combisystem for minimum life cycle cost, energy use and exergy destroyed. *Solar Energy*, *100*, 102-113.

Nguyen, A. T., Reiter, S., & Rigo, P. (2014). A review on simulation-based optimization methods applied to building performance analysis. *Applied Energy*, *113*, 1043-1058.

Nyboer, J., & Lutes, K. (2011). *A Review of Renewable Energy in Canada, 2009.* Natural Resources Canada and Environment Canada, Canadian Industrial Energy End-use Data and Analysis Centre Simon Fraser University. Burnaby, BC, Canada.

OECD/IEA. (2013). *Transition to Sustainable Buildings Strategies and Opportunities to 2050.* Paris, France: International Energy Agency (IEA). Retrieved on July 06, 2017, from `http://www.iea.org/publications/freepublications/publication/Building2013_free.pdf`

Pasandideh, S. H. R., Niaki, S. T. A., & Sharafzadeh, S. (2013). Optimizing a bi-objective multi-product EPQ model with defective items, rework and limited orders: NSGA-II and MOPSO algorithms. *Journal of Manufacturing Systems*, *38*(4), 764-770.

Patela, R. (1964). Exergy of heat radiation. *Heat Transfer*, *86*, 187-192.

Perlman, M., & Mills, B. (1985). Development of residential hot water use patterns. *ASHRAE Transactions*, *91*, 657-679.

Peyvanddi, M., Zafarani, M., & Nasr, E. (2011). Comparison of Particle Swarm Optimization and the Genetic Algorithm in the Improvement of Power System Stability by an SSSC-based Controller. *Journal of Electrical Engineering & Technology*, *6*(2), 182-191.

Pichler, M. F., Lerch, W., Heinz, A., Goertler, G., Schranzhofer, H., & Rieberer, R. (2014). A novel linear predictive control approach for auxiliary energy supply to a solar thermal combistorage. *Solar Energy*, *101*, 203-219.

Poppi, S., Bales, C., Haller, M. Y., & Heinz, A. (2016). Influence of boundary conditions and component size on electricity demand in solar thermal and heat pump combisystems. *Applied Energy*, *162*, 1062-1073.

Poppi, S., Bales, C., Heinz, A., Hengel, F., Chèze, D., Mojic, I., & Cialani, C. (2016). Analysis of system improvements in solar thermal and air source heat pump combisystems. *Applied Energy*, *173*, 606-623.

Pulido, G. T., & Coello Coello, C. A. (2003). The Micro Genetic Algorithm 2: Towards On-Line Adaptation in Evolutionary Multiobjective Optimization. In *International Conference on Evolutionary Multi-Criterion Optimization* (p. 252-266). Berlin Heidelberg: Springer.

Raffenel, Y., Fabrizio, E., Virgone, J., Blanco, E., & Filippi, M. (2009). Integrated solar heating systems: from initial sizing procedure to dynamic simulation. *Solar Energy*, *83*, 657-663.

Ramesh, T., Prakash, R., & Shukla, K. K. (2010). Life cycle energy analysis of buildings: An overview. *Energy and Buildings*, *42*, 1592-1600.

Ravindran, A., Reklaitis, G. V., & Ragsdell, K. M. (2006). *Engineering OptimizationP: Methods and Applications*. New York, US: John Wiley & Sons.

Ray, T., Tai, K., & Seow, K. C. (2001). MULTIOBJECTIVE DESIGN OPTIMIZATION BY AN EVOLUTIONARY ALGORITHM. *Engineering Optimization*, *33*(4), 399-424.

Reddy, T. A. (2011). *Applied Data Analysis and Modeling for Energy Engineers and Scientists*. New York, USA: Springer.

RESOL. (2015a). *RESOL® - V40 Flowmeter.* Retrieved on September 24, 2015, from http://www.resol.de/index/produktdetail/kategorie/4/id/57/sprache/en

RESOL. (2015b). *RESOL® - WMZ Calorimeter.* Retrieved on September 24, 2015, from http://www.resol.de/index/produktdetail/kategorie/2/id/41/sprache/en

Revenu Québec. (2016). *Revenu Québec - Tables of GST and QST Rates.* Retrieved on April 13, 2016, from http://www.revenuquebec.ca/en/entreprises/taxes/tpstvhtvq/reglesdebase/historiquetauxtpstvq.aspx

Rey, A., & Zmeureanu, R. (2016). Multi-objective optimization of a residential solar thermal combisystem. *Solar Energy*, *139*, 622-632.

Rey, A., & Zmeureanu, R. (2017). Micro-Time Variant Multi-Objective Particle Swarm Optimization (micro-TVMOPSO) of a solar thermal combisystem [in press]. *Swarm and Evolutionary Computation*. doi: https://doi.org/10.1016/j.swevo.2017.04.005

Reyes-Sierra, M., & Coello Coello, C. A. (2006). Multi-Objective Particle Swarm Optimizers: A Survey of the State-of-the-Art. *International Journal of Computational Intelligence Research*, *2*(3), 287-308.

Roy, R., Hinduja, S., & Teti, R. (2008). Recent advances in engineering design optimisation: challenges and future trends. *CIRP Annals - Manufacturing Technology*, *57*(2), 697-715.

RSMeans. (2014). *RSMeans® Mechanical Cost Data.* Norwell, MA, USA: Author.

RSMeans. (2016). *RSMeans® Building Construction Cost Data.* Norwell, MA, USA: Author.

Ruicheng, Z., & Jingjingm, N. (2015). Analysis for makertization development prospect of large-scale solar heating combisystems in China. *Energy Procedia*, *70*(4), 574-579.

Schimpf, S., & Span, R. (2015). Techno-economic evaluation of a solar combined heat pump-Organic Rankine Cycle system. *Energy Conservation and Management*, *94*, 430-437.

Schwartz, Y., Raslan, R., & Mumovic, D. (2016). Implementing multi objective genetic algorithm for life cycle carbon footprint and life cycle cost minimisation: A building refurbishment case study. *Energy*, *97*, 58-68.

Shakerian, R., Kamali, S. H., Hedayati, M., & Alipour, M. (2011). Comparative Study of Ant Colony Optimization and Particle Swarm Optimization for Grid Scheduling. *The Journal of Mathematics and Computer Science*, *2*(3), 469-474.

Shariah, A., & Shalabi, B. (1997). Optimal design for a thermosyphon solar water heater. *Renewable Energy*, *11*(3), 351-361.

Shi, Y., & Eberhart, R. (1998). A modified particle swarm optimizer. In *IEEE World Congress on Computational Intelligence.* Anchorage, AK, US.

Silicon Solar. (2016). *StorMaxx Solar Hot Water Storage Tanks.* Retrieved on May 11, 2016, from `http://www.siliconsolar.com/shop/solar-store/solar-hot-water-heaters/solar-water-storage-tanks/`

Srinivas, N., & Deb, K. (1994). Multiobjective optimization using nondominated sorting in genetic algorithms. *Evolutionary Computation*, *2*(3), 221-248.

Stephan, A., & Stephan, L. (2016). Life cycle energy and cost analysis of embodied, operational and user-transport energy reduction measures for residential buildings. *Applied Energy*, *161*, 445-464.

Stricher, E., Heidemann, W., & Müller-Steinhagen, H. (2004). Energy Payback Time - A Key Number for the Assessment of Thermal Solar Systems. In *Proceedings of EuroSun2004.* Freiburg, Germany.

Suter, J.-M., Letz, T., & Weiss, W. (2000). *Solar Combisystems in Austria, Denmark, Finland, France, Germany, Sueden, Switzerland, the Netherlands and the USA – Overview 2000.* IEA SHC Task 26 Solar Combisystems.

Suzuki, A. (1988). GENERAL THERORY OF EXERGY-BALANCE ANALYSIS AND APPLICATION TO SOLAR COLLECTORS. *Energy*, *13*, 153-160.

TESS. (2014). *Welcome to TESS.* Retrieved from `http://www.tess-inc.com/` (Last visited on December 13, 2014)

The Home Depot. (2016). *Water heaters.* Retrieved on June 20, 2016, from https://www.homedepot.ca/en/home/ideas-how-to/buying-guides/building-materials/water-heaters.html

Thermo Dynamics Ltd. (2016). *Thermo Dynamics Ltd. – Solar Products.* Retrieved on May 11, 2016, from http://www.thermo-dynamics.com/products.html#storagetanks

Thundil, R. K. R., Pavan, P., & Rajeev, D. R. (2012). Experimental Investigation of a New Solar Flat Plate Collector. *Research Journal of Engineering Sciences*, *14*, 1-8.

Timilsina, G. R., Kurdgelashvili, L., & Narbel, P. A. (2012). Solar energy: Markets, economics and policies. *Renewable and Sustainable Energy Reviews*, *16*(1), 449-465.

Tokarik, M. S., & Richman, R. C. (2016). Life cycle cost optimization of passive energy efficiency improvements in a Toronto house. *Energy and Buildings*, *118*, 160-169.

Torío, H., Angelotti, A., & Schmidt, D. (2009). Exergy analysis of renewable energy-based climatisation systems for buildings: A critical view. *Energy and Buildings*, *41*, 248-271.

Torío, H., & Schmidt, D. (2010). Framework for analysis of solar energy systems in the built environment from an exergy perspective. *Renewable Energy*, *35*, 2689-2697.

Tripathi, P. K., Bandyopadhyay, S., & Pal, S. K. (2007). Multi-objective particle swarm optimization with time variant inertia and acceleration coefficients. *Information Sciences*, *177*(22), 5033-5049.

United States Department of Labor. (2016). *Inflation Calculator: Bureau of Labor Statistics.* Retrieved on May 11, 2016, from http://www.bls.gov/data/inflation_calculator.htm

ur Rehman, H., Hirvonen, J., & Sirn, K. (2016). Design of a Simple Control Strategy for a Community-size Solar Heating System with a Seasonal Storage. *Energy Procedia*, *91*, 486-495.

U.S. Energy Information Administration. (2016). *U.S. Energy Information Administration (EIA).* Retrieved on May 11, 2016, from https://www.eia.gov/

Žandeckis, A., Kirsanovs, A., Dzikēvičs, M., & Klavina, K. (2016). Solar and pellet combisystem for apartment buildings: Heat losses and efficiency improvements of the pellet boiler. *Energy Efficiency*, *101*, 1-13.

Žandeckis, A., Timma, L., Blumderga, D., & Rochas, C. (2011). Possibilities for Utilization of solar Thermal Energy in Multi-Family Building in Latvia. *Scientific Journal of Riga technical University Environmental and Climate technologies*, *6*(1), 138-146.

Žandeckis, A., Timma, L., Blumderga, D., Rochas, C., & Rošā, M. (2013). Solar and pellet combisystem for apartment buildings: Heat losses and efficiency improvements of the pellet boiler. *Applied Energy*, *101*, 244-252.

Van Veldhuizen, D. A., & Lamont, G. B. (1998). Evolutionary computation and convergence to a pareto front. In *Genetic programming 1998 conference* (p. 221-228). Stanford, CA, USA.

Viennet, R., Fontiex, C., & Marc, I. (1996). Multicriteria optimization using a genetic algorithm for determining a Pareto set. *Journal System Science*, *27*(2), 255-260.

Wang, W., Rivard, H., & Zmeureanu, R. (2005). An object-oriented framework for simulation-based green building design optimization with genetic algorithms. *Advanced Engineering Informatics*, *19*(1), 5-23.

Weather Analytics. (2016). *Weather Analytics - Get Weather Smart.* Retrieved on July 10, 2017, from `http://www.weatheranalytics.com/wa/`

Weiss, W. (2003). *Solar Heating Systems for Houses: A Design Handbook for Solar Combisystems.* London, UK: James & James.

Wetter, M. (2004). *Simulation-Based Building Energy Optimization* (Ph.D. thesis). Dept. Mech. Eng., University of California, Berkeley, Berkeley, CA.

Wetter, M. (2011). *GenOpt: Generic Optimization Program, User Manual Version 3.1.0.* Lawrence Berkeley National Laboratory. Retrieved from `https://simulationresearch.lbl.gov/GO/`

Wetter, M., & Wright, J. (2004). A comparison of deterministic and probabilistic optimization algorithms for nonsmooth simulation-based optimization. *Building and Environment*, *39*(8), 989-999.

Wolpert, D. H., & Macready, W. G. (1997). No Free Lunch Theorems for Optimization. *IEEE Transactions on Evolutionary Computation*, *1*(1), 67-82.

Yan, Q., & Li, N. (2012). Comparative Studies on Solar Combisystem by Different Auxiliary Heat Sources. *Applied Mechanics and Materials*, *178*, 76-79.

Yang, J., Zhou, J., Liu, L., & Li, Y. (2009). A novel strategy of pareto-optimal solution searching in multi-objective particle swarm optimization (MOPSO). *Computers & Mathematics with Applications*, *57*(11), 1995-2000.

Yang, R., & Wang, L. (2012). Multi-objective optimization for decision-making of energy and comfort management in building automation and control. *Sustainable Cities and Society*, *2*(1), 1-7.

Yang, S., Li, M., Liu, X., & Zheng, J. (2013). A grid-based evolutionary algorithm for many-objective optimization. *IEEE Transactions on Evolutionary Computation*, *17*(5), 721-736.

Yazdanshenas, E., & Furbo, S. (2010). Theoretical study of solar combisystems based on bikini tanks and tank-in-tank stores. *International Journal of Numerical Methods for Heat & Fluid Flow*, *22*(2), 251-262.

Yuan, Y., Xu, H., Wang, B., Zhang, B., & Yao, X. (2016). Balancing Convergence and Diversity in Decomposition-Based Many-Objective Optimizers. *IEEE Transactions on Evolutionary Computation*, *20*(2), 180-198.

Zeng, Y., & Sun, Y. (2014). Application of hybrid MOPSO algorithm to optimal reactive power dispatch problem considering voltage stability. *Journal of Electrical and Computer Engineering*, 1-12.

Zhan, Z.-H., Zhang, J., Li, Y., & Shu-Hung, H. (2009). Adaptive Particle Swarm Optimization. *IEEE Transactions on Systems, Man, and Cybernetics – Part B: (Cybernetics)*, *39*(6), 1362-1381.

Zhang, Q., & Li, H. (2007). MOEA/D: A Multiobjective Evolutionary Algorithm Based on Decomposition. *IEEE Transactions on Evolutionary Computation*, *11*(6), 712-731.

Zhang, Q., Zhou, A., Zhao, S., Suganthan, P., Liu, W., & Tiwari, S. (2009). *Multiobjective optimization test instances for the CEC 2009 special session and competition.* University of Essex and Nanyang Technological University, Tech. Rep. CES-487. Retrieved on July 06, 2017, from `http://dces.essex.ac.uk/staff/zhang/MOEAcompetition/cec09testproblem0904.pdf`

Zhang, X., Tian, Y., Y., & Jin. (2015). A Knee Point-Driven Evolutionary Algorithm for Many-Objective Optimization. *IEEE Transactions on Evolutionary Computation*, *19*(6), 761-776.

Zhang, Y., Gong, D.-W., & Ding, Z.-H. (2011). Handling multi-objective optimization problems with a multi-swarm cooperative particle swarm optimizer. *Expert Systems with Applications*, *38*, 13933-13941.

Zhou, A., Qu, B.-Y., Li, H., Zhao, S.-Z., Suganthan, P. N., & Zhang, Q. (2011). Multiobjective evolutionary algorithms: A survey of the state of the art. *Swarm and Evolutionary Computation*, *1*, 32-49.

Zitzler, E., Deb, K., & Thiele, L. (2000). Comparison of Multiobjective Evolutionary Algorithms: Empirical Results. *Evolutionary Computation*, *8*(2), 173 - 195.

Zitzler, E., Laumanns, M., & Thiele, L. (2001). *SPEA2: Improving the strength Pareto evolutionary algorithm.* Comput. Eng. Netw. Lab. (TIK), ETH, Zurich, Switzerland, Tech. Rep. 103. Retrieved from `http://e-collection.library.ethz.ch/eserv/eth:24689/eth-24689-01.pdf` (Last visited on June 07, 2016)

Zitzler, E., & Thiele, L. (1999). Multiobjective evolutionary algorithms: A comparative case study and the strength Pareto approach. *IEEE Transactions on Evolutionary Computation*, *3*(4), 257-271.

Appendix A

Details of the uncertainty calculation

The overall uncertainty in the thermal efficiency of the flat-plate collectors was calculated in Section 9.3.2 as follows:

$$U_{\eta_{\text{coll}}} = \left[\left(\frac{\partial \eta_{\text{coll}}}{\partial \dot{m}_{\text{coll,F1}}} \cdot U_{\dot{m}_{\text{coll,F1}}} \right)^2 + \left(\frac{\partial \eta_{\text{coll}}}{\partial T_{\text{S5}}} \cdot U_{T_{\text{S5}}} \right)^2 + \left(\frac{\partial \eta_{\text{coll}}}{\partial T_{\text{S12}}} \cdot U_{T_{\text{S12}}} \right)^2 \right]^{1/2} \tag{A.1}$$

in which:

$$\frac{\partial \eta_{\text{coll}}}{\partial \dot{m}_{\text{coll,F1}}} = \frac{c_{\text{p,coll}} \cdot (T_{\text{S5}} - T_{\text{S12}})}{A_{\text{A1}} \cdot G_{\text{tot,A1}} + A_{\text{A2}} \cdot G_{\text{tot,A2}}} \tag{A.2a}$$

$$\frac{\partial \eta_{\text{coll}}}{\partial T_{\text{S5}}} = \frac{\dot{m}_{\text{coll,F1}} \cdot c_{\text{p,coll}}}{A_{\text{A1}} \cdot G_{\text{tot,A1}} + A_{\text{A2}} \cdot G_{\text{tot,A2}}} \tag{A.2b}$$

$$\frac{\partial \eta_{\text{coll}}}{\partial T_{\text{S12}}} = \frac{-\dot{m}_{\text{coll,F1}} \cdot c_{\text{p,coll}}}{A_{\text{A1}} \cdot G_{\text{tot,A1}} + A_{\text{A2}} \cdot G_{\text{tot,A2}}} \tag{A.2c}$$

The overall uncertainty in the calculation of the thermal energy stored in the storage tank was formulated in Section 9.3.2 as follows:

$$U_{Q_{\text{stored}}} = \sqrt{U_{Q_{\text{supply}}}^2 + U_{Q_{\text{DHW,tank}}}^2 + U_{Q_{\text{SH,tank}}}^2} \tag{A.3}$$

where:

$$\begin{aligned} U_{Q_{\text{supply}}} = \Bigg[& \left(\frac{\partial Q_{\text{supply}}}{\partial \dot{m}_{\text{coll,F1}}} \cdot U_{\dot{m}_{\text{coll,F1}}} \right)^2 + \left(\frac{\partial Q_{\text{supply}}}{\partial c_{\text{p,coll}}} \cdot U_{c_{\text{p,coll}}} \right)^2 \\ & + \left(\frac{\partial Q_{\text{supply}}}{\partial T_{\text{S5}}} \cdot U_{T_{\text{S5}}} \right)^2 + \left(\frac{\partial Q_{\text{supply}}}{\partial T_{\text{S12}}} \cdot U_{T_{\text{S12}}} \right)^2 \Bigg]^{1/2} \end{aligned} \tag{A.4}$$

$$U_{Q_{\mathrm{DHW,tank}}} = \left[\left(\frac{\partial Q_{DHW,tank}}{\partial \dot{m}_{\mathrm{DHW,F2}}} \cdot U_{\dot{m}_{\mathrm{DHW,F2}}} \right)^2 + \left(\frac{\partial Q_{\mathrm{supply}}}{\partial c_{\mathrm{p,water}}} \cdot U_{c_{\mathrm{p,water}}} \right)^2 + \left(\frac{\partial Q_{DHW,tank}}{\partial T_{\mathrm{S11}}} \cdot U_{T_{\mathrm{S11}}} \right)^2 + \left(\frac{\partial Q_{DHW,tank}}{\partial T_{\mathrm{S10}}} \cdot U_{T_{\mathrm{S10}}} \right)^2 \right]^{1/2} \tag{A.5}$$

$$U_{Q_{\mathrm{SH,tank}}} = \left[\left(\frac{\partial Q_{SH,tank}}{\partial \dot{m}_{\mathrm{SH,F3}}} \cdot U_{\dot{m}_{\mathrm{SH,F3}}} \right)^2 + \left(\frac{\partial Q_{\mathrm{supply}}}{\partial c_{\mathrm{p,water}}} \cdot U_{c_{\mathrm{p,water}}} \right)^2 + \left(\frac{\partial Q_{SH,tank}}{\partial T_{\mathrm{S13}}} \cdot U_{T_{\mathrm{S13}}} \right)^2 + \left(\frac{\partial Q_{SH,tank}}{\partial T_{\mathrm{S3}}} \cdot U_{T_{\mathrm{S3}}} \right)^2 \right]^{1/2} \tag{A.6}$$

in which:

$$\frac{\partial Q_{\mathrm{supply}}}{\partial \dot{m}_{\mathrm{coll,F1}}} = c_{\mathrm{p,coll}} \cdot (T_{\mathrm{S5}} - T_{\mathrm{S12}}) \tag{A.7a}$$

$$\frac{\partial Q_{\mathrm{supply}}}{\partial c_{\mathrm{p,coll}}} = \dot{m}_{\mathrm{coll,F1}} \cdot (T_{\mathrm{S5}} - T_{\mathrm{S12}}) \tag{A.7b}$$

$$\frac{\partial Q_{\mathrm{supply}}}{\partial T_{\mathrm{S5}}} = \dot{m}_{\mathrm{coll,F1}} \cdot c_{\mathrm{p,coll}} \tag{A.7c}$$

$$\frac{\partial Q_{\mathrm{supply}}}{\partial T_{\mathrm{S12}}} = -\dot{m}_{\mathrm{coll,F1}} \cdot c_{\mathrm{p,coll}} \tag{A.7d}$$

$$\frac{\partial Q_{\mathrm{DHW,tank}}}{\partial \dot{m}_{\mathrm{DHW,F2}}} = c_{\mathrm{p,water}} \cdot (T_{\mathrm{S11}} - T_{\mathrm{S10}}) \tag{A.8a}$$

$$\frac{\partial Q_{\mathrm{DHW,tank}}}{\partial c_{\mathrm{p,water}}} = \dot{m}_{\mathrm{DHW,F2}} \cdot (T_{\mathrm{S11}} - T_{\mathrm{S10}}) \tag{A.8b}$$

$$\frac{\partial Q_{\mathrm{DHW,tank}}}{\partial T_{\mathrm{S11}}} = \dot{m}_{\mathrm{DHW,F2}} \cdot c_{\mathrm{p,water}} \tag{A.8c}$$

$$\frac{\partial Q_{\mathrm{DHW,tank}}}{\partial T_{\mathrm{S10}}} = -\dot{m}_{\mathrm{DHW,F2}} \cdot c_{\mathrm{p,water}} \tag{A.8d}$$

$$\frac{\partial Q_{\mathrm{SH,tank}}}{\partial \dot{m}_{\mathrm{SH,F3}}} = c_{\mathrm{p,water}} \cdot (T_{\mathrm{S13}} - T_{\mathrm{S3}}) \tag{A.9a}$$

$$\frac{\partial Q_{\mathrm{SH,tank}}}{\partial c_{\mathrm{p,water}}} = \dot{m}_{\mathrm{SH,F3}} \cdot (T_{\mathrm{S13}} - T_{\mathrm{S3}}) \tag{A.9b}$$

$$\frac{\partial Q_{\mathrm{SH,tank}}}{\partial T_{\mathrm{S13}}} = \dot{m}_{\mathrm{SH,F3}} \cdot c_{\mathrm{p,water}} \tag{A.9c}$$

$$\frac{\partial Q_{\mathrm{SH,tank}}}{\partial T_{\mathrm{S3}}} = -\dot{m}_{\mathrm{SH,F3}} \cdot c_{\mathrm{p,water}} \tag{A.9d}$$